PERMEABILITY AND PORE STRUCTURE OF ROCKS UNDER PRESSURE

by

Yves Bernabe

Doctorat de specialite, Universite Paris 6 (1977)

Submitted to the Department of Earth,
Atmospheric, and Planetary Sciences
in partial fulfillment of the
requirements of the degree of

DOCTOR OF PHILOSOPHY

at the

December 6, 1985

Signature of Author: _____
Department of Earth, Atmospheric, and Planetary Sciences

Certified by: _____
William F. Brace
Thesis Supervisor

Accepted by: _____
Chairman, Department Committee on Graduate Students

PERMEABILITY AND PORE STRUCTURE OF ROCKS UNDER PRESSURE

by

Yves Bernabe

submitted to the Department of Earth, Atmospheric, and Planetary Sciences on December 6, 1985 in partial fulfillement of the requirements for the degree of Doctor of Philosophy in Geophysics

ABSTRACT

Permeability may be altered in the Earth by plastic flow of the rock matrix. In order to better understand the relation between plastic flow and pore geometry, we measured the permeability of a suite of hot-pressed calcite samples with differing porosities. We found that the permeability dramatically decreased with decreasing porosity, particularly in the range of 10 to 4% total porosity. These results agree with a model for pore geometry changes during hot-pressing as previously developed for ceramics. Measurements of unconnected and interconnected porosity showed that the interconnected porosity virtually disappeared in samples with a total porosity of 4% or less. Scanning electron microscope observations showed that the porosity of samples above 10% total porosity were composed of large "spheroidal" pores which were often connected by "tubular" pores. During the last stage of hot-pressing, these "tubes" are thought to collapse making the pore network disconnected.

We measured the permeability of three samples of Chelmsford granite cored in mutually perpendicular directions, while simultaneously cycling the confining pressure P_c and the pore pressure P_p. At intervals along the cycles we calculated "local" values of the coefficient α of the effective pressure law ($P_{eff}=P_c-\alpha P_p$). We found α ranging between 0.6 and 0.7 for the three samples, showing almost no directional effect. Similar procedures were applied on two samples of Barre granite. The measurements were made during unloading as well as loading. We observed a large hysteresis in permeability, and α was found to be strongly stress history dependent (α depended on the order in which P_c and P_p were applied to the samples). A simple model based on frictional sliding inside the rock seems to explain well these observations. Also, our data suggest a decrease of α with increasing confining pressure in both rocks. This can be explained by an increase in the mean aspect ratio of cracks during closure (the number of asperities coming into contact increases with pressure).

Similar experiments were performed on samples of Pottsville sandstone, Pigeon Cove granite, and Westerly granite. Just as in the previous section, α took values near 1.0 when the pore pressure was changed before the confining pressure, and was significantly lower in the other case. However, this dependency on stress path decreased rapidly with the number of cycles. After a

few cycles, α approached 1.0, which seems to favor the use of the simple pressure difference, $P_c - P_p$, for evaluating the effective pressure.

During the experiments mentioned above, we also measured the pore volume variations caused by changing the confining pressure. A recent version of the "equivalent channel model" provided appropriate means for interpreting these data jointly with permeability and electrical resistivity data collected for the same rocks. Thus, we could evaluate the following geometrical parameters: the standard deviation of the asperity heights distribution h, the pore wetted area per unit volume A_c/V, and the product of the initial mean hydraulic radius $\langle m_o \rangle$ by the initial mean tortuosity $\langle \tau_o \rangle$ squared.

A_c/V appeared very poorly correlated with the rocks permeability or porosity. However, we found that, the more permeable the rocks, the larger h and $\langle m_o \rangle \langle \tau_o \rangle^2$ were. This confirms that permeability in rocks is controlled by the hydraulic radius.

Finally, within the precision limits of this study, these three parameters did not seem to be affected either by the loading and unloading stages, or by further cycles, although the pore volume change data showed a strong hysteresis. This conclusion is not definitive because the uncertainty on certain parameters was quite large in some of the rocks studied. The uncertainty on h, A_c/V, and $\langle m_o \rangle \langle \tau_o \rangle^2$ can be considerably reduced by measuring the needed quantities on the same samples and during the same runs.

Thesis supervisor: Professor William F. Brace.

ACKNOWLEDGEMENTS

First, I would like to express my profound gratitude to Bill Brace and Joe Walsh. I certainly find fascinating to work with such great scientists, but even more important for me is the extraordinary spirit of free communication, mutual aid, and friendship that Bill and Joe have communicated to the 7th floor rock mechanics group.

I am also grateful to the other members of my thesis examination committee Ted Madden and Ronald Scott for their thorough and pertinent comments.

I always found encouragement, concern and help among the members of the rock mechanics group: Brian Evans, Sheila Gardner, Lind Gee, Randy Hay, Steve Hickman, Derek Hirst, and Dave Olgaard. I am also thankful to Lou Caruso, Karl Coyner, Gene Simmons, Roy Wilkens, and Tom Wissler, whose suggestions and advices were always very helpul.

Finally, I would like to affectionately thank the many friends I met at MIT, with a special attention to Rafael Benites, my office-mates Helene Lyon-Caen, Kaye Shedlock, and Joanne Fredrich, the members of the "french connection" Wafik Beydoun, Bernard Celerier, Carlos Del Pozo, and Marc Larrere, my soccer and volley-ball team-mates Craig Jones, Mike Nelson, Fico Pardo, Steve Roecker, Joao and Jose Rosa, and last but not least Kiyoshi "Kamikaze" Yomogida.

TABLE OF CONTENTS

PREFACE

One of the main characteristics of in-situ crustal rocks is that they are "wet". The fluids (mostly water) within the pores of the rocks play an important role both chemically and mechanically in almost all of the geological processes in the crust (for example, see Fyfe et al., 1978, Martin, 1979, or quoting Walder and Nur, 1984: "Certainly the mechanisms by which crustal rocks deform during tectonic activity are strongly influenced by the presence or absence of water as well as by the pore pressure, with brittle behavior favored under some conditions, ductile behavior under others"). In all these processes, permeability (here denoted k) is a vital controlling parameter. As a matter of fact, the need for accurate measurements of k in rocks submitted to high pressures was very early felt among the geophysicists (for a review see De Wiest, 1965). Inside this broad area, I tried to address two specific subjects: first, characterization of the pore structure of rocks based on transport properties measurements; second, the coupled effect of pore pressure and confining pressure on the transport properties of rocks.

The presence of pores and cracks inside rocks strongly affects their physical properties (Walsh and Brace, 1966). Because of the high connectivity of the pore network in crustal rocks, transport properties are very helpful for characterizing the pore structure of rocks under pressure, especially when used jointly with other data like porosity. In the case of crystalline rocks with their predominantly crack-like pores, the so-called "equivalent channel model"

(Paterson, 1983) provided an appropriate tool for interpreting the data. Also, measuring permeability is the most direct way to study the disappearance of pore connectivity in rocks undergoing bulk inelastic deformation.

The mechanical effect of pore pressure is usually incorporated into the analyses of crustal processes through the so-called "effective stress law" (or "effective pressure law" when only hydrostatic stresses are considered). It is written as follows (for example, see Paterson, 1978)

$$P_{eff} = P_c - \alpha P_p \qquad (1)$$

where P_{eff}, P_c, and P_p respectively are the effective pressure, the confining pressure, and the pore pressure. α is usually assumed to be a constant close to 1. But, both theoretical and experimental evidences exist showing that α may be significantly lower than unity, which can be extremely important in practical cases. For example, Fyfe et al. (1978) reported that rocks with an internally generated pore pressure higher than confining pressure behave differently if they obey the "simple" effective pressure law ($\alpha=1$), or the "general" law ($\alpha<1$). Fragmentation is usually observed in the former case, while propagation of hydraulic fractures occurs in the latter one.

Since the five chapters constituting this thesis were written in the form of independent articles, it seems necessary now to briefly comment on each one of them separately.

Chapter 1

The Earth sciences literature contains a large body of evidences showing that pore pressure may temporarily approach or even exceed the lithostatic

(or confining) pressure in the crust (Fyfe et al., 1978). Persistence of high pore pressure for a significant amount of time implies very low permeability. There are several possible mechanisms capable of lowering k in rocks. The first one mentioned by Walder and Nur (1984) is: "inelastic deformation, leading to pore closure", and, consequently, loss of connectivity, as should be added. We tested this type of process in hot-pressed calcite (sintered under pressure), which provides a good experimental model for indurated sedimentary rocks (Olgaard, 1985). As an a posteriori justification of our use of synthetic rocks, we can also cite Bourbie and Zinszner (1985) who observed a relation between permeability and porosity for a suite of natural sandstones very close to the one we found for synthetic marble. Our main conclusion was that the drop in permeability during densification was predominantly controlled by the disappearance of pore connectivity. If the connected porosity rather than the total porosity is used in the formation factor versus porosity log chart (Schlumberger Well Services, 1984), the Humble formula can apparently be successfully used even for low-porosity carbonates (Roberts, personal communication).

As noticed by Paterson (1983), equation (7) in our paper comes from an incorrect version of the equivalent channel model, but using the correct expression does not significantly change our conclusions. The permeability data tend to show that the connectivity was already reduced for samples with a porosity as large as 10%. This seems to disagree with the experimental curve of unconnected porosity versus total porosity which shows no significant amount of unconnected porosity above 5% total porosity. A possible explanation is that, in these early stages, connectivity is lost by development of dead-end pores

which contibute to the connected porosity but not to the conducting pore space.

Chapter 2

In this study, I attempted to experimentally determine the law of effective pressure for permeability in two granites. Two important observations were made: α depended on confining pressure, and on the order in which P_c and P_p were applied to the sample (similar stress history dependency effects were previously observed by others; for a review see Martin, 1979). The decrease of α with increasing confining pressure can be reasonably attributed to an increase of the crack aspect ratio (ratio of the width by the length of the crack) during pressurization. If the crack network in the rock was formed of flat cracks with a broad distribution of aspect ratios, the network connectivity should decrease rapidly with the closure of the low aspect ratio cracks. As I showed in the first chapter, this should yield a dramatic drop in permeability. Since such a drop was not observed, we must consider cracks with rough walls which would be transformed into an array of smaller cracks with higher aspect ratios during closure. Finally, the stress history dependency observed could be explained with a very simple model based on frictional sliding inside the rock. It should be remarked that shear stresses can easily develop in rock under hydrostatic pressure because of the anisotropy of the rock constituents.

Chapter 3

Here, I performed the same type of experiment as in Chapter 2 on other crystalline rocks. The results I obtained confirmed the conclusions of Chapter 2. Furthermore, certain samples were subjected to several confining pressure cycles, and I found that the stress history dependency decreased with the

number of cycles. Neglecting the pressure dependence, α was observed to approach 1 after a few cycles were applied. The frictional sliding model proposed in Chapter 2 can also account for these new observations. Another possible explanation for irreversible hysteresis and stress history dependency is that pressure cycles may damage the rocks. However, only tiny changes were observed by Sprunt and Brace (1974) in rock samples subjected to pressure cycles. Furthermore, the development of residual stresses predicted by the frictional sliding model can explain the recovery observed by Morrow (personal communication) in a Westerly granite sample that was cycled and, then, let free to relax under atmospheric pressure. I attempted to reproduce this experiment on Pottsville sandstone, but failed either because I used too different a rock, or because I let the sample rest under dry conditions. Wissler and Simmons (1985) measured the volumetric strain of rock submitted to several confining pressure cycles. They also based their interpretation on frictional sliding inside the rock. From these studies, the following question arises: are the rocks at depth in "post-stress" state (in the laboratory, equivalent to the state of samples subjected to several seasoning cycles), or "pre-stress" state? An experiment performed by Brace and reported by Walsh (1965) showed that strong vibrations can eliminate a large part of the hysteresis in a sample under load. Perhaps, natural vibrations can similarly "reset" the rocks in the crust to their pre-stress state.

Chapter 4

Changes in the pore volume were also measured during the experiments described in Chapter 2 and Chapter 3. Pores in crystalline rocks are known to consist almost exclusively in low aspect ratio cracks. I tried to apply the

equivalent channel model, which is greatly favored by narrow pore shape and/or size distributions, to these data. But, resistivity formation factor (here denoted F) data were necessary for this purpose. Measurements of electrical resistivity were available on some of my samples (Barre granite and Chelmsford granite; Gee and Brace, 1985). For the remaining rocks, I had to use data collected on other samples of the same rocks, which considerably augmented the uncertainty on the results. Examination of these data showed that, for effective pressures ranging between 20 and 200MPa, permeability and formation factor could be adequately related by the following power law: k proportional to F^{-2}. Adding both this empirical relation and some elements of elastic joint mechanics to the equivalent channel model (we saw in Chapter 2 that the cracks in rocks can be considered as microjoints with rough walls) made possible the evaluation of h, A_c/V, and $\langle m_o \rangle \langle \tau_o \rangle^2$, where h is the standard deviation of the distribution of the asperity heights, A_c the pore wetted area, V the pore volume, $\langle m_o \rangle$ the initial mean hydraulic radius, and $\langle \tau_o \rangle$ the initial tortuosity. Within the uncertainty limits of this study, these parameters appeared unchanged by loading, unloading, and further cycling. In the case of h and A_c/V as well as $\langle \tau_o \rangle$, this observation is consistent with the model proposed in the previous chapters, which states that there is no significant amount of inelastic deformation taking place except by frictional sliding. But, the hydraulic radius was expected to decrease with the number of cycles, which I failed to observe because of the large uncertainty introduced by my using data from different samples. However, I think that, even small variations in hydraulic radius can be detected in this manner, provided that all the measurements are made on the same samples during the same runs. Finally, we can

note that the largest hydraulic radii and largest h corresponded to the most permeable rocks. To the contrary, such a correlation could not be found for the pore wetted area A_c/V.

Chapter 5

The final chapter is a technical note devoted to the description of the apparatus used for the permeability and pore volume change measurements. Designing and building it was a very important part of my work. Despite a few arguments we had at the beginning, I think this machine certainly deserves a full chapter in my thesis. The dependability it always demonstrated should be acknowledged.

References

Bourbie, T., and B. Zinszner, Hydraulic and acoustic properties as a function of porosity in Fontainebleau sandstone, J. Geophys. Res., 90, 11524-11532, 1985.

De Wiest, R., Geohydrology, Wiley, New York, pp.366, 1965.

Fyfe, W.S., N.J. Price, and A.B. Thompson, Fluids in the Earth's Crust, Elsevier, Amsterdam, pp.383, 1978.

Gee, L.S., and W.F. Brace, The dependence of electrical resistivity in granites on effective pressure (abstr.), Trans. Am. Geophys. Union, 66, 366, 1985.

Martin, R.J., Pore pressure effects in crustal processes, Rev. Geophys. Space Phys., 17(6), 1132-1137, 1979.

Olgaard, D.L., Grain growth and mechanical processes in two-phased synthetic marbles and natural fault gouge, Ph.D. Thesis, M.I.T., Cambridge, 1985.

Paterson, M.S., Experimental Rock Deformation: the Brittle Field, Springer-Verlag, New York, pp.254, 1978.

Paterson, M.S., The equivalent channel model for permeability and resistivity in fluid-saturated rock - a re-appraisal, Mech. Mat., 2, 345-352, 1983.

Schlumberger Well Services, Log Interpretation Charts, 1984.

Sprunt, E., and W.F. Brace, Some permanent structural changes in rocks due to pressure and temperature, in Advances in Rock Mechanics, Proc. 3rd Congr. Int. Soc. Rock Mech., Denver 1974, Washington, D.C., Nat. Acad. Sci.,

Vol. 2, Part A, 524-529, 1974.

Walder, J., and A. Nur, Porosity reduction and crustal pore pressure development, J. Geophy. Res., 89, 11539-11548, 1984.

Walsh, J.B., The effect of cracks on the uniaxial elastic compression of rocks, J. Geophys. Res., 70, 399-411, 1965.

Walsh, J.B., and W.F. Brace, Cracks and Pores in rocks, Int. Cong. Rock Mechanics, Lisbon, 643-646, 1966.

Wissler, T.H., and G. Simmons, The physical properties of a set of sandstones, II: permanent and elastic strains in hydrostatic compression to 200MPa, Int. J. Rock Mech. Min. Sci. Geomech. Abstr., in press, 1985.

CHAPTER 1:

PERMEABILITY, POROSITY AND PORE GEOMETRY OF HOT-PRESSED CALCITE.

The co-authors B. Evans and W.F. Brace initiated this research and thoroughly reviewed the paper. B. Evans indicated the ceramics literature to me.

Mechanics of Materials 1 (1982) 173–183
North-Holland Publishing Company

PERMEABILITY, POROSITY AND PORE GEOMETRY OF HOT-PRESSED CALCITE *

Yves BERNABE and W.F. BRACE

Department of Earth and Planetary Sciences, Massachusetts Institute of Technology, Cambridge, MA 02139, U.S.A.

Brian EVANS

Department of Geological and Geophysical Sciences, Princeton University, Princeton, NJ 08544, U.S.A.

Received 4 May 1982; revised version received 1 June 1982

Permeability may be altered in the Earth by plastic flow of the rock matrix. In order to better understand the relation between plastic flow and pore geometry, we measured the permeability of a suite of hot-pressed calcite samples with differing porosities. We found that the permeability dramatically decreased with decreasing porosity, particularly in the range of 10 to 4% total porosity. These results agree with a model for pore geometry changes during hot-pressing as previously developed for ceramics. Measurements of unconnected and interconnected porosity showed that the interconnected porosity virtually disappeared in samples with a total porosity of 4% or less. Scanning electron microscope observations showed that the porosity of samples above 10% total porosity were composed of large 'spheroidal' pores which were often connected by 'tubular' pores. During the last stage of hot-pressing, these 'tubes' are thought to collapse making the pore network disconnected.

1. Introduction

The circulation of fluid in the crust is a vital factor in many different subjects including induced seismicity, fault mechanics, the deposition of ores, and heat and magma transport. The permeability of crustal rocks is thought to be relatively high (around 10^{-16} m^2, or 0.1 md) even at 10 km depth (Brace, 1980). However, the interconnected porosity may be reduced at depth by several processes including crack 'healing' or 'sealing' (Sprunt and Nur, 1979; Batzle et al., 1980) and plastic flow of the rock matrix (Brace, 1980). The kinetics of these processes are probably enhanced with increasing depth, but the lower depth limit of interconnecting pore space is presently unknown.

Material scientists have expended considerable effort investigating hot-pressing, and although exact quantitative prediction of porosity of the finished compact is not yet possible, many details of the processes involved have been clearly explained (for reviews, see Kingery et al., 1976; Waldron and Daniell, 1978; Wilkinson and Ashby, 1975; Coble, 1970). The reduction of porosity of a granular aggregate due to loading of the solid (geologically, the lithostatic pressure) at high temperature involves straining of the solid via one or more of the following mechanisms: self-diffusion through the lattice or along the grain boundaries, motion of dislocations, diffusion of solid material through the pore fluid. To the extent that these processes operate to reduce porosity in geologic situations the hot-pressing models may be helpfully applied to earth sciences problems such as induration of sediments or welding of fault gouge. We believe that some understanding of the influence of plastic flow on permeability can be gleaned from investigations of hot-pressed aggregates. In this study, we worked with synthetic aggregates of pure calcite powder hot-pressed to different porosities.

2. Experimental techniques

2.1. Description of the samples

Three different specimens of hot-pressed calcite, each a few centimeters long, were prepared using the hot-pressing technique of Caristan et al. (1981). Since the temperature changed from the central part of the furnace to the end, a gradient in porosity was obtained

* This research was supported by Army Research Office as Contract No. DAAG 29-79-C-003, and by National Sciences Foundation under Grant No. EAR-8008284.

0167-6636/82/0000-0000/$02.75

along the specimens. The specimens were then cut into three suites of smaller samples of differing porosity. The individual samples were ground into right cylinders 1.25 cm in diameter and from 0.5 to 1.0 cm in length, and carefully dried. Sample densities were obtained by measuring the dimensions and weight of the samples and were compared to the density of single crystal calcite. Thus, we could determine the total porosity η for each sample. The total porosity is composed of two terms: the interconnected porosity η_i and the unconnected porosity η_u ($\eta = \eta_i + \eta_u$). After saturation by water, the samples were weighed while immersed in water to determine the relative amount of interconnected and unconnected porosity.

2.2. The permeability measurement system

The sample assembly shown schematically in Fig. 1 permitted independent control of the confining pressure P_c and the pore pressure P_p. Calibration tests on inpermeable glass samples showed that there was no detectable flow along the rubber jacket as long as the confining pressure was more than 5 MPa above the pore pressure. The spiral tubing allowed adjustment for samples of differing lengths.

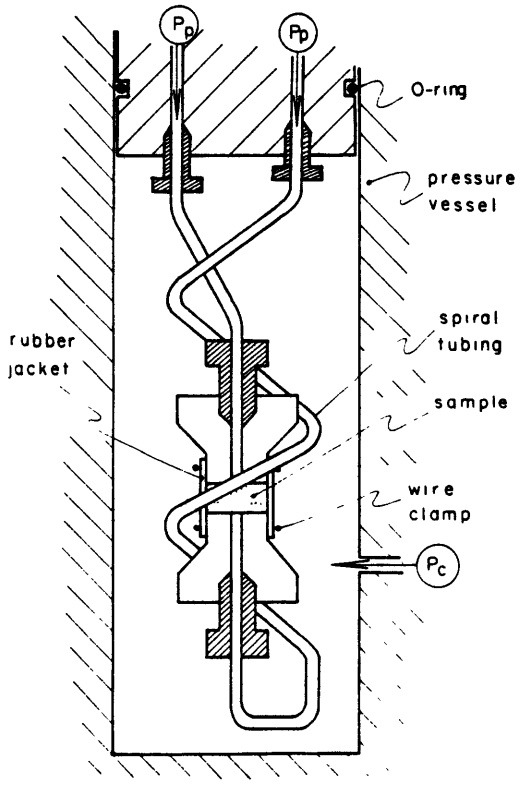

Fig. 1. A schematic drawing of the sample assembly.

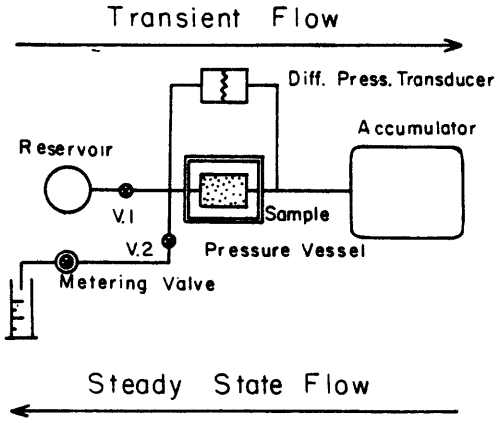

Fig. 2. A schematic drawing of the permeability measurement system.

The permeability measurement system shown schematically in Fig. 2 was designed to use both the steady-state and the transient methods under the same conditions of pressure. As shown in Fig. 3, the system was capable of measuring a wide range of permeability. This feature was desirable because of the wide range of permeability covered by geologic materials (Brace, 1980). Furthermore, the accuracy of permeability measurements could be tested by applying both methods to the same sample under the same experimental conditions.

2.2.1. The steady-state flow method

Steady-state flow was generated by closing the valve V.1 (see Fig. 2), opening V.2, and adjusting the metering valve to keep the differential pressure ΔP between the two ends of the sample at a constant value between 1 to 5% of the pore pressure. ΔP was accurately measured by a differential pressure transducer (B.L.H.) with a 0.001

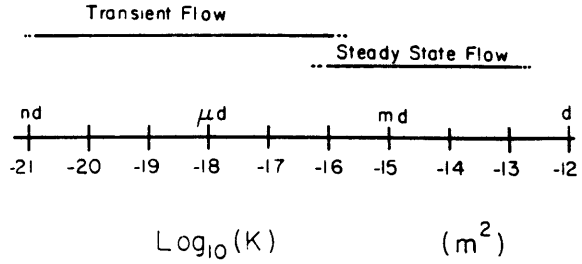

Fig. 3. The range of permeability covered by the system.

MPa sensitivity. A bladder-type accumulator (Greer Olaer Products) was used to maintain a nearly constant fluid pressure on the upstream side of the sample in spite of large changes in the volume of fluid.

The permeability k is simply given by Darcy's law,

$$k = (V_f L\mu)/(T\Delta P A), \tag{1}$$

where V_f is the volume of fluid flowing through the metering valve during the interval of time T, L the length, A the cross-sectional area of the sample, and μ the dynamic viscosity of distilled water which was used in this study as pore fluid.

2.2.2. The transient flow method

V.2 was closed, isolating the sample from the outside. V.1 was opened, connecting the so-called upstream and downstream reservoirs through the sample. The downstream reservoir was considered as infinite, since it included the accumulator. A pressure pulse ΔP_0 of 5 to 10% of the fluid pressure was generated in the upstream reservoir, and the differential pressure decay recorded.

Brace et al. (1968) analysed the transient flow method and derived an approximate expression for the differential pressure as a function of time:

$$\Delta P(t) = \Delta P_0 \exp\{-\alpha t\} \tag{2}$$

where t is the time and α is a constant related to the permeability k by

$$\alpha = (Ak)/(\mu L C_{up}) \tag{3}$$

where C_{up} is the upstream compressive storage, defined as the change in volume of fluid in the upstream reservoir per unit change in fluid pressure. C_{up} had to be experimentally determined since the upstream reservoir was not perfectly rigid.

There were two possible sources of error: Firstly, ambient temperature changes might induce parasitic changes of ΔP, and so the system had to be thermally isolated and kept at a constant temperature. An isothermal bath was used, which was not very effective for periods of time greater than several hours. Thus, the permeability was not determined for samples with a decay time longer than 1 hour. Secondly, the approximate solution suggested by Brace et al. (1968) could be not accurate enough. This point has been extensively studied in many papers (for example: Yamada and Jones, 1980; Trimmer, 1981; Hsieh et al., 1981; Neuzil et al., 1981). In the case of an infinite downstream reservoir, the general solution was derived by Hsieh et al. (1981), and is given as

$$\Delta P(t) = 2\Delta P_0 \sum_{m=1}^{\infty} \exp\{-at\Phi_m^2\}/(\Phi_m^2/b + b + 1) \tag{4}$$

where $a = (kA)/(\mu L C_s)$ and $b = C_s/C_{up}$, C_s being the sample compressive storage similar to C_{up}. The Φ_m's are solutions of

$$\tan\Phi = b/\Phi. \tag{5}$$

In this case, Neuzil et al. (1981) showed that the general solution is very close to the approximate one if b is lower than 0.1 (Fig. A.2 in their paper). This result is in agreement with the conclusions of Yamada and Jones (1980) and Trimmer (1981). b is given by

$$b = (\eta\beta_w + \beta_{eff} - \{1+\eta\}\beta_c)V_s/(\beta_w V_{up}) \tag{6}$$

where β_w, β_c and β_{eff} are respectively the compressibility of water, the compressibility of calcite and the effective compressibility of the material being studied. V_s is the volume of the sample, and V_{up} is the volume of the upstream reservoir. As will be shown later, in hot-pressed calcite the main part of the pore volume may be considered as almost spherical pores with a diameter of 4 μm. Given this assumption, β_{eff} can be computed from the porosity and the calcite compressibility as showed by Walsh (1965). The value found is of the order of 1.5 β_c. V_s was typically of the order of 1 cm^3. Two values 5 and 50 cm^3 of V_{up} were used to keep the decay times at reasonable values for samples with either high or low porosity. In either case, b was found to be lower than 0.05. Therefore, Neuzil's condition was satisfied.

2.3. The accuracy of the system

Four samples of hot-pressed quartz were used to experimentally test the accuracy of the system. The permeability of these fell in the overlapping region where both transient and steady-state methods can be applied (around 10^{-16} m^2). Permeability was measured under different conditions of pressure, using both methods for each of the samples. The results plotted in Fig. 4 are very consistent, and show a precision of 10% for both methods. Also, neither method systematically underestimated or overestimated the permeability.

2.4. Experimental procedure

In a typical experiment, the sample was subjected to a cycle of confining pressure to season the sample. The confining pressure was then increased and decreased by

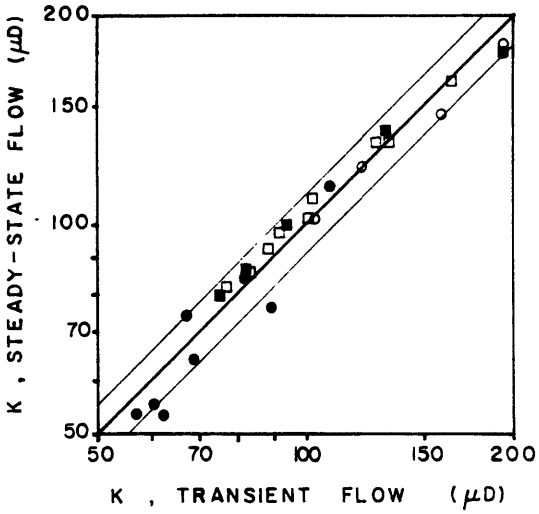

Fig. 4. Comparison of the two methods for four hot-pressed quartz samples indicated by different symbols. The measurements were made under different conditions of pressure. The solid line corresponds to $k_{\text{steady-state}} = k_{\text{transient}}$. A 10% interval is also indicated.

steps between a minimum value of 30 MPa and a maximum value of 180 MPa while the pore pressure was kept constant at 15 MPa. The permeability was measured at each step, except during the seasoning cycle.

In the case of a sample with low permeability, the loading and unloading steps each required several hours to be completed, making it difficult to complete a cycle in one working day. Thus, to be consistent, even in the case of samples with high permeability, loading and unloading stages were separated by around 12 hour during which time both the pore pressure and the confining pressure were kept unchanged.

3. Observations and discussion

The numerical data given in Table 1 can be examined from different view-points. In the following sections we will distinguish several different effects each of which is discussed separately.

3.1. Hysteresis and time effect

Cycling the confining pressure seems to cause non-recoverable changes in permeability especially for samples with a high porosity (Fig. 5). These irreversible changes seem to have occurred mainly during the 'rest' time which separated the loading and unloading stages, when the confining pressure was at its maximum (180 MPa). Thus, processes of irreversible sliding between grains do not seem to have occurred perhaps because of grain interlocking. It seems likely that time-dependent processes such as yielding at contacts of asperities, or slow crack growth, were taking place. Such a time effect was previously observed by Sutherland and Cave (1980) on rock salt.

Another time-dependent phenomena should be noted. Some samples showed a slight increase of permeability during the 'rest' time which separated two cycles, when the confining pressure was at its minimum (30 MPa). Kranz et al. (1979) previously observed a similar effect under different experimental conditions. In order to keep the 'effective' pressure $P_{\text{eff}} = P_c - P_p$ unchanged, Kranz et al. changed P_p and P_c by the same amount. According to them, changes in P_p and P_c produce deformations of pores which may not compensate each other. This explanation cannot be used in this study since neither P_p nor P_c were changed. A time-dependent process of relaxation of residual stresses

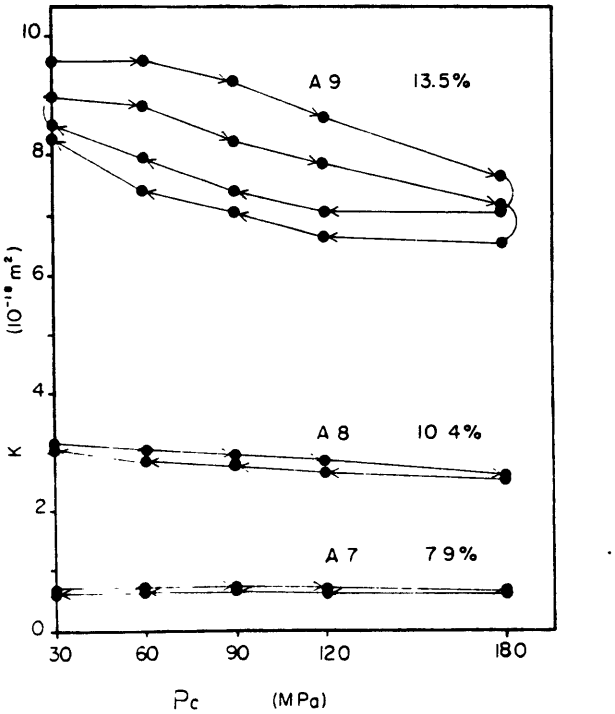

Fig. 5. The variations of the permeability k during confining pressure cycles for three typical hot-pressed calcite samples.

Table 1 [a]
The permeability k as a function of the confining pressure P_c

Sample	η (%)		k (10^{-18} m^2)				
			30 MPa	60 MPa	90 MPa	120 MPa	180 MPa
A1	1.6	L2			*		
A2	1.9	L2			*		
A3	2.7	L2			*		
A4	4.3	L2			*		
A5	6.3	U2	0.058	0.058	0.055	0.052	0.052
A6	7.1	L2	0.16	0.13	0.14	0.13	0.13
		U2	0.12	0.12	0.12	0.11	0.10
A7	7.9	L2	0.70	0.69	0.67	0.64	0.64
		U2	0.67	0.63	0.63	0.61	0.61
A8	10.4	L2	3.1	3.0	2.9	2.8	2.6
		U2	3.0	2.8	2.7	2.6	2.5
A9	13.5	L2	9.6	9.6	9.2	8.6	7.6
		U2	8.5	7.9	7.4	7.0	7.0
		L3	9.0	8.8	8.2	7.9	7.0
		U3	8.3	7.3	7.1	6.7	6.5
B1	10.8	U2	4.7	4.2	4.1	4.0	3.9
		L3	4.8	4.5	4.4	4.2	4.1
B2	11.6	L2	10.5	10.3	10.1	9.8	9.2
		U2	10.3	9.9	9.5	9.3	9.2
		L3	10.1	10.1	9.9	9.6	9.0
B3	12.4	L2	10.2	10.0	9.9	9.9	9.6
		U2	10.1	9.5	9.4	9.4	9.4
C1	14.1	L2	40.0	38.0	37.0	35.0	33.0
		U2	32.0	29.0	28.0	28.0	28.0
C2	15.4	U2	23.0	21.0	20.0	19.0	19.0
		L3	22.0	21.0	19.0	18.0	16.0
C3	16.0	L2	48.0	46.0	45.0	43.0	41.0
		U2	40.0	37.0	35.0	35.0	35.0
C4	17.1	L2	34.0	33.0	32.0	31.0	29.0
		U2	25.0	24.0	23.0	23.0	23.0
C5	18.4	L2	46.0	45.0	44.0	44.0	43.0
		U2	43.0	40.0	39.0	37.0	37.0
C6	19.5	L2	70.0	70.0	69.0	65.0	59.0
		U2	49.0	46.0	44.0	43.0	44.0

[a] The letters L and U indicate whenever the measurement was made during a loading or an unloading stage of a cycle, the number of which is given next. As previously reported, the permeability of the first four samples was below the resolution of the system. The porosity η is also indicated. The underlined values define the 'intrinsic' permeability for each sample.

at the locations where plastic flow previously occurred, is rather suggested.

3.2. Pressure sensitivity

As compared to the large decrease of permeability of crystalline rocks with increasing P_c (Fig. 6; Brace et al., 1968; Coyner et al., 1979), the pressure sensitivity of permeability of hot-pressed calcite is small. k decreases by a factor of 20% for a six fold increase in confining pressure. Since their behavior is so different, crystalline rocks and hot-pressed calcite must have quite different pore geometries.

The permeability of many crystalline rocks is thought to be due to interconnected networks of cracks of low aspect ratio (ratio of crack width to length). Since low aspect ratio cracks can close under relatively small confining pressure (Batzle et al., 1980), P_c strongly affects the permeability of crystalline rocks.

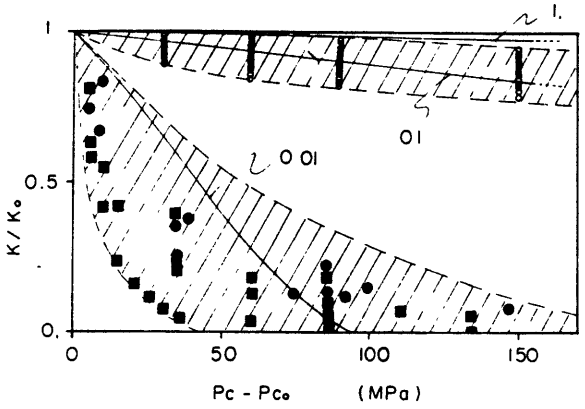

Fig. 6. Comparison of the behaviour of hot-pressed calcite (open circles), and various crystalline rocks (closed circles: Brace et al. (1968): closed squares: Coyner et al. (1979)). The three curves computed in Appendix A for three values of the aspect ratio (1, 0.1 and 0.01) are also plotted.

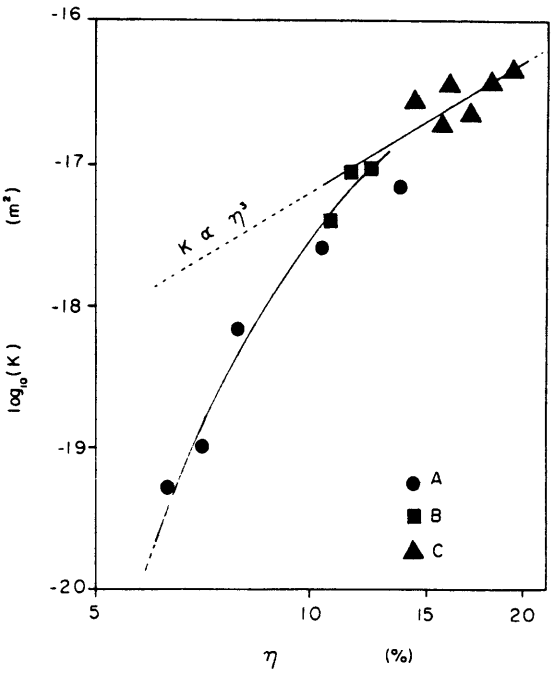

Fig. 7. The 'intrinsic' permeability k of hot-pressed calcite as a function of the porosity η.

In contrast, the interconnected pores of hot-pressed calcite must have a greater aspect ratio than the cracks of crystalline rocks, since the permeability of our samples exhibites a smaller pressure sensitivity. We verified this by computing the permeability changes with confining pressure for an infinitely long cylindrical pore of elliptical cross-section (Appendix A). The results are plotted in Fig. 6 for three values of the aspect ratio ϵ defined in this case as the ratio of the minor to the major axis of the cross-sectional surface. $\epsilon = 0.1$ agrees fairly well with our data, whereas the data for crystalline rocks are in better agreement with $\epsilon = 0.01$.

3.3. Permeability–porosity relationship

In contrast to the rather small pressure sensitivity, the hot-pressed calcite data shows a strong porosity dependence (k decreases by three orders of magnitude when η decreases from 20 to 5%). In order to quantify this, the value measured at the starting of the unloading stage of second cylce (underlined in Table 1) was arbitrarily defined as the 'intrinsic' permeability of each sample. The permeability could then be plotted against porosity (Fig. 7). To relate k and η, we used the following classical expression (Brace, 1977):

$$k = (m^2\eta^3)/C \qquad (7)$$

where C is a constant number ranging between 2 and 3, and m the hydraulic radius (the ratio of the volume of pores to the void-solid interface area). The slope of the $\log k$ vs. $\log \eta$ curve was determined by least squares analysis. It is equal to 3.3 for the samples with a porosity greater than 11%. This implies that the hydraulic radius does not vary significantly over the porosity range from 20 to 11%. The value of m computed from our data is of the order of 0.1–0.2 μm. As it will be seen

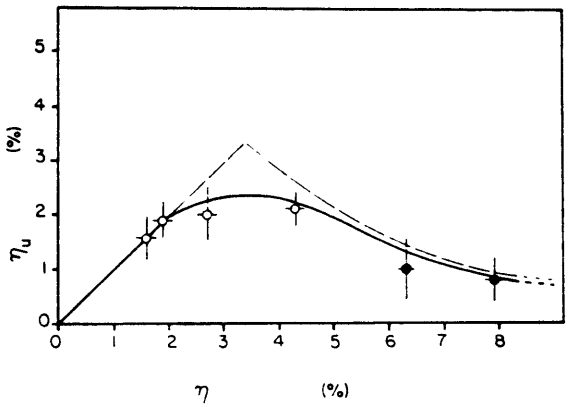

Fig. 8. The unconnected porosity η_u as a function of the total porosity η. The theoretical model is illustrated by the broken line. The solid line is a curve fitting our experimental points. The open circles represent samples, the permeability of which is below the resolution of our system (10^{-11} m^2 or 1 nd).

later, during the intermediate stage of hot-pressing (the porosity ranging from 20 to 11%) both the volume of pores and the pore-solid interface area are thought to vary. An almost constant hydraulic radius (the permeability being roughly proportional to the cubed porosity) implies that the diminution of the volume of pores and of the void–solid interface area occurred at almost the same rate.

For porosities less than 11%, the permeability shows a startling departure from the porosity cubed law, falling quite rapidly until, at around 5% porosity, the permeability was too small to be measured accurately ($k \leqslant 10^{-21}$ m^2). We needed further data to observe the transition from connected pore network to isolated inclusions which was predicted by Waldron and Daniell (1978). From the measurements of interconnected and

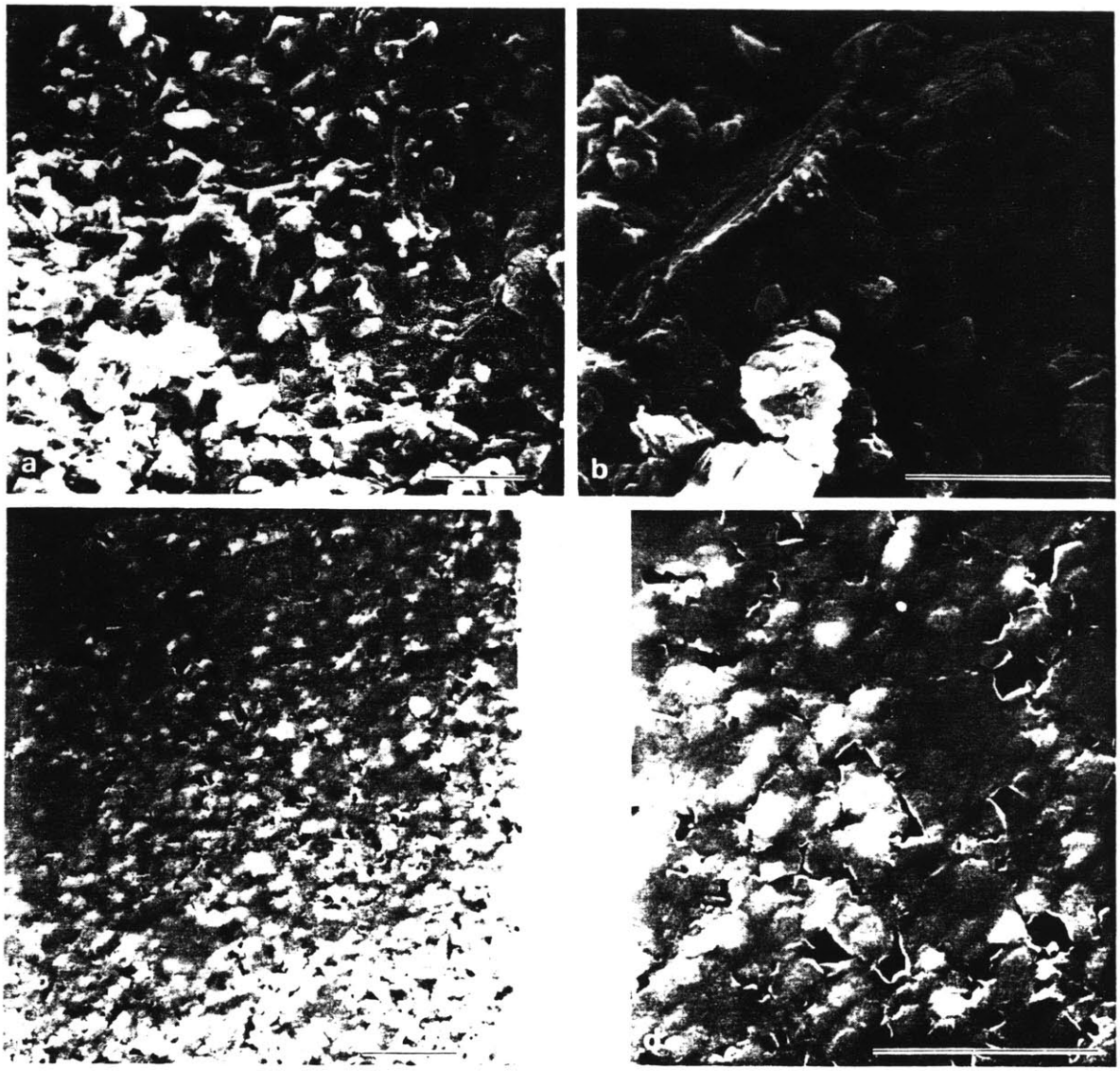

Fig. 9. (a) and (b) The surface of an intergranular tensile fracture in the sample A9 ($\eta = 13.5\%$), which corresponds to the second stage of hot-pressing. (c) and (d) A cross-section of the pores in the same sample. (*Note*: The length of the line in the right lower corner of (a), (b), (c) and (d) indicates 10 μm.)

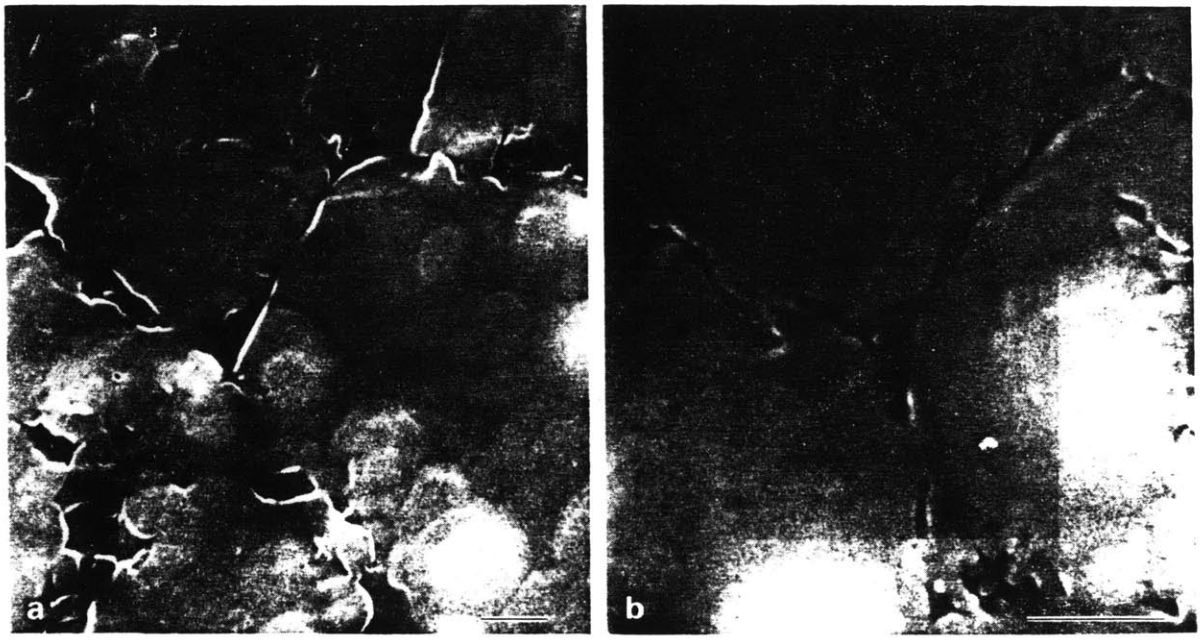

Fig. 10. (a) A view of 'tubular' pores with a triangular cross-section which are thought to be situated at three-grain edges, and to bond the larger cavities observable in the previous micrographs. (b) A detailed view of a triangular pore and the three narrow throats extending from the vertices along two-grain faces. (*Note*: The length of the line in the right lower corner of (a) and (b) indicates 1 μm.)

unconnected porosity a critical porosity of about 3–4% could be determined, below which the pore connectivity become vanishingly small (Fig. 8). Yen and Coble (1972) and Gupta (1976) observed in Al_2O_3 that, under high temperature, tubular pores become unstable and are pinched off into rows of isolated bubbles; perhaps such a process occurs in the hot-pressed material. As the porosity decreases, the number of closed pores becomes larger and larger, until a critical number is reached above which the pore network becomes totally disconnected.

Because the samples were hot-pressed at different temperatures, it is possible that the partitioning of strain amongst the various diffusional and dislocation mechanisms also was different from sample to sample. Since we did not attempt to determine the dominant mechanism of plastic flow during hot-pressing, this study alone cannot conclude wether or not the relationship between porosity and permeability is sensitive to the mode of plastic flow. However, because of the similarity of these results to those noted above for ceramics, we suspect that the porosity at which the pore connectivity disappears does not depend on the mechanism of plastic flow during hot-pressing.

3.4. The microstructure of a typical sample

Sample A9 ($\eta = 13.5\%$) was used to make two different series of micrographs. In the first case, the cross-sectional surface was polished, ion-milled and sputter-coated with about 20 nm of gold-palladium. The pores could be seen in cross-section. In the second case, the sample was broken in tension. Since the cohesion of our material was relatively low, the tensile fracture was intergranular. The fracture surface was then coated with 20 nm of gold-palladium, and micrographs were taken. All the observations were made on a JEOL JSM-35 microscope with an accelerating voltage of 20 kV and a resolution of 0.02 μm.

Several typical micrographs are presented in Figs. 9 and 10. The grain size is relatively inhomogeneous ranging from 2 to 20 μm. All the pores are situated at grain boundaries, and there is no evidence of cracking. Three classes of pores can be distinguished: relatively large cavities (2 to 4 μm) with an almost equidimensional shape (the mean distance separating them is of the order of the grain size); smaller 'tubular' pores (0.1 to 0.4 μm) with variable triangular cross-section (some are almost equilateral, whereas some others look like very long

arrows); very narrow pores (less than 0.1 μm) which extend from the vertices of the triangular pores following the grain boundaries. Examples of these three different classes of pores can be seen on the micrographs in Figs. 9 and 10. Except those of the last class, the pores show relatively high aspect ratio. Although we did not carry out a quantitative study of the pore geometry from these micrographs, a mean hydraulic radius of 0.1–0.2 μm seems reasonable.

To summarize, the permeability of hot-pressed calcite may be due to a network of 'tubes' with triangular cross-section along three-graind edges and of narrow sheet-like throats at two-grain faces bonding larger cavities at four-grain corners. These cavities contribute most of the porosity, whereas the 'tubes' control the permeability of the aggregates. Examples of such networks were observed by Wardlaw (1976) on carbonate rocks. Simmons et al. (1982) used S.E.M. stereo-pair micrographs to visualize such pore networks in three dimensions for a suite of sandstones.

4. Conclusion

In conclusion, Fig. 11 shows a schematic representation of the pore geometry for the three successive stages of hot-pressing as predicted by Waldron and Daniell (1978) and Coble (1961), and the corresponding permeability changes with porosity. We could not prepare any sample corresponding to the first (or initial) stage because of its very short duration. Therefore, we can only speculate the shape of the permeability vs. porosity curve. During this stage, as the volume of pores decreases, the number of individual contact points of grains is thought to increase, but not the total area of contact. This implies that the hydraulic radius should decrease as the porosity decreases and the permeability does not follow the porosity cubed law. During the second (or intermediate) stage, the void–solid interface area is thought to decrease in proportion to the volume of pores. We observed that the hydraulic radius tended to remain constant the permeability being roughly proportional to the cube of the porosity. During the third (or final) stage, the 'tubular' pores are thought to become unstable, and to be pinched off into rows of isolated bubbles. During this process, the hydraulic radius decreases rapidly and, again, the permeability does not follow the porosity cubed law. Below a critical porosity (3–4% for hot-pressed calcite), the number of closed 'tubular' pores becomes large enough to make the pore network totally disconnected.

Finally, we wish to remark that the relationship between permeability and porosity noted here presupposes that the material has been plastically deformed, and that no significant amount of brittle deformation has occurred after the plastic straining. Thus, rock formations near the surface of the earth cannot be expected to exhibit such a simple permeability–porosity relationship because of their varied and complex strain history involving, among other things, the introduction of microcracks during uplift.

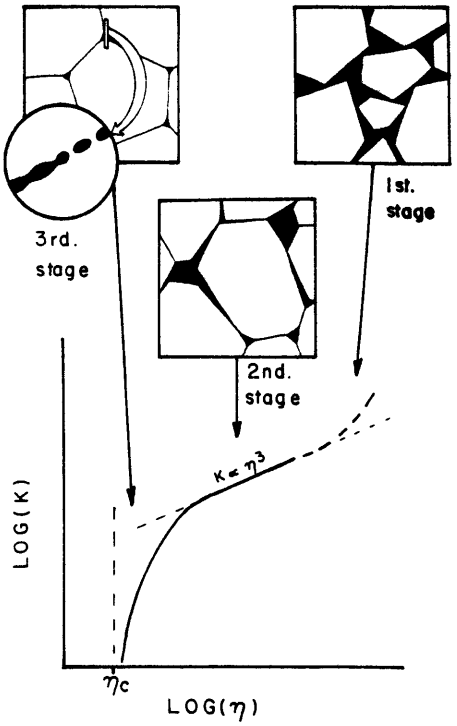

Fig. 11. A schematic representation of the theoretical model of changes of pore geometry during hot-pressing, and the corresponding permeability vs. porosity curve. The critical porosity η_c corresponding to the point where the tubular pores along three-grain edges are pinched off is also indicated. This process is schematically shown in a section parallel to the long dimension of one of these pore (inside the circle).

Acknowledgement

We would like to thank D. Olgaard who was very helpful in preparing some of the hot-pressed calcite specimens. We are also grateful to J. Walsh and J. Blendell for their suggestions and comments.

Appendix A

Assume that an infinite elastic solid contains an infinitely long cylindrical pore with an elliptical cross-section as sketched in Fig. A1. At infinity, the solid is subjected to a confining pressure P_c. The fluid pressure P_p in the pore is assumed to be constant. A change in the confining pressure ΔP_c produces displacements u and v only along the x and y directions (plane strain), which can be written

$$u+iv=1/(2G)\{-(3-4\nu)\Phi(Z) + Z\overline{d\Phi(Z)}/dZ+\overline{\Psi(Z)}\} \tag{A1}$$

where G is the shear modulus, and the overbar represents the complex conjugate of the quantity written below the bar. The functions Φ and Ψ are classically given by

$$\Phi=(\tfrac{1}{2}c)\Delta P_c \sinh\zeta, \qquad \Psi=(\tfrac{1}{2}c)\Delta P_c(\cosh 2\xi/\sinh\zeta) \tag{A2}$$

where ξ and ζ are defined in Fig. A1. (For a review of the complex function method, see Jaeger and Cook (1979).)

The radial displacements at points A and B are equal to the variations of the cross-sectional dimensions,

$$u_A=\Delta a=-b(1-\nu)\Delta P_c/G, \qquad v_B=\Delta b=-a(1-\nu)\Delta P_c/G \tag{A3}$$

where a and b are the major and minor axis. This yields

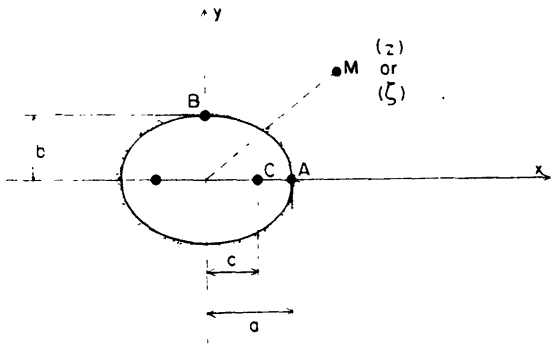

Fig. A1. An infinitely long cylindrical pore with an elliptical cross-section inside an infinite elastic medium. A point M in this plane can be represented by a complex number Z ($Z=x+iy$). The elliptical coordinates ξ and η can also be used ($\zeta=\xi+i\eta$, $Z=c\cosh\zeta$, $x=c\cosh\xi\cos\eta$ and $y=c\sinh\xi\times\sin\eta$).

the following pair of coupled differential equations:

$$da/dP_c=-b(1-\nu)/G, \qquad db/dP_c=-a(1-\nu)/G. \tag{A4}$$

Taking the second derivative uncouples the equations, yielding

$$d^2a/dP_c^2=a(1-\nu)^2/G^2, \qquad d^2b/dP_c^2=b(1-\nu)^2/G^2, \tag{A5}$$

the solution of which is

$$a=\tfrac{1}{2}(a_0+b_0)\exp\left\{-\frac{(1-\nu)}{G}(P_c-P_{c0})\right\} +\tfrac{1}{2}(a_0-b_0)\exp\left\{\frac{(1-\nu)}{G}(P_c-P_{c0})\right\}, \tag{A6}$$

$$b=\tfrac{1}{2}(a_0+b_0)\exp\left\{-\frac{(1-\nu)}{G}(P_c-P_{c0})\right\} -\tfrac{1}{2}(a_0-b_0)\exp\left\{\frac{(1-\nu)}{G}(P_c-P_{c0})\right\}$$

where a_0, b_0 and P_{c0} are the initial values of a, b and P_c. When the cross-section is circular ($a=b=r$), (A5) is reduced to a single equation, and the solution is

$$r=r_0\exp\left\{-\frac{(1-\nu)}{G}(P_c-P_{c0})\right\}. \tag{A7}$$

It is interesting to compute the confining pressure at which the pore is entirely closed ($b=0$, $a=c$). It is given by

$$P_c-P_{c0}=(E/4(1-\nu^2))\ln\frac{1+\epsilon_0}{1-\epsilon_0} \simeq(E\epsilon_0/2(1-\nu^2)) \tag{A8}$$

where E is the Young's modulus and ϵ_0 the initial aspect ratio. This expression is very close to the one obtained by Walsh (1965) in the case of a penny-shaped crack.

In absence of body-forces, the fluid flow is controlled by the Navier–Stokes equation:

$$\vec{V}\,\mathrm{grad}\,\vec{V}+\partial\vec{V}/\partial t+ +1/\rho\,\mathrm{grad}\,P_p+\mu/\rho\,\mathrm{curl\,curl}\,\vec{V}=0 \tag{A9}$$

where $\vec{V}$ is the local velocity vector of the fluid, ρ the fluid density and μ the dynamic viscocity of the fluid. In the case of steady-state laminar flow, the fluid velocity is everywhere parallel to the pore axis, and vanishes at the pore–solid interface. The Navier–Stokes equation is

then reduced to

$$\partial^2 V/\partial x^2 + \partial^2 V/\partial y^2 = -1/\mu\, \partial P_p/\partial z \qquad \text{(A10)}$$

where z is the coordinate along the infinite dimension of the pore. The solution is

$$Q = \frac{\pi a^3 b^3}{4(a^2+b^2)\mu} \frac{\partial P_p}{\partial z} \qquad \text{(A11)}$$

where Q is the volume of fluid flowing per unit time. Using Darcy's law, this expression yields the normalized permeability

$$\frac{k}{k_0} = \frac{a^2 b^2 (a_0^2 + b_0^2)}{a_0^2 b_0^2 (a^2+b^2)}. \qquad \text{(A12)}$$

It is easy to see that, when a and b are replaced by their values from (A6), the solution only contains the aspect ratio $\epsilon_0 = b_0/a_0$ and $P_c - P_{c0}$.

With appropriate values of the constants, this model permits to evaluate the effect of a change of the confining pressure on the permeability for various aspect ratios.

Appendix B

The values of the density and dynamic viscosity of water come from the Steam Tables of Keenan et al. (1978). The values of the density of calcite and of the elastic constants of a pure calcite aggregate come from Simmons and Wang (1971).

References

Batzle, M.L., G. Simmons and R.W. Siegfried (1980), "Microcrack closure in rocks under stress: direct observation", *J. Geophys. Res. 85*, 7072.

Brace, W.F. (1977), "Permeability from resistivity and pore shape", *J. Geophys. Res. 82*, 3343.

Brace, W.F. (1980), "Permeability of crystalline and argillaceous rocks", *Internat. J. Rock. Mech. Min. Sci. Geomech. Abstr. 17*, 241.

Brace, W.F., J.B. Walsh and W.T. Frangos (1969), "Permeability of granite under high pressure", *J. Geophys. Res. 73*, 2225.

Caristan, Y., R.J. Harpin and B. Evans (1981), "Deformation of porous aggregates of calcite and quartz using the isostatic hot-pressing technique", *Tectonophysics 78*, 629.

Coble, R.L. (1961), "Sintering crystalline solids Part I. Intermediate and final state diffusion models", *J. Appl. Phys. 32(5)*, 787.

Coble, R.L. (1970), "Diffusional models for hot-pressing with surface energy and pressure effects as driving forces", *J. Appl. Phys. 41*, 4798.

Coyner, K.B., W.F. Brace and J.B. Walsh (1979), "New laboratory measurements of permeability and electric resistivity of crystalline rocks", *Trans. Amer. Geophys. Union 60*, 943.

Gupta, T.K. (1976), "Alterations of cylindrical voids during crack healing in alumina", in: R.M. Fulrath and J.A. Park, eds., *Ceramic Microstructures '76: With Emphasis on Energy Related Applications*, Westview Press, Boulder, CO, 354.

Hsieh, P.A., J.V. Tracy, C.E. Neuzil, J.D. Bredehoeft and S.E. Silliman (1981), "A transient laboratory method for determining the hydraulic properties of 'tight' rocks – Theory", *Internat. J. Rock. Mech. Min. Sci. Geomech. Abstr. 18*, 245.

Jaeger, J.C. and N.C. Cook (1979), *Fundamentals of Rock Mechanics*, Chapman and Hall, London.

Kingery, W.D., H.K. Bowen and D.R. Uhlmann (1976), *Introduction to Ceramics*, Wiley, New York, 501.

Keenan, J.H., F.G. Keyes, P.G. Hill and J.G. Moore (1978), *Steam Tables: Thermodynamic Properties of Water Including Vapor, Liquid, and Solid Phases*, Wiley, New York.

Kranz, R.L., A.D. Frankel, T. Engelder and C.H. Scholz (1979), "The permeability of whole and jointed Barre granite", *Internat. J. Rock Mech. Min. Sci. Geomech. Abstr. 16*, 225.

Neuzil, C.E., C. Cooley, S.E. Silliman, J.D. Bredehoeft and P.A. Hsieh (1981), "A transient laboratory method for determining the hydraulic properties of 'tight' rocks – Application", *Internat. J. Rock Mech. Min. Sci. Geomech. Abstr. 18*, 253.

Simmons, G., R. Wilkens, L. Caruso, T. Wissler and F. Miller (1982), "Physical properties and microstructures of a set of sandstones", Ann. Rept. to the Schlumberger –Doll Research Center.

Simmons, G. and H. Wang, eds. (1971), *Single Crystal Elastic Constants and Calculated Aggregate Properties: A Handbook*, M.I.T. Press, Cambridge.

Sprunt, E.S. and A. Nur (1979), "Microcracking and healing in granites: new evidence from cathodoluminescence", *Science (AAAS) 205 (4405)*, 495.

Sutherland, H.J. and S.P. Cave (1980), "Argon gas permeability of New Mexico rock salt under hydrostatic compression", *Internat. J. Rock Mech. Min. Sci. Geomech. Abstr. 17*, 281

Trimmer, D.A. (1981), "Design criteria for laboratory measurements of low permeability rocks", *Geophys. Res. Lett. 8*, 9, 973.

Waldron, M.B. and B.L. Daniell (1978), *Sintering*, Heyden, London, 4.

Walsh, J.B. (1965), "The effect of cracks on the compressibility of rock", *J. Geophys. Res. 70(2)*, 381.

Wardlaw, N.C. (1976), "Pore geometry of carbonate rocks as revealed by pore casts and capillary pressure", *Amer. Assoc Petrol. Geol. Bull. 60(2)*, 245.

Wilkinson, D.S. and M.F. Ashby (1975), "The development of pressure sintering maps", *Proc. 4th Internat. Conf. on Sintering and Related Phenomena*, Notre Dame; *Mater. Sci. Res 10*, 475.

Yamada, S.E. and A.H. Jones (1980), "A review of pulse technique for permeability measurements", *Soc. Pet. Engrg J. 20*, 357.

Yen, C.F. and R.L. Coble (1972), "Spheroidization of tubular voids in Al_2O_3 crystals at high temperature", *J. Amer Ceram. Soc. 55(10)*, 507.

CHAPTER 2:

THE EFFECTIVE PRESSURE LAW FOR PERMEABILITY IN CHELMSFORD GRANITE AND BARRE GRANITE.

INTRODUCTION

When working on problems where porous rocks or soils and pore fluid pressure are involved, geophysicists and engineers commonly use the concept of effective pressure, a notion which stems from experimental considerations. It has been observed that the strength of rocks remained fairly constant when the confining pressure P_c and the pore pressure P_p were simultaneously changed by the same amount, in comparison with the large variations measured when P_c or P_p was changed alone ([1] to [7]). Assuming that this is true for any physical property k (here, permeability), the knowledge of k as a function of P_c at zero pore pressure is sufficient to derive the value of k for any pair (P_c, P_p) using the expression

$$k(P_c, P_p) = k(P_{eff}, 0) \qquad (1)$$

where the effective pressure P_{eff} is defined by

$$P_{eff} = P_c - P_p \qquad (2)$$

This is the ordinary effective pressure law, the simplicity of which made it so popular. However, it has been found both theoretically and experimentally that this law does not always hold ([8] to [17]). Rather, the law of effective pressure should be written in the form

$$P_{eff} = P_c - \alpha P_p \qquad (3)$$

where α is a constant taking values other than 1.0, depending on many factors like porosity, pore geometry, the rock constituents and their geometrical arrangement. In fact, the confining pressure and the pore pressure can significantly affect some of these factors and, therefore, α itself. In this case, the expression (3) cannot be conveniently used. However, alternative formulations allowing for a variable α will be presented in the next section.

Finally, it should be remembered that the effective pressure law may not be the same if different physical properties are considered ([10] and [12]). Consequently, comparing values of α obtained for different properties may be fairly misleading. This remark also applies to the rare theoretical expressions of α available in the literature (for example, the well-known expression derived by Skempton [8] is valid only for the bulk volumetric strain; see also [10] and [12]).

In the past, soils and sedimentary rocks were principally investigated. There are only few data about α on crystalline rocks available in the literature. Our objective was to measure α for permeability in typical crystalline rocks and study the effect of some of the factors listed above. We specifically addressed the following questions.

1 - In certain sandstones the permeability takes very different values when measured in directions parallel or perpendicular to the bedding (see [18]). Do crystalline rocks with an anisotropic distribution of cracks like Chelmsford granite (see [19]) produce a similar directional effect on permeability and the law of effective pressure?

2 - We know that the physical properties of crystalline rocks are deeply altered during pressurization because of the closure of cracks. The variations of α with confining pressure may yield useful information about the changes in crack geometry during closure.

3 - Hysteresis is an important feature of materials containing cracks when submitted to loading cycles [20]. Similar stress history and hysteresis effects were observed on permeability in the past (for example, on Barre granite [21]). It can be important for the users of the law of effective

pressure to know how pressure cycles affect α.

EXPERIMENTAL TECHNIQUES

Description of the samples

After the studies cited above, Chelmsford and Barre granites seemed quite appropriate for our purpose. In a previous work [22], samples of Chelmsford granite were cored with different orientations, namely perpendicular to rift plane, perpendicular to grain plane, and perpendicular to hardway plane (we will call them R-, G-, and H-samples respectively, following Peng and Johnson [19]). We took one sample for each orientation, the dimensions of which had to be reduced to 1.90cm in diameter and around 2.5cm in length in order to fit into our apparatus. Samples of this size contain a very large number of cracks and it can be reasonably assumed that they provide good representations (in the statistical sense) of the block from which they were cored. Also, several samples of Barre granite were similarly prepared from a long cylindrical specimen cored in a non-oriented block. Special care was taken to produce parallel faces precisely perpendicular to the cylinder axis. The samples were carefully cleaned from cutting-oil, and saturated with distilled water by immersion under vacuum. With this technique, the amount of air trapped inside the pores was very small, and, total saturation was certainly achieved after a pore pressure of 30MPa was applied to the samples.

Permeability measurements

Since the permeability of granites is of the order of $10^{-18}m^2$ (or 1μd) or less, only the pulse decay technique is applicable. Very briefly, this method

can be sketched as follows: the sample is the only communication between two reservoirs containing the pore fluid (here, distilled water) under pressure. The fluid pressure is suddenly changed in one of the reservoirs (a pore pressure pulse is generated). Thereafter the system is let free to return to equilibrium. Under certain conditions the differential pressure decay is exponential and the permeability is inversely proportional to the decay time τ.

$$k = \{\mu L\ C_s\ C_s'\}/\{A\tau\ (C_s+C_s')\} \qquad (4)$$

where L is the length of the sample, A the cross-sectional area, μ the viscosity of the pore fluid, and, C_s and C_s' the compressive storages of the two reservoirs (the compressive storage is the ratio of a given fluid volume variation to the change in fluid pressure which accompanies it). These last two parameters, which must be experimentally determined, are responsible for a good part of the uncertainty on the absolute values of k. More details on this technique as well as a description of the measurement system we used can be found in [23]. It was pointed out at that time that the noise in the data is mostly due to the variations of ambient temperature. Therefore, the whole system was enclosed inside an isothermal oven, the temperature of which was permanently recorded during the experiments. With this improved temperature control ($\pm 0.1^{o}C$ for intervals of time of 1 hour) the estimated uncertainty on the absolute value of the permeability was of the order of 20%, even for permeabilities as low as $10^{-21}m^2$ (or 1nd). In order to test the repeatability, the measurements were made twice using pulses of opposite sign. For practically all the pairs of measurements, the results differed by 8% or less, which gave an evaluation of the uncertainty on the relative values of permeability. When large discrepancies occurred, the system was probably not completely at

equilibrium at the beginning of the measurements. The uncertainty introduced by these data points of dubious quality was limited by assigning them a smaller weight in the calculations.

Experimental procedure

The procedures followed here are schematized in Figure 1. In order to study the confining pressure effect, P_c was raised (loading) and lowered (unloading) with an increment of 10MPa. We investigated a range of confining pressure (40-180MPa) large compared to the range of pore pressure permitted by our equipment (up to 30MPa). Testing the stress history dependency necessitated that different experiments were run with the pore pressure cycled under different procedures. In procedure #1 the cycles on pore pressure were: 10MPa, 20MPa, 30MPa, and 10MPa; they were 30MPa, 20MPa, 10MPa, and 30MPa in procedure #2. Previous experiments suggested that hysteresis was negligible for the pore pressure cycles because of their small amplitude. Therefore, we could save time by measuring permeability only during the first half of a P_p cycle. The three samples of Chelmsford granite and a sample of Barre granite were tested following procedure #1. Procedure #2 was used only with a second sample of Barre granite. Since we did not test the effect of stress history or hysteresis on Chelmsford granite, the measurements were made only during loading.

Computation of α

The equation (1) can be graphically represented by a family of curves $k(P_c, P_p)$=constant. When equation (3) is satisfied, these curves simply are parallel straight lines with a slope α. When equation (3) is not valid, we can consider a range of pressure small enough so the curves of constant k can be

approximated by parallel straight lines with an equation P_c-αP_p=constant (different of P_{eff}). Hence, we can determine α "locally" by applying ordinary techniques on small intervals of pressure. Two different methods were used here, one inspired from Walls and Nur [15], and the other from Walsh [17].

Method #1:

The differential of k can be written

$$dk = (\partial k/\partial P_c)\, dP_c + (\partial k/\partial P_p)\, dP_p \qquad (5)$$

In the close vicinity of the point $M(P_c, P_p)$ the curves of constant k are approximated by parallel straight lines (P_c-αP_p=constant). By definition, dk is equal to zero when traveling on one of these lines. Hence, the following two differential equations must be simultaneously satisfied:

$$dP_c - \alpha\, dP_p = 0 \qquad (6)$$

and

$$(\partial k/\partial P_c)\, dP_c + (\partial k/\partial P_p)\, dP_p = 0 \qquad (7)$$

From (6) and (7) we deduce

$$\alpha = -(\partial k/\partial P_c)/(\partial k/\partial P_p) \qquad (8)$$

In order to evaluate these two partial derivatives we can perform the following experiments successively. In the first one we measure δK_c the variation in permeability corresponding to changing the confining pressure and the pore pressure as follows: $dP_c=\delta P$ and $dP_p=0$ (δP can be either positive or negative corresponding to loading and unloading). Using (5) we find

$$\delta k_c = (dk/dP_c)\, \delta P \qquad (9)$$

In the second experiment we measure δk_p corresponding to $dP_c=0$ and $dP_p=\delta P$. δk_p can be written

$$\delta k_p = (dk/dP_p)\, \delta P \qquad (10)$$

Combining (8), (9), and (10) we find

$$\alpha = - (\delta k_p / \delta k_c) \qquad (11)$$

The order in which the two experiments are made has no effect on α except in the case of stress history dependency (or path dependency).

Since α is defined as a ratio, σ_α the uncertainty on α only depends on σ_k the uncertainty on the relative values of permeability (5-10%). σ_α becomes large when σ_k is comparable to the δk's. As we will see latter the δk's decrease with increasing P_c, which makes the method less accurate in the high confining pressure range.

Method #2:

Alternatively, we can use a technique similar to the cross-plotting method described by Walsh [17]. First, k is plotted as a function of confining pressure at fixed values of pore pressure (here, 10MPa, 20MPa, and 30MPa). Then, these data are cross-plotted yielding P_c as a function of P_p for constant values of permeability. This method allows us to directly determine the curves of constant k. If the range of pressure considered is small enough, these curves are well approximated by parallel straight lines, α the slope of which is simply given by a linear regression.

In the cross-plotting process we need to interpolate the values of k between the data points. We naturally used the simple linear interpolation. Furthermore, since Walsh and Brace [24] showed that k elevated to a certain power n (with $0 \leq n \leq 1/3$) should be proportional to the logarithm of P_c, we also used the following expression

$$k = (A \log(P_c) + B)^{1/n} \qquad (12)$$

where A and B are fitting parameters depending on P_p, and n is chosen to

produce the least variance (the contributions of the different values of pore pressure were added to ensure that n is independent of P_p). Because we use curves fitting the data over the whole range of pressure, the α's determined in this way bear more global information than the ones obtained from linear interpolation between only two data points. Of course, this type of interpolation can be adapted to method #1 as well.

As before, this method is less accurate in the high confining pressure range because k tends to vary more slowly as P_c increases. In this case, a small error in k produces a large error in P_c when interpolating.

OBSERVATIONS

Chelmsford granite

The results of permeability measurements for R-, G-, and H-samples are listed in Table 1. In the case of H-sample the experiment was stopped at P_c=90MPa because of a leak at the jacket isolating the sample from the confining fluid. The permeabilities of the three samples do not differ by more than 20% (Figure 2). Our results are in good agreement with the measurements previously made by Coyner et al. [22]. During loading, permeability decreased by about an order of magnitude at a rate which constantly diminished with increasing P_c (the curves k vs P_c tend to become horizontal at high P_c). A similar effect can be noted with pore pressure (the three curves in Figure 3 tend to get closer with increasing confining pressure). Finally, the exponent n was found to be noticeably less than 1/3 (0.009, 0.18, and 0.095 for G-, H-, and R-samples respectively), but it was also rather poorly constrained by the

data.

The values of α calculated are plotted versus P_c in Figure 4. The uncertainty on α was estimated around 15% at low P_c and 35% at high P_c. The results are quite comparable for the three samples (about 0.65). A slight diminution of α with increasing confining pressure (0.68 at 60MPa and 0.57 at 160MPa) can be noted. A similar effect was observed by Todd and Simmons [11], α decreasing with increasing confining pressure and increasing with increasing pore pressure.

Barre granite

The values of permeability for the two samples of Barre granite are presented in Table 2. The general features described above are also present here. The permeability of the two samples differ by about 15%. Our values are about a tenth of those measured by Kranz et al. [21]. The shape of the curves k vs P_c are very similar to those for Chelmsford granite. In addition, we can notice a strong hysteresis effect and a permanent change in permeability after a cycle is completed (Figures 5 and 6; loading and unloading cycles are respectively represented by solid and open symbols). This behavior is observed with both procedures. As before, the exponent n was found much smaller than 1/3 (0.009 and 0.001 for loading and unloading with procedure #1, and 0.001 with procedure #2).

The α's calculated are plotted on Figures 7 and 8. The values obtained are very different for loading and unloading, and it can also be remarked that the two cycling procedures give quite dissimilar results (procedure #1: 0.55 for loading, and 1.1 for unloading; procedure #2: 1.0 for loading, and 0.85 for unloading without taking into account few aberrant points). In the first case,

α showed a strong tendency to decrease with increasing confining pressure (0.65 at 60MPa and 0.43 at 140MPa). There is no obvious trend in the other cases. The uncertainty in α was estimated to range between 15 and 30% at low P_c, and between 20 and 100% at high P_c (the largest uncertainties were always obtained for unloading).

DISCUSSION

Anisotropy effect

Peng and Johnson [19] found that the crack density of Chelmsford granite in thin sections parallel to the rift plane was about half that in other planes. If only the cracks parallel to the macroscopic flow direction contributed to the flow, the permeability of the R-sample should be twice as small as the permeability of the G- and H-samples. In fact, differences of only 20% were observed, which can be better explained by a slight disparity of the samples. Similarly, there is no anisotropy effect appearing in the values of α (the mean values are 0.66 for G-sample, 0.69 for H-sample, and 0.61 for R-sample). We can conclude that the same cracks participate to the flow almost independently of its direction. The two-dimensional examples of Figure 9 illustrate this point. In a) the permeability along Y would be lower than along X for cracks of same aperture. In b) and c) the total length of crack along X and Y are the same than in a), but the directional effect is reduced. In b) the cracks in excess in the X direction are disconnected. Zoback and Byerlee [25] observed an example of this type of situation. They measured the permeability of rocks under uniaxial load. They found that the axial cracks

due to dilatancy were poorly connected to the rest of the crack network (the permeability remained almost unchanged during the experiments). In c) the offset of the cracks in the X direction tends to reduce the difference between the permeabilities measured in both directions. Although difficult to sketch in two dimensions, it is not difficult to imagine that this situation is more easily achieved in a three-dimensional network of cracks. Our results agree with Madden's proposition that transport properties of a crack network are not very sensitive to the topology of the network [26]. The situation could be quite different in rocks with a strong layering of materials with different permeabilities [27].

Effect of confining pressure

The non-linear behavior of crystalline rocks at pressures up to 200MPa has been almost universally attributed to the closure of cracks. The rock stiffness increases with P_c and reaches a limit which is interpreted as the stiffness of the rock in absence of cracks. However, measurements of transport properties ([28], [29], or this study) show that, at least, some cracks do not completely close in this range of pressure, but simply become more resistant to pressure.

Simple models of elliptic cracks ([23] and [30]) show that cracks are less compliant when their aspect ratio approaches 1.0. After Witherspoon et al. [31], an "effective" crack length can be defined as the mean distance separating the points where the crack walls come into contact. With the number of contacts increasing, a single crack could be progressively transformed into an array of coplanar, interconnected cracks with higher aspect ratios (Figure 10). These smaller cracks are more resistant to pressure than the initial one. A simple

two-dimensional model (see Appendix) shows that α is of the order of 1.0 for very low aspect ratio cracks and noticeably smaller for circular tubes (aspect ratio of 1.0). Therefore, an increase in mean crack aspect ratio due to the rugosity of the crack walls may explain the decrease of α with increasing confining pressure observed in some cases.

The low values taken by the exponent n also support this interpretation. Walsh [17] derived the following expression

$$k = (1 - A \log P_c)^3 (B - B'P_c)/(B + B'P_c) \qquad (13)$$

where A, B, and B' are constants depending on the geometry of the crack and the elastic moduli of the rock constituents. The first term of this expression is interpreted as the "aperture" term, and the other one as the "tortuosity" term. We can see that n is equal to 1/3 only if the tortuosity term is equal to unity (B'=0). Therefore, our observations indicate a strong "tortuosity" effect ($|B'|$ large), which is consistent with our model. Indeed, each asperity coming into contact changes the tortuosity of the flow path by forming an obstacle around which the pore fluid has to flow.

It could be argued that the crack network may be formed of cracks with different aspect ratios. The low aspect ratio cracks would close first with increasing confining pressure, leaving only the pressure resistant, high aspect ratio pores open. But, microscope observations show an overwhelming predominance of the low aspect ratio cracks over high aspect ratio pores in crystalline rocks. Also, this model cannot properly explain the persistence of transport properties of rocks under pressure (it is difficult to imagine that so few high aspect ratio pores randomly distributed would form a fully connected network).

Hysteresis and stress history effect

There are many examples of observations of hysteresis on rocks in the literature. Most of them are related to the dilatancy of rocks under uniaxial or triaxial loading [32]. Under these conditions large shear stresses can develop in the rock and friction seems the best candidate to explain the hysteresis observed. Walsh [33] reported an experiment made by Brace during an uniaxial test, which clearly demonstrates the role of friction. "At stages in the unloading cycle, a sample was strongly vibrated while still loaded. This caused the strain in the sample to fall at constant stress to nearly the same value as obtained in the loading cycle. Apparently the additional energy of the vibration was sufficient to overcome friction at crack surfaces. The usual hysteresis loop could be almost eliminated by this procedure." During loading, frictional sliding might have occurred at favorable configurations of cracks and grains. During unloading, some of these sites remained blocked in an intermediate position, introducing residual shear stresses. The vibration unblocked most of these places, probably by temporarily releasing the normal stress across the sliding surfaces, therefore allowing the residual stresses to relax.

However, models based on sliding cracks are still controversial (see [34] and [35]). The main reason is that the configurations of cracks proposed by Brace et al. [32] where sliding should take place, were very rarely observed [36]. But, sliding could easily occur in other configurations (Figure 11) like en echelon cracks (observed by Kranz [37]) or oblique contacts (discussed by Scholz and Hickman [20]). Electron microscope observations showed examples with strong evidences of past shear motion ([38] and [39]). Finally, the reversible

Griffith crack proposed as an alternative model by Holcomb and Stevens [40] is not very attractive because it requires a perfect matching of the crack walls, which is not consistent with the persistence of the transport properties of rocks at high pressure.

Hysteresis and stress history effects can also be observed under hydrostatic pressure ([21], [22], or this study). This indicates that the stress is inhomogeneously distributed in the rock and that shear stresses can develop locally at places where cracks and grains interact. Therefore, the model proposed above can also be applied here. Because of friction, a portion of the pores and cracks do not reopen fully during unloading, causing the permanent change in permeability observed at the end of a confining pressure cycle. Moreover, this model can explain why α was found so strongly path dependent. The cycling procedures we used can be described as series of "mixed cycles". We know that P_c and P_p have roughly opposite effects on permeability. Therefore, we can create a loop on permeability by successively changing P_c and P_p by δP ($\delta P>0$ or <0). Such a loop is similar to the loops obtained by cycling confining pressure or pore pressure alone with an amplitude δP. There are four possible mixed cycles: increasing P_c first and P_p second, increasing P_p first and P_c second, decreasing P_c first and P_p second, and finally decreasing P_p first and P_c second. Our model predicts that the lack of sliding should make P_p (or P_c) less efficient whenever it is applied in the second place. In other words, α, which compares the efficiency of P_c and P_p, should take lower values when P_p is changed after P_c, and higher values in the other case. This is indeed what we observed. P_c was shifted before P_p in procedure #1 during loading and in procedure #2 during unloading with the

corresponding α's significantly lower than 1.0. Accordingly, α took values near 1.0 in the other cases.

APPENDIX

The simple two-dimensional model of a "tunnel" crack with an elliptical cross-section in an infinite body (see [22]) can help us estimate the influence of crack aspect ratio on α. In this model the crack aspect ratio ε is defined as the ratio of the cross-sectional minor axis b to the major axis a. This model is adequate in the case of a dilute solution of cracksin the rock. We will first treat the case of plane strain. The partial derivatives of a and b with respect to the two-dimensional confining pressure P_c' and the pore pressure P_p are written

$$\partial a/\partial P_c' = -\, b(1-\nu)/G; \quad \partial a/\partial P_p = -\, \partial a/\partial P_c' - a(1-2\nu)/2G \qquad (A1)$$

and

$$\partial b/\partial P_c' = -\, a(1-\nu)/G; \quad \partial b/\partial P_p = -\, \partial b/\partial P_c' - b(1-2\nu)/2G \qquad (A2)$$

where G is the shear modulus and ν the Poisson's ratio. The differential of the crack permeability can be expressed in function of a, b, da, and db as follows (see [22])

$$dk = ab(b^3\, da + a^3\, db)/2(a^2 + b^2)^2 \qquad (A3)$$

We can evaluate α from (A1), (A2), and (A3) by using the first method described in this paper. The change in permeability δk_c corresponds to $dP_c'=\delta P$ and $dP_p=0$. It is given by

$$\delta k_c = -\, \delta P(1-\nu)a^2\varepsilon(\varepsilon^4+1)/2G(1+\varepsilon^2)^2 \qquad (A4)$$

δk_p corresponding to $dP_c'=0$ and $dP_p=\delta P$ is written

$$\delta k_p = \delta k_c - \delta P(1-2\nu)a^2\varepsilon^2/4G(1+\varepsilon^2) \quad (A5)$$

Since α is given by $-\delta k_p/\delta k_c$ we obtain

$$\alpha = 1 - [(\varepsilon/2)(1+\varepsilon^2)(1-2\nu)/(1-\nu)(1+\varepsilon^4)] \quad (A6)$$

Therefore α is equal to 1.0 in the case of a flat crack (ε=0), and to $1/2(1-\nu)$ in the case of a circular tube (ε=1). We can obtain α for plane stress in a similar manner. We just replace $(1-\nu)$ by $(1+\nu)^{-1}$ and $(1+\nu)$ by $(1-\nu)$ in the equations (A1) and (A2).

$$\alpha = 1 - [\varepsilon(1+\varepsilon^2)(1-\nu)/2(1+\varepsilon^4)] \quad (A7)$$

α is still equal to 1.0 for a flat crack, but now takes the new value $(1+\nu)/2$ for a circular tube.

Walsh (personnal communication) solved the three-dimensional problem of the infinite "tunnel" crack submitted to confining pressure and pore pressure. He found α=1.0 as usual in the case of a flat crack and $\alpha=2(1+\nu)/(5-4\nu)$ in the case of a circular tube. Walsh's values are a little different than ours because he treated a true three-dimensional problem, but he was not able to solve it for any value of the aspect ratio. We can see that all the values are close in a reasonable range of Poisson's ratios (α around 0.6).

REFERENCES

[1] Robinson, L.H., The effect of pore and confining pressure on the failure process in sedimentary rocks, in Proc. 3rd Symp. Rock Mech., Quart. Colo. School Min., 54, 177-199, 1959.

[2] Heard, H.C., Transition from brittle fracture to ductile flow in Solenhofen limestone as a function of temperature, confining pressure, and interstitial fluid pressure, in Rock Deformation, Griggs, D., and J. Handin (eds), Geol. Soc. Am., Memoir 79, 193-226, 1960.

[3] Handin, J., R.V. Hayer, M. Friedman, and J.N. Feather, Experimental deformation of sedimentary rocks under confining pressure; pore pressure effects, Bull. Am. Assoc. Petrol. Geol., 47, 717-755, 1963.

[4] Murrell, S.A.F., A criterion for brittle fracture of rocks and concrete under triaxial stress, and the effect of pore pressure on the criterion, in Rock Mechanics, Fairhurst, C. (ed), Proc. 5th Symp. Rock Mech., Pergamon Press, New York, 563-577, 1963.

[5] Brace, W.F., and R.J. Martin, A test of the law of effective stress for crystalline rocks of low porosity, Int. J. Rock Mech. Min. Sci., 5, 415-426, 1968.

[6] Byerlee, J.D., The fracture strength and frictional strength of Weber sandstone, Int. J. Rock Mech. Min. Sci. Geomech. Abstr., 12, 1-4, 1975.

[7] Gowd, T.N., and Rummel, Effect of fluid injection on the fracture behaviour of porous rock, Int. J. Rock Mech. Min. Sci. Geomech. Abstr., 14, 203-208, 1977.

[8] Skempton, A.W., Effective stress in soils, concrete and rocks, in Conf.

on Pore Pressure and Suction in Soils, Butterworth, London, 4-16, 1960.

[9] Banthia, B.S., M.S. King, and J. Fatt, Ultrasonic shear wave velocities in rocks subjected to simulated overburden pressure and internal pore pressure, Geophysics, 30(1), 117-121, 1965.

[10] Nur, A., and J.D. Byerlee, An exact effective stress law for elastic deformation of rock with fluids, J. Geophys. Res., 76(26), 6414-6419, 1971.

[11] Todd, T., and G. Simmons, Effect of pore pressure on the velocity of compressional waves in low-porosity rocks, J. Geophys. Res., 77(2), 3731-3743, 1972.

[12] Robin, P-Y.F., Note on effective pressure, J. Geophys. Res., 78(14), 2434-2437, 1973.

[13] Garg, S.K., and A. Nur, Effective stress laws for fluid-saturated rocks, J. Geophys. Res., 78(26), 5911-5921, 1973.

[14] Zoback, M.D., and J.D. Byerlee, Permeability and effective stress, Amer. Assoc. Petrol. Geolog. Bull., 59(1), 154-158, 1975.

[15] Walls, J., and A. Nur, Pore pressure and confining pressure dependence of permeability in sandstone, in 7th Formation Evaluation Symposium Proceedings, Canadian Well Logging Society, Calgary, pp.1, 1979.

[16] Carroll, M.M., An effective stress law for anisotropic elastic deformation, J. Geophys. Res., 84, 7510-7512, 1979.

[17] Walsh, J.B., Effect of pore pressure and confining pressure on fracture permeability, Int. J. Rock Mech. Min. Sci. Geomech. Abstr., 18, 429-435, 1981.

[18] Dullien, F.A.L., Porous Media: Fluid Transport and Pore Structure, Academic Press, New York, pp.396, 1979.

[19] Peng, S.S., and A.M. Johnson, Crack growth and faulting in cylindrical

specimens of Chelmsford granite, Int. J. Rock Mech. Min. Sci., 9, 37-86, 1972.

[20] Scholz, C.H., and S.H. Hickman, Hysteresis in the closure of a nominally flat crack, J. Geophys. Res., 88, 6501-6504, 1983.

[21] Kranz, R.L., A.D. Frankel, T. Engelder, and C.H. Scholz, The permeability of whole and jointed Barre granite, Int. J. Rock Mech. Min. Sci. Geomech. Abstr., 16, 225-234, 1979.

[22] Coyner, K.B., W.F. Brace, and J.B. Walsh, New laboratory measurements of permeability and electrical resistivity of crystalline rocks (abstr.), Trans. Am. Geophys. Union, 60, 943, 1979.

[23] Bernabe, Y., W.F. Brace, and B. Evans, Permeability, porosity, and pore geometry of hot-pressed calcite, Mech. of Materials, 1, 173-183, 1982.

[24] Walsh, J.B., and W.F. Brace, The effect of pressure on porosity and the transport properties of rocks, J. Geophys. Res., 89, 9425-9431, 1984.

[25] Zoback, M.D., and J.D. Byerlee, The effect of microcrack dilatancy on the permeability of Westerly granite, J. Geophys. Res., 80(5), 752-755, 1975.

[26] Madden, T.R., Random networks and mixing laws, Geophysics, 41, 1104-1125, 1976.

[27] Simmons, G., R. Wilkens, L. Caruso, T. Wissler, and F. Miller, Physical Properties and Microstructures of a set of sandstones, Ann. Rept. to the Schlumberger-Doll Research Center, 1982.

[28] Brace, W.F., A.S. Orange, and T.R. Madden, The effect of pressure on the electrical resistivity of water-saturated crystalline rocks, J. Geophys. Res., 70, 5669-5678, 1965.

[29] Brace, W.F., J.B. Walsh, and W.T. Frango, Permeability of granite under high pressure, J. Geophys. Res., 73, 2225-2236, 1968.

[30] Walsh, J.B., The effect of cracks on the compressibility of rock, J. Geophys. Res., 70(2), 381-389, 1965.

[31] Witherspoon, P.A., Y.W. Tsang, J.C.S. Long, and J. Nooriphad, New approaches to problems of fluid flow in fractured rock masses, in Proceedings to the 22nd U.S. Symposium on Rock Mechanics, MIT, Cambridge, pp.1, 1982.

[32] Brace, W.F., B.W. Paulding, and C.H. Scholz, Dilatancy in the fracture of crystalline rocks, J. Geophys. Res., 71, 3939-3953, 1966.

[33] Walsh, J.B., The effect of cracks on the uniaxial elastic compression of rocks, J. Geophys. Res., 70(2), 399-411, 1965.

[34] Stevens, J.L., and D.J. Holcomb, A theoretical investigation of the sliding crack model of dilatancy, J. Geophys. Res., 85(12), 7091-7100, 1980.

[35] Moss, W.C., and Y.H. Gupta, A constitutive model describing dilatancy and cracking in brittle rocks, J. Geophys. Res., 87, 2985-2998, 1982.

[36] Tapponnier, P., and W.F. Brace, Development of stress-induced microcracks in Westerly granite, Int. J. Rock Mech. Min. Sci. Geomech. Abstr., 13, 103-112, 1976.

[37] Kranz, R.L., Crack-crack and crack-pore interactions in stressed granite, Int. J. Rock Mech. Min. Sci. Geomech. Abstr., 16, 37-47, 1979.

[38] Batzle, M.L., G. Simmons, and R.W. Siegfried, Microcrack closure in rocks under stress: direct observation, J. Geophys. Res., 85(12), 7072-7090, 1980.

[39] Kranz, R.L., Crack growth and development during creep of Barre granite, Int. J. Rock Mech. Min. Sci. Geomech. Abstr., 16, 23-35, 1979.

[40] Holcomb, D.J., and J.L. Stevens, The reversible Griffith crack: a viable model for dilatancy, J. Geophys. Res., 85(12), 7101-7107, 1980.

	G-sample			H-sample			R-sample		
	10MPa	20MPa	30MPa	10MPa	20MPa	30MPa	10MPa	20MPa	30MPa
P_c (MPa)									
40	590.	786.	1340.	728.	950.		931.	1230.	1970.
	629.	802.	1400.	659.	901.		891.	1220.	1940.
50	447.	540.	744.	560.	693	950.	717.	869.	1160.
	455.	561.	746.	540.	664.	919.	724.	855.	1240.
60	325.	405.	495.	434.	512.	617.	527.	622.	758.
	338.	395.	498.	372.	472.	619.	523.	617.	789.
70	257.	294.	376.	334.	385.	460.	421.	482.	569.
	258.	304.	349.	306.	357.	449.	398.	471.	578.
80	204.	224.	294.	265.	299.	340.	335.	377.	427.
	204.	245.	276.	242.	278.	337.	319.	366.	433.
90	168.	185.	224.	207.	234.	274.	279.	305.	346.
	174.	193.	220.	193.	216.	261.	256.	295.	349.
100	137.	158.	187.				222.	245.	270.
	145.	159.	176.				210.	240.	274.
110	118.	126.	154.				184.	211.	230.
	123.	137.	145.				177.	204.	231.
120	94.0	109.	129.				150.	172.	185.
	100.	117.	120.				151.	163.	189.
130	88.1	95.4	125.				140.	151.	153.
	92.8	99.3	101.				130.	144.	161.
140	76.3	81.3	98.0				115.	123.	132.
	80.3	86.9	93.7				110.	119.	137.
150	71.1	77.1	81.9				101.	107.	116.
	74.6	75.0	82.4				101.	108.	119.
160	63.7	67.5	77.6				88.0	92.2	96.1
	66.2	66.9	72.9				88.6	92.4	103.
170	56.1	60.5	62.5				78.2	80.8	90.6
	56.5	61.7					67.8	81.2	88.9
180	49.9	54.0	67.4				71.8	71.3	80.7
	51.7	56.2	54.0				69.7	77.4	81.8

Table 1: Results of the permeability measurements for Chelmsford granite (G-, H-, and R-samples at P_p=10, 20, 30MPa). k is in $10^{-21}m^2$ or nd.

	procedure #1			procedure #2		
	10MPa	20MPa	30MPa	10MPa	20MPa	30MPa
P_c (MPa)						
40	39.4	48.7	96.1	47.5	74.2	121.
	40.3	52.7	98.5	48.9	75.4	118.
60	18.7	23.9	31.9	24.7	34.3	46.0
	20.2	23.9	32.9	25.6	35.1	46.3
80	11.5	15.1	16.0	14.8	18.5	24.7
	11.5	15.0	16.4	14.7	18.8	24.9
100	8.94	9.76	10.7	9.10	12.2	14.3
	8.81	9.65	9.97	10.3	12.2	14.4
120	6.15	6.96	7.60	6.82	7.89	9.57
	6.56	6.17	6.39	7.22	7.96	9.62
140	4.55	5.25	5.45	5.13	5.83	6.73
	4.93	5.08	5.43	5.27	5.88	6.84
160	3.50	3.75	4.19	4.39	4.85	5.41
	3.51	3.69	4.03	4.41	4.83	5.26
140	4.28	4.27	5.21	4.80	4.60	5.73
	4.38	4.29	4.25	4.78	4.98	5.75
120	4.37	5.18	6.24	5.34	6.50	7.37
	4.55	5.44	6.17	5.89	6.73	6.83
100	6.25	7.68	9.29	7.86	8.03	9.47
	5.88	7.56	9.02	7.75	8.32	9.76
80	8.19	8.97	10.8	9.52	11.4	13.6
				10.0	11.9	14.2
60	12.8	13.9	21.0	14.1	18.4	23.7
				15.1	20.0	25.3
40	22.4	33.8	72.7	29.1	46.6	80.7
	21.7	36.1	79.7	32.5	50.3	83.8

Table 2: Results of the permeability measurements for Barre granite (procedures #1 and #2, during loading and unloading, at P_p=10, 20, and 30MPa). k is in $10^{-21}m^2$ or nd.

FIGURE CAPTIONS

Figure 1: Diagram sketching the cycling procedures #1 and #2.

Figure 2: Permeability vs confining pressure for Chelmsford granite (R-, G-, and H-samples at P_p=20MPa). The best fit curves k^n=A$\log P_c$+B are indicated. The ±5% error bars represent the expected error on the relative values of permeability. These features will be also given in all the Figures showing the permeability data.

Figure 3: Permeability vs confining pressure for Chelmsford granite (R-sample at P_p=10, 20, and 30MPa; procedure #1, loading).

Figure 4: α vs confining pressure for Chelmsford granite (R-, G-, and H-samples). Since the results are very similar for the three samples, we used only one symbol for the whole collection of data. Estimated error bars are plotted for high and low P_c.

Figure 5: Permeability vs confining pressure for Barre granite (procedure #1; P_p=10 and 30MPa).

Figure 6: Permeability vs confining pressure for Barre granite (procedure #2; P_p=10 and 30MPa).

Figure 7: α vs confining pressure for Barre granite (procedure #1). The solid symbols correspond to loading and the open ones to unloading. Estimated error bars are plotted for high and low P_c.

Figure 8: α vs confining pressure for Barre granite (procedure #2). The solid symbols correspond to loading and the open ones to unloading. Estimated error bars are plotted for high and low P_c.

Figure 9: Examples of two-dimensional anisotropic distributions of cracks

with: a) a strong directional effect on permeability; b) no directional effect (the cracks in excess are not connected); c) a reduced effect (the cracks perpendicular to the macroscopic flow direction are essential for the network connectivity; they contribute to the flow independently of its direction).

Figure 10: Model of crack closure. The "effective" crack length diminishes and the "effective" aspect ratio increases during closure.

Figure 11: Examples of configurations where sliding can occur: a) sliding cracks [32]; b) en echelon crak [36]; c) oblique contact [20].

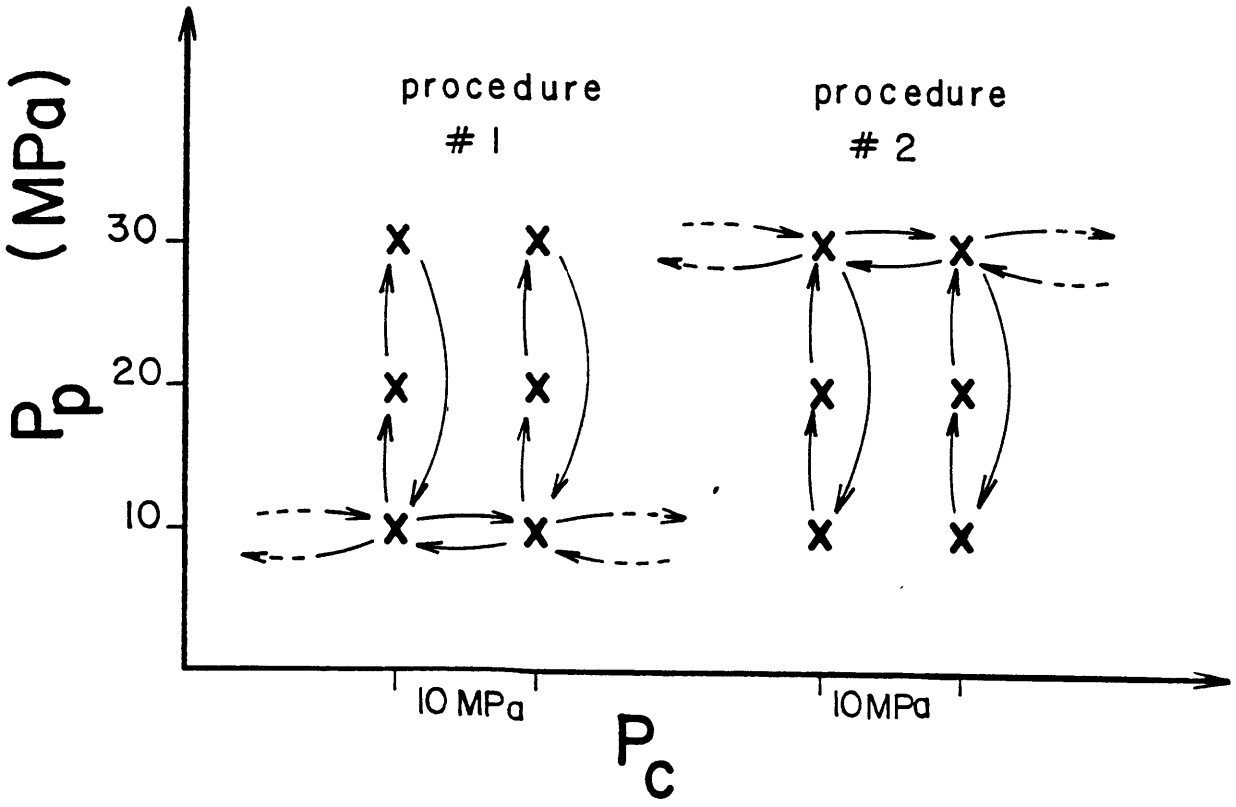

Figure 1:

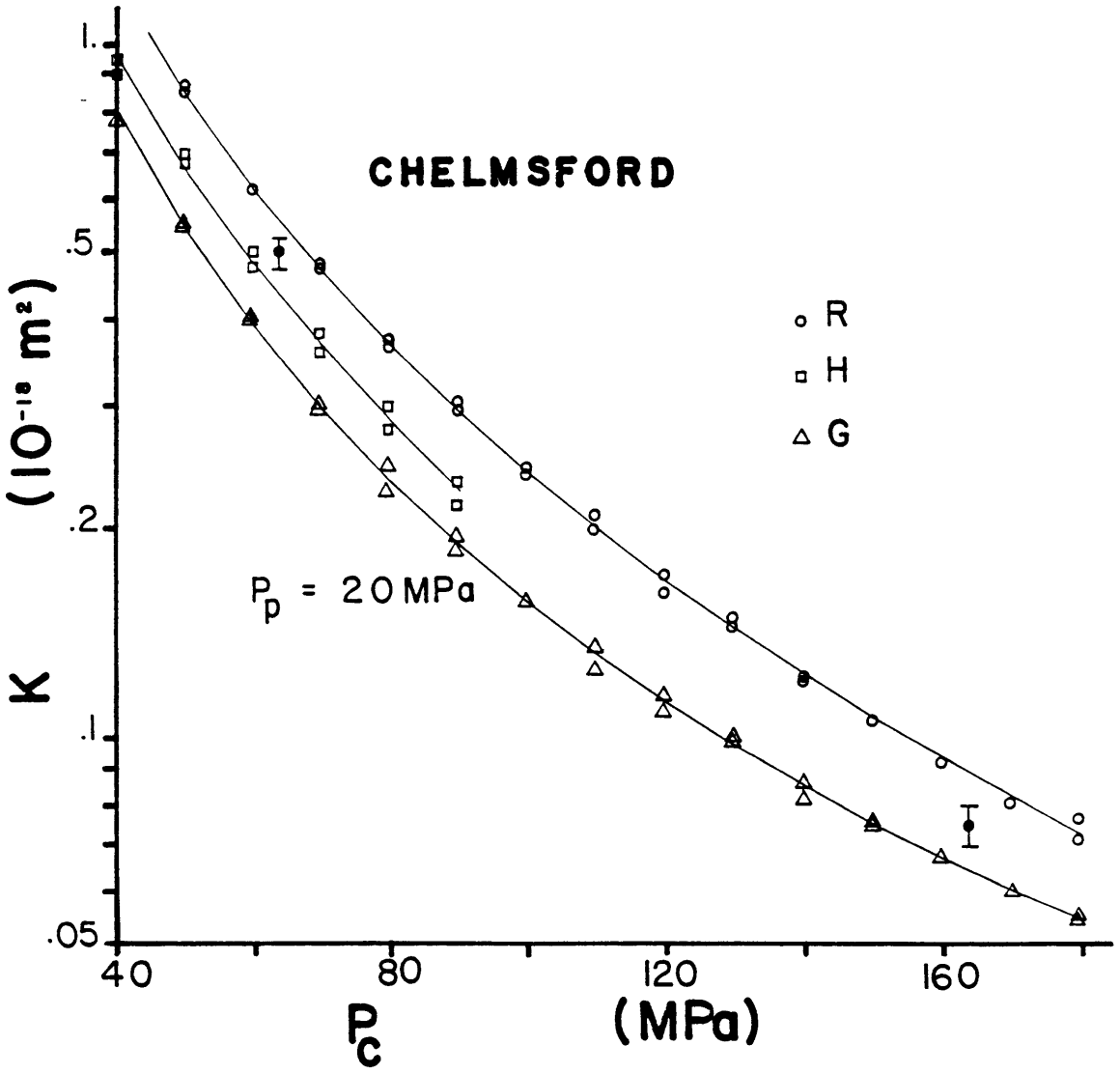

Figure 2:

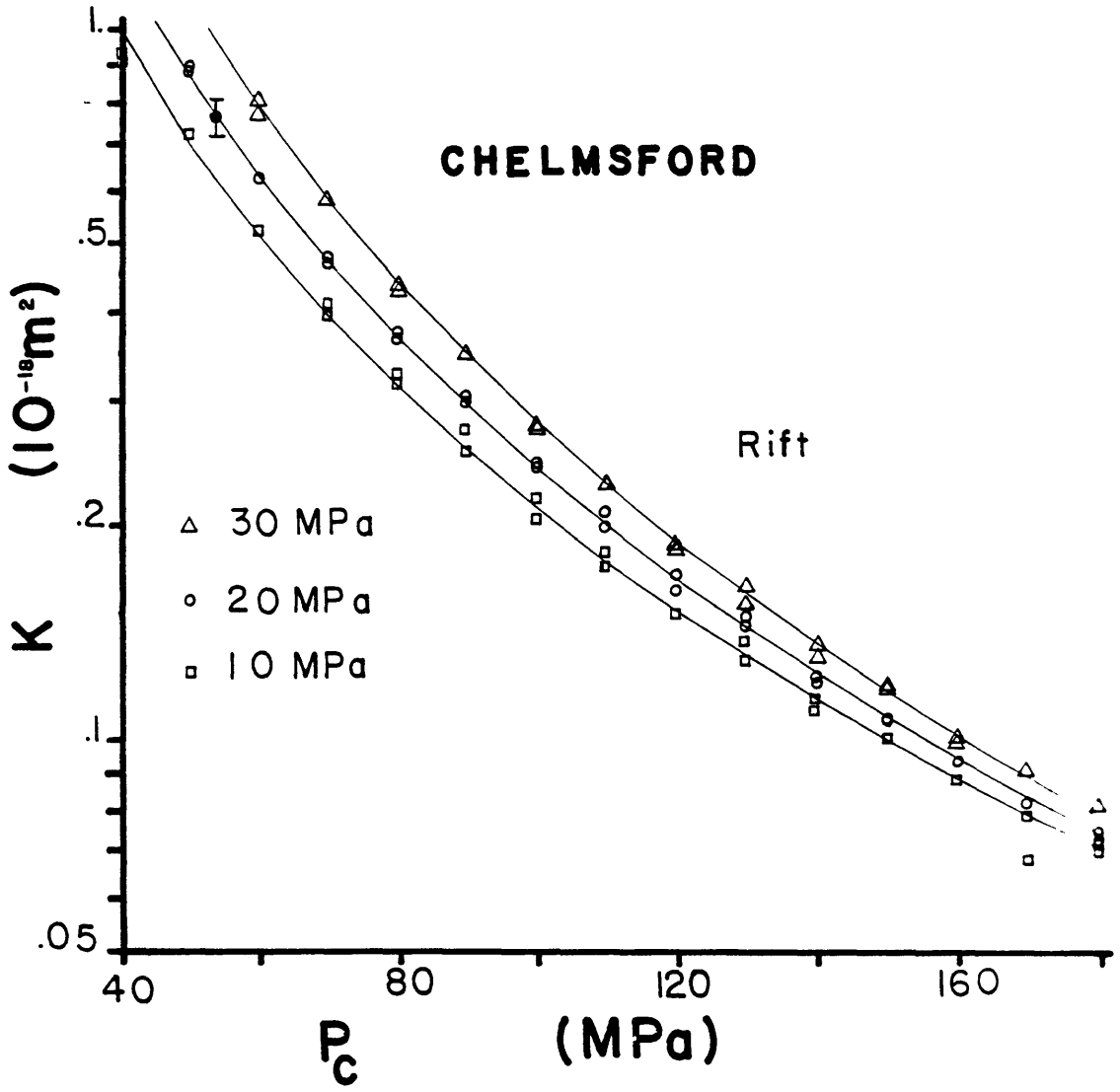
CHELMSFORD
Rift
30 MPa
20 MPa
10 MPa
K (10⁻¹⁸m²)
1.
.5
.2
.1
.05
40
80
120
160
Pc (MPa)

Figure 3:

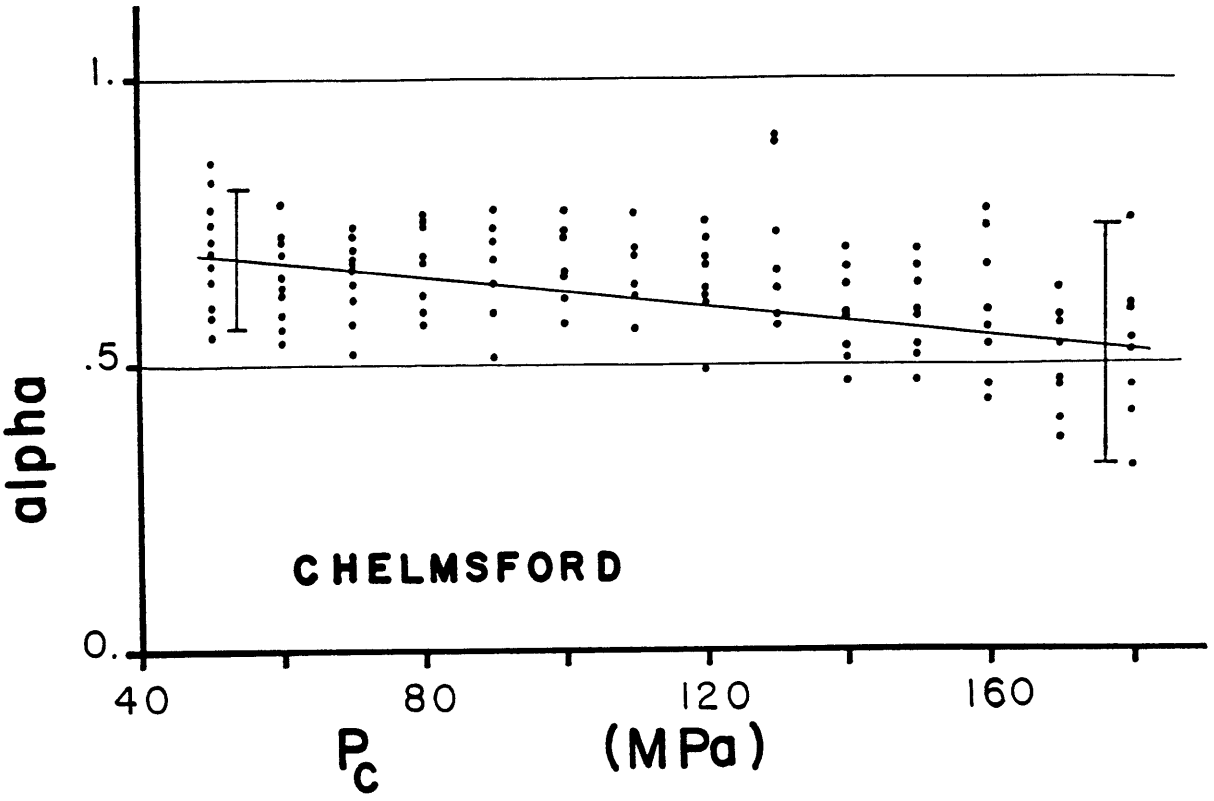

Figure 4:

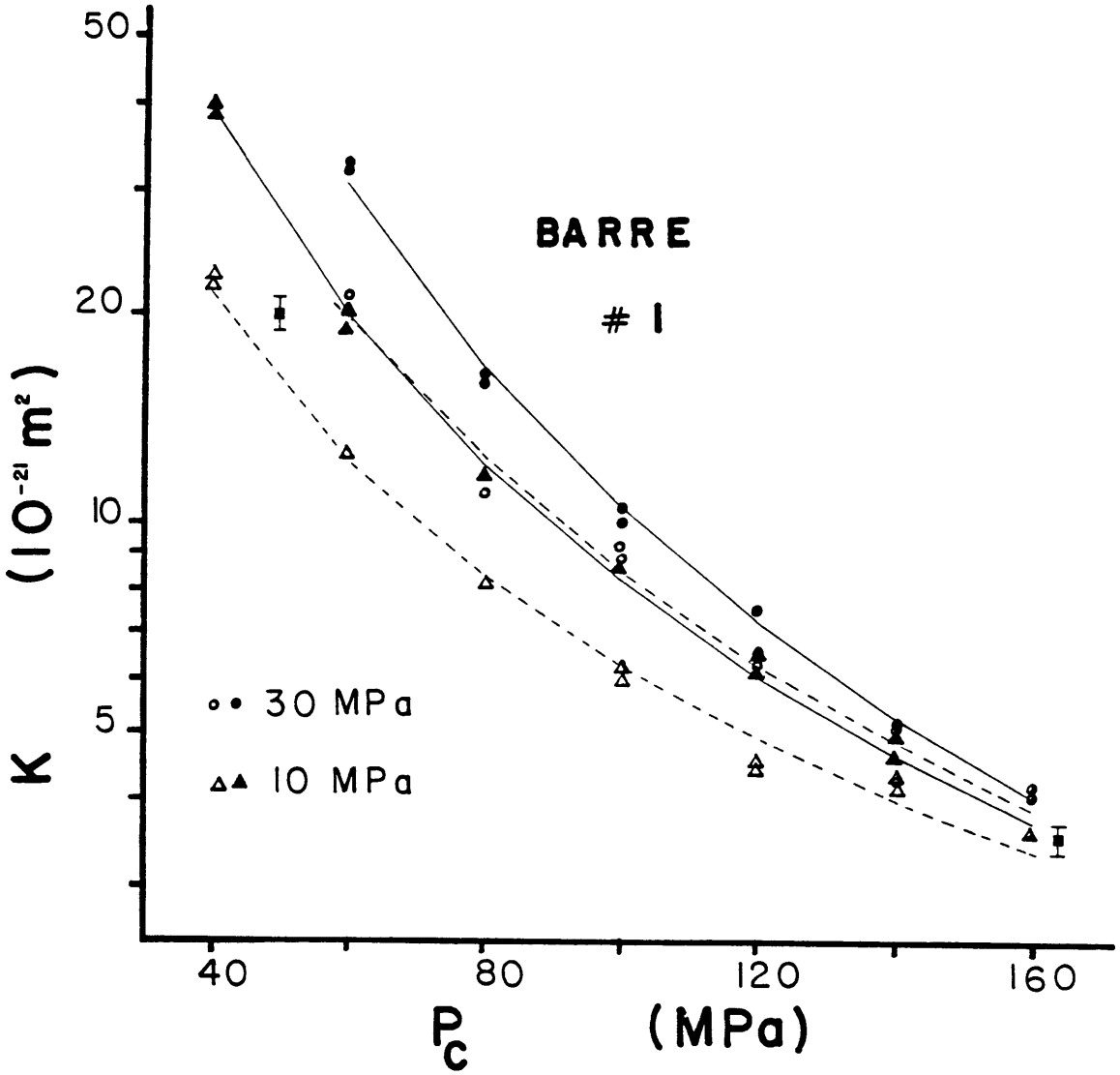

Figure 5:

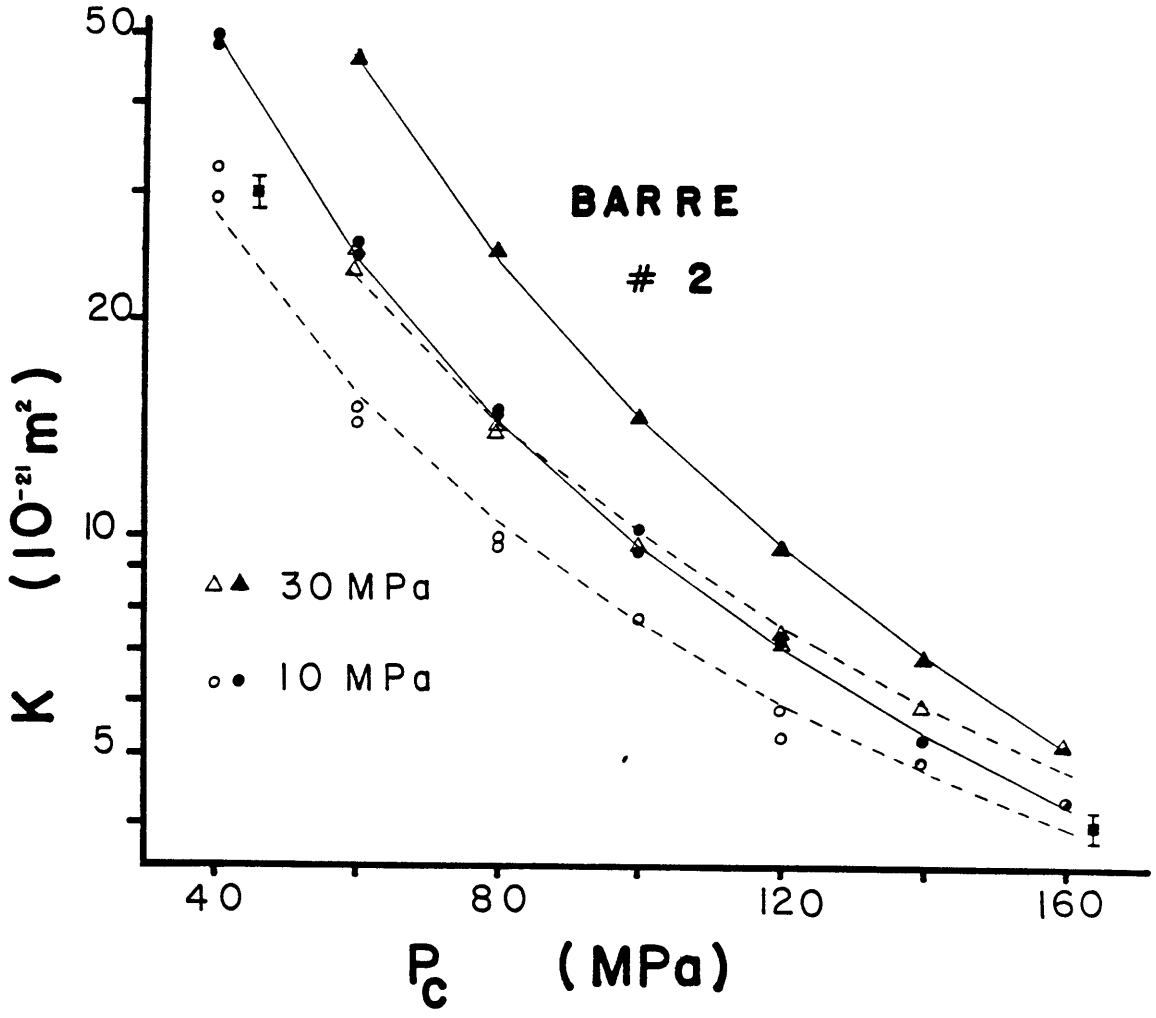

Figure 6:

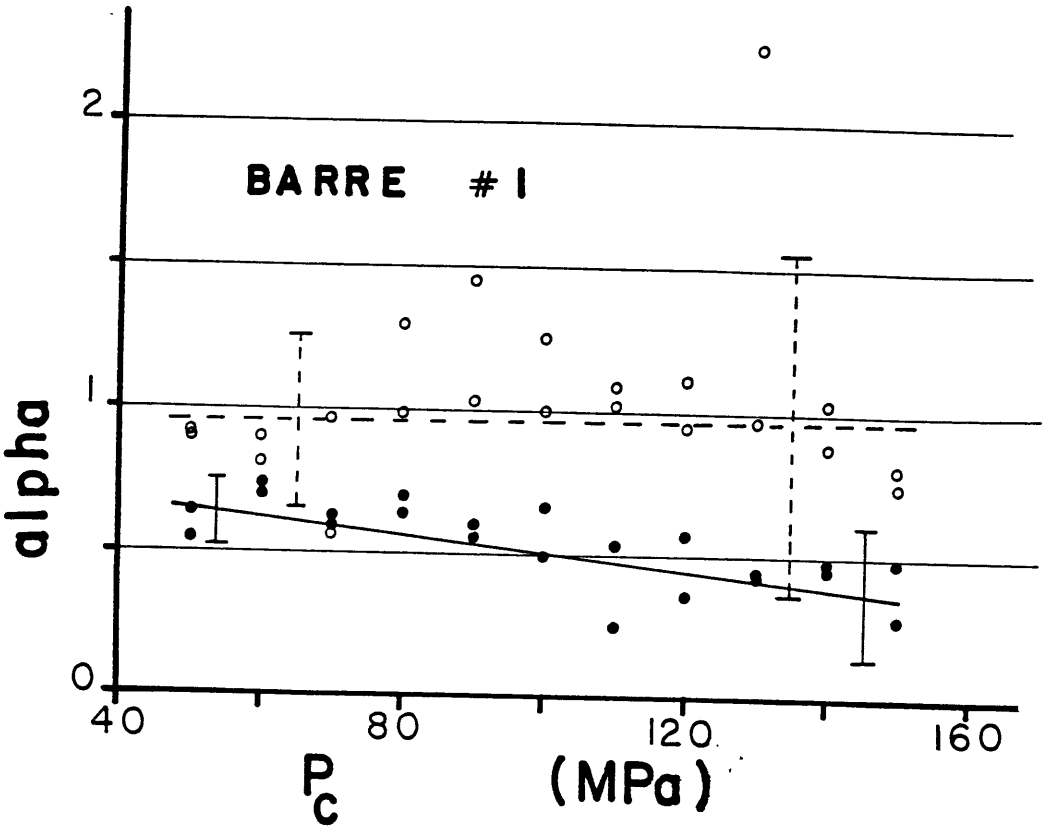

Figure 7:

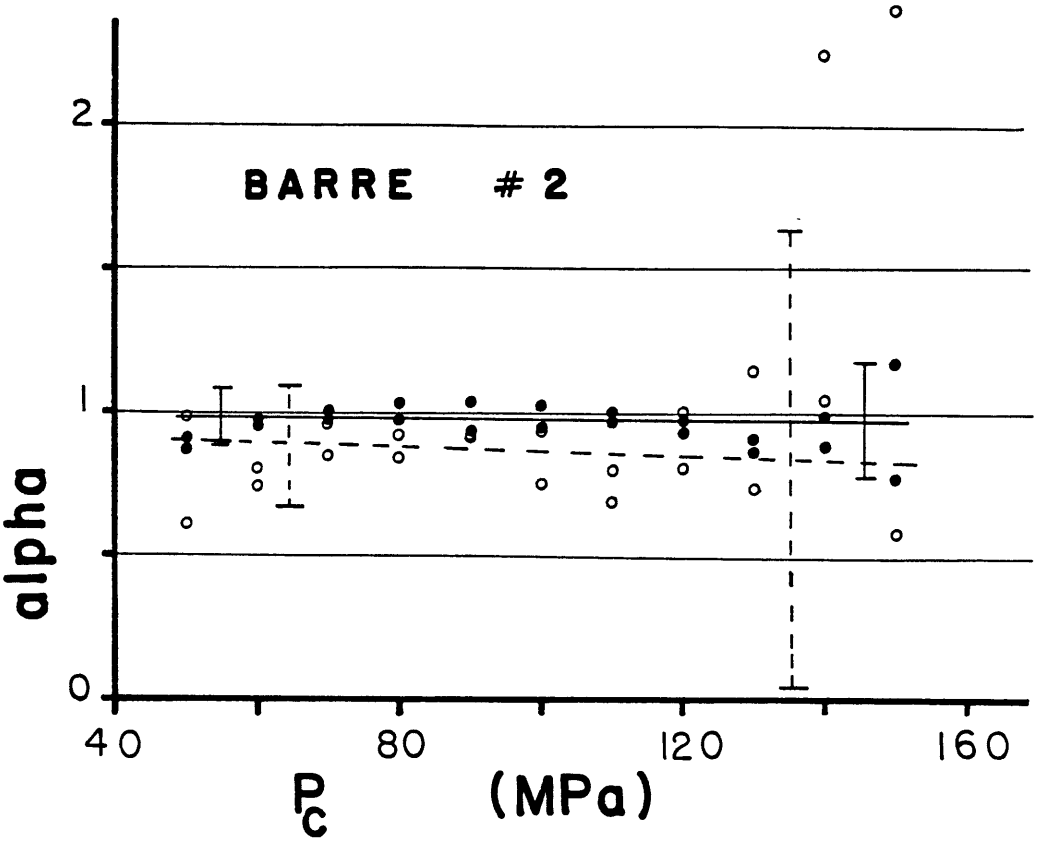

Figure 8:

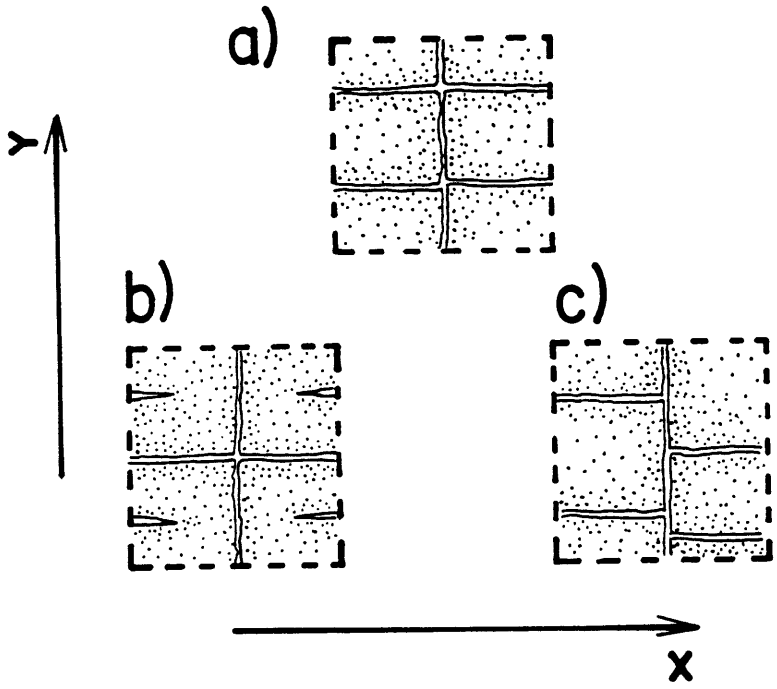

Figure 9:

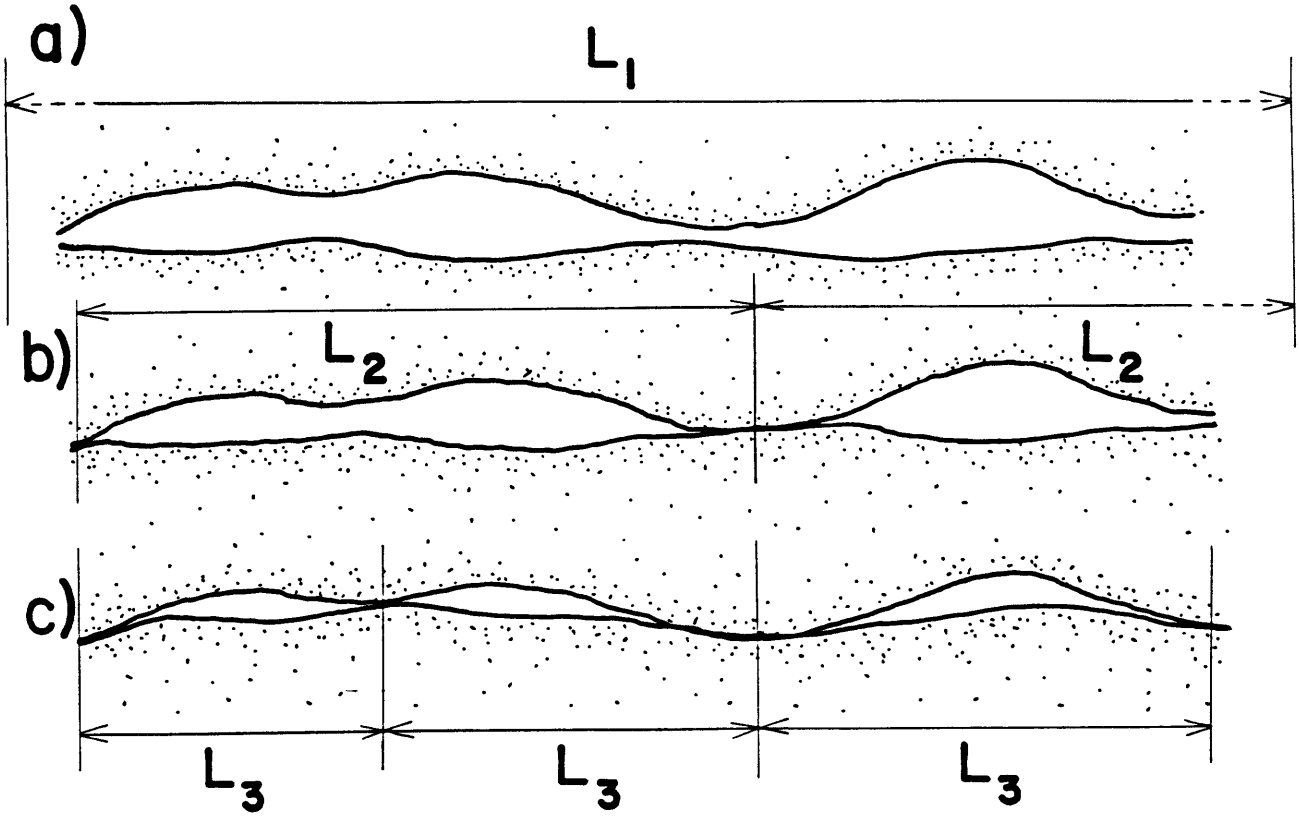

Figure 10:

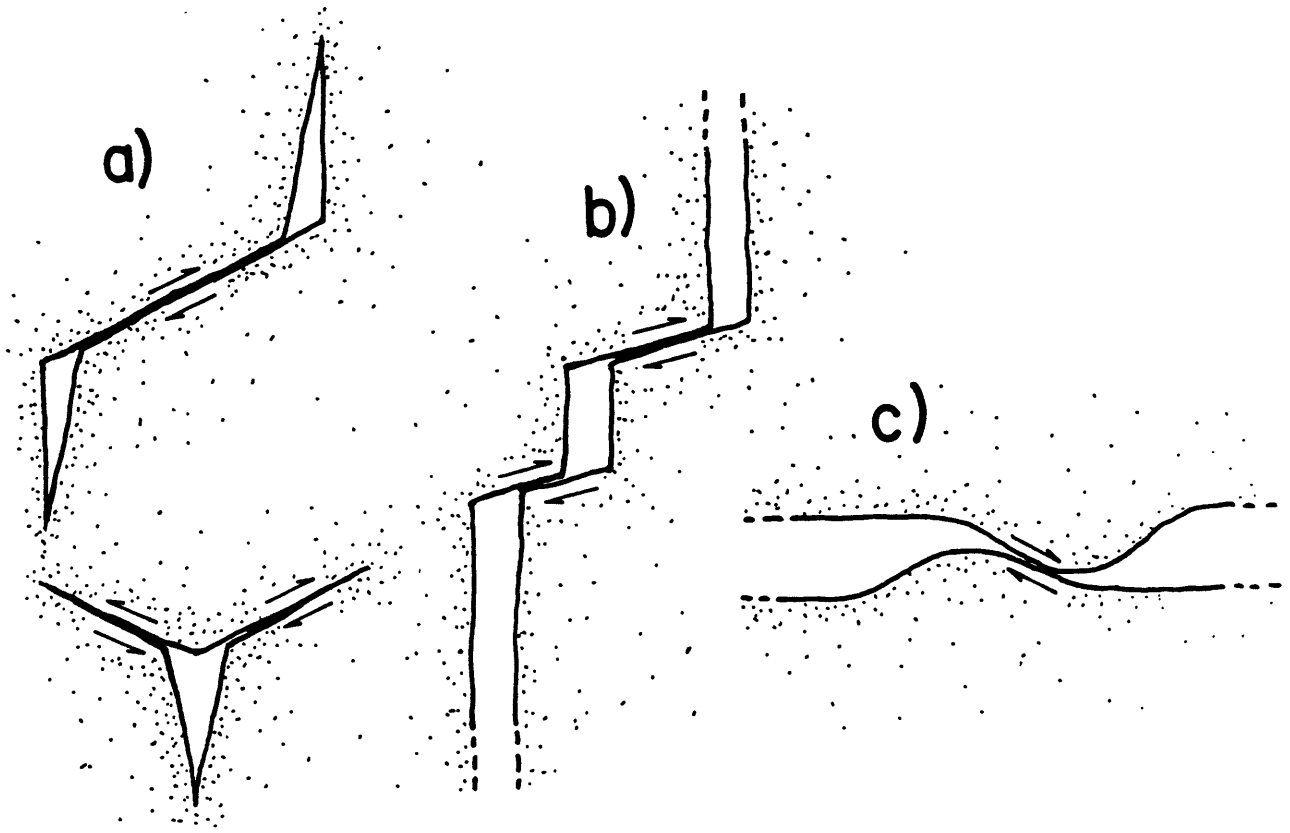

Figure 11:

CHAPTER 3:

THE EFFECTIVE PRESSURE LAW FOR PERMEABILITY DURING PORE PRESSURE AND CONFINING PRESSURE CYCLING OF SEVERAL CRYSTALLINE ROCKS.

Introduction

In the rock mechanics literature the terms "stress history dependency" or "path dependency" refer to a dependency of some rock properties on past state of stress. This feature appears most clearly when the rock samples are submitted to a number of stress cycles. Examples are given by Scholz and Koczinski (1979), Hadley (1976), Zoback and Byerlee (1975), and Haimson (1974) who studied the effect of such cycles on the dilatancy or the strength of rocks. Similar stress history and hysteresis effects were also observed on rocks submitted to cycles of the confining pressure P_c and/or the pore fluid pressure P_p. Wissler and Simmons (1985) reported observations of recoverable and irrecoverable hysteresis in strain on sandstones. Knutson and Bohor (1963), Coyner et al. (1979), Kranz et al. (1979), Bernabe et al. (1984), and others found that permeability depended on the path followed from one point to another in the plane (P_c, P_p). As will be showed in the next section, the usual definition of the effective pressure becomes inappropriate in such a case. In a previous work (Bernabe, 1985), we used alternative formulations allowing α, the coefficient of the effective pressure law, to vary with pressure and path. We found that α was strongly affected by the order in which confining pressure and pore pressure increments were applied to the samples.

In this paper we wanted, first, to check if other rocks (namely Pottsville sandstone, Pigeon Cove granite, and Westerly granite) showed a similar path dependency of α, and second to investigate the influence of further cycles. The motivation for the latter came from a recent study by Coyner (1984) in which the effective pressure law for permeability was invariably found to be

$P_{eff}=P_c-P_p$. This difference with our results was specially puzzling since we both worked on the same rocks. Some of our samples were even cored from the same blocks. The important point was that Coyner used to subject his samples to several seasoning cycles before starting the measurements. Seasoning is a familiar practice for eliminating (or minimizing) hysteresis (for example, Wilhelmi and Somerton, 1967, or Gregory, 1976). As an explanation, it seems possible that, after several cycles, an equilibrium state is reached where the effective pressure law no longer depends on stress history. We tried to verify this hypothesis by submitting some of our samples to up to 5 pressure cycles.

A local definition of α the coefficient of the effective pressure law

There is a good deal of confusion in the effective pressure terminology, perhaps due to a too wide variety of applications. For example, "effective pressure" is often meant as a straight synonym of the pressure difference P_c-P_p. To avoid ambiguity, we will first present the definition we used (based on the analysis by Robin, 1973). Then, we will show an alternative formulation yielding "local" values of α, the coefficient of the effective pressure law.

Consider a physical property k (here, permeability), and let it be a single valued function of P_c and P_p, noting $k_o(P_c)$ the value of k at zero pore pressure (in this theoretical discussion we do not consider the feasibility of measuring permeability at $P_p=0$). The effective pressure at the point $M(P_c, P_p)$ is defined as the confining pressure which, applied alone, would yield the same permeability. Therefore, it is given by the following functional relation

$$k_o(P_{eff}) = k(P_c, P_p) \qquad (1)$$

From (1) it is sometimes possible to express P_{eff} as a function of P_c and P_p.

$$P_{eff} = F(P_c, P_p) \tag{2}$$

This is graphically represented by the family C of curves $k(P_c, P_p)$=constant in the plane (P_c, P_p). Each curve corresponds to a different value of P_{eff} given by the point where it intersects the P_c axis. An important experimental result is that, often, these curves can be approximated by parallel straight lines. Their equation is then written

$$P_{eff} = P_c - \alpha P_p \tag{3}$$

where α is a constant. Equation (3) is the form under which the effective pressure law is really useful in practice. It has a very simple meaning: suppose the confining pressure is shifted by a given amount δP, we must change the pore pressure by $\delta P/\alpha$ in order to keep the permeability of the rock unchanged.

However, several quite restrictive remarks must be made at this point:

1 - The curves C and, therefore, the law of effective pressure can be entirely different if another property is considered.

2 - The equation (3) does not always hold. The effective pressure law may not even have an analytical expression when the material considered is not linear elastic.

3 - The above definition does not apply anymore if k is not a single valued function of P_c and P_p. This is important since it obviously applies to the case of stress history dependency.

In view of these complications, a "local" definition of the coefficient α allowing it to vary with pressure and path is needed.

In the vicinity of a point $M(P_c, P_p)$ the curves C can be approximated by a family of straight lines parallel to the tangent to C in M. Their equation

can be written

$$P_c - \alpha P_p = \text{constant} \qquad (4)$$

where α is the slope of the tangent in M. In general, the constant in (4) is not equal to P_{eff} (that happens only when the equation (3) is satisfied). In this formulation, we do not determine P_{eff} directly. The principal parameter now becomes α which is given by the following equation (Bernabe, 1985)

$$\alpha = - (\partial k/\partial P_p) (\partial P_c/\partial k) \qquad (5)$$

In practice, these two partial derivatives can be evaluated by measuring the variations of permeability caused by changing P_c and P_p independently. α is then given by

$$\alpha = - \delta k_p/\delta k_c \qquad (6)$$

where δk_p is the variation of k due to shifting P_p by δP while P_c is kept unchanged (a similar definition applies to δk_c with the subscripts c and p interchanged).

If α is known everywhere, all the curves C can be constructed point by point and their intersects with the P_c axis found. Hence, both formulations lead to equivalent definitions of P_{eff}. But the local formulation puts more emphasis on the coefficient α which represents a measure of the efficiency of the pore pressure in comparison with the confining pressure. At the present time, little is known about the variations of α in the plane (P_c, P_p) even when stress history can be ignored. The common assumption that α is everywhere constant, is probably not valid. Some observations suggest that α decreases with increasing P_c and with decreasing P_p (Todd and Simmons, 1972; Bernabe et al., 1984). Figure 1 illustrates this behavior.

Let's now consider the path dependency case. Two different paths can be

followed for determining α at the point $M(P_c, P_p)$ as showed in Figure 2. We start in $A(P_c-\delta P/2, P_p-\delta P/2)$ and go to $B(P_c+\delta P/2, P_p+\delta P/2)$ passing by either P_1 or P_2. The two paths only differ by the order in which the increments in P_c and P_p are applied to the sample (we changed P_c before P_p when passing through P_1, and the reverse in the other case). We can notice that, what precedes is only true for loading (raising P_c or $\delta P>0$). During unloading the order of application of confining pressure and pore pressure is reversed. The importance of distinguishing these two paths was demonstrated in a previous study on Barre granite (Bernabe et al., 1984). It was observed that α was roughly equal to 1.0 when the pore pressure was applied first, and significantly smaller when it was applied second ($\alpha\approx0.55$ and 0.85 in two different experiments). In other words, P_p was more efficient when it was applied in the first place than otherwise.

Since α is defined as a ratio, σ_α the uncertainty in α only depends on σ_k the uncertainty on the relative values of permeability (around 5% for k higher than $10^{-21}m^2$ or 1.0nd, and 10% otherwise). σ_α becomes large when σ_k is comparable to the δk's which are primarily controlled by the pressure increment δP. Therefore, using a smaller δP would allow determining a more "local" α, but with much less precision. We found that δP=20MPa was a good compromise value. Finally, this method becomes less accurate in the high pressure range because the δk's decrease with increasing P_c.

Description of the samples

Several samples were cored in non-oriented blocks of Pottsville sandstone

(Tennessee), Pigeon Cove granite (Massachusetts), and Westerly granite (Rhode Island). They were then ground to a cylindrical shape, 1.90cm in diameter and about 2.5cm in length. Special care was taken to produce parallel faces, precisely perpendicular to the cylinder axis. The samples were carefully cleaned of cutting-oil, and saturated with distilled water by immersion under vacuum. Modal analyses as well as evaluations of density, porosity and grain size can be found in Brace and Martin (1968) [Westerly, Pottsville], Brace and Orange (1968) [Pigeon Cove], and Siegfried and Simmons (1978) [Westerly]. Despite the name, Pottsville sandstone can be considered a crystalline rock; in fact, it is a quartzite with a porosity of 3%.

Experimental procedures

We used the cycling procedure schematically represented in Figure 3. It corresponds to going through the point P_1 in Figure 2. P_c was cycled with an increment δP=20MPa. At each step, the pore pressure was cycled between 10MPa and 30MPa (distilled water was the pore fluid). The permeability was measured using the pulse decay technique (a description of the apparatus and details about the method are given in Bernabe et al., 1982). The measurements were usually made twice with pulses of opposite signs allowing for detection of small leaks. This technique also demonstrated the excellent repeatability of our measurements. But, because of the large number of measurements required, this procedure was highly time consuming and we tried to minimize the duration of the experiments by reducing the amplitude of the cycles and/or measuring k only during the first and the last cycle.

As an exploratory step, we subjected a sample of Pottsville sandstone to a full confining pressure cycle (40MPa-200MPa) and to the very beginning of a second one. Since the effect we were looking for appeared to be quite spectacular (α drastically increased in the second cycle), we repeated the experiment on other rocks. A sample of Pigeon Cove granite was submitted to two successive cycles (40MPa-160MPa). The sample of Pottsville sandstone already used was kept at atmospheric pressure under dry conditions for about one month, and then, subjected to five more cycles (40MPa-140MPa). The purpose was to see if it had recovered its initial state after such a long relaxation time and to investigate the effect of further cycling. Finally, we tried to apply a similar procedure to a sample of Westerly granite. But its permeability was so low that it was not possible to even complete a single cycle (20MPa-120MPa). Rather, this experiment served the purpose of testing the capability of our apparatus in the very low permeability range (less than $10^{-21}m^2$ or 1nd).

According to Walsh and Brace (1984) the permeability measured at a given pore pressure should satisfy the following equation

$$k = [a \log(P_c) + b]^{1/n} \tag{7}$$

where a and b are fitting parameters depending on P_p, and n ranges between 0 and 1/3. n must be chosen to produce the lowest possible variance independently of P_p. However, it seemed to be poorly constrained by the data, making its significance questionable. Therefore, the equation (7) was only used to generate a new set of data smooth in comparison with the raw data. The α's obtained from both sets were quite comparable with more scatter for the raw data as expected.

Observations

The results of the permeability measurements are listed in Tables 1 and 2 (Pottsville), 3 (Pigeon Cove), and 4 (Westerly). For Pigeon Cove granite we found permeabilities very close to those reported by Coyner et al. (1979). For Westerly granite we measured permeabilities lower than the ones previously mentioned in the literature (for example, an order of magnitude less than the values from Coyner et al., 1979). The observations in this paper agree very well with the ones made in our previous work on Chelmsford granite and Barre granite (Bernabe et al., 1984). For each rock, the equation (7) (with n much lower than 1/3) fitted well the permeability k as a function of P_c (see Figure 4). We noticed that n took its minimum values during unloading, but we cannot provide an explanation for that at this point. For all the samples, cycling the confining pressure produced a large permanent change in permeability (k varied from about 300nd to 90nd for Pottsville sandstone, and from 80nd to 40nd for Pigeon Cove granite). But this effect decreased significantly with further cycles. Probably due to their relatively low amplitude, pore pressure cycles did not noticeably affect k except at low P_c during unloading.

The α's calculated are presented in Figures 5 and 6 (Pottsville), 7 (Pigeon Cove), and 8 (Westerly). The Westerly granite sample showed slightly higher α's than the other rocks ($\alpha \approx .7$). In all the cases, α clearly decreased with increasing confining pressure, and appeared to be strongly path dependent. α took values near 1.0 when P_p was applied before P_c (with our procedure this happens during unloading), and was much lower in the other case ($\alpha \approx .4$-.5 for Pottsville sandstone, and .6 for Pigeon Cove granite during loading). But this

effect diminished rapidly with the number of cycles. The values of α for loading increased constantly with the number of cycles ($\alpha \approx .5$ for the 1st cycle and .8 for the 5th one in the case of Pottsville sandstone; $\alpha \approx .6$ and .7 for the 1st and 2nd cycles in Pigeon Cove granite) approaching a limit near 1.0. On the contrary, α remained almost unchanged around 1.0 during unloading.

In a similar study C. Morrow (personal communication) subjected a sample of Westerly granite to two sets of pressure cycles separated by a long relaxation time under room conditions. She observed that, after relaxation, the sample permeability almost totally recovered its initial value (before the first set of cycles). To the contrary, our sample of Pottsville sandstone did not recover its initial state after resting one month at atmospheric pressure under dry conditions. At the beginning of the second set of measurements, k took a value just slightly higher than the final value reached at the end of the initial cycle (70nd instead of 60nd). But, the difference between the two rocks makes these contradictory results hard to interpret.

Discussion

For the interpretation of the decrease of α with increasing P_c we refer to Bernabe (1985) who discussed similar observations on Chelmsford granite and Barre granite. The model proposed can be briefly sketched as follows: the cracks in the rocks are supposed to have rough walls; during closure, when more and more asperities come into contact, a typical crack is progressively transformed into an array of coplanar, interconnected, smaller cracks with higher aspect ratio (see also Walsh and Grosenbaugh, 1979; Walsh, 1981;

Witherspoon et al., 1982); and Bernabe (1985) showed that α should decrease with increasing aspect ratio.

The hysteresis and path dependency effects can be simply attributed to frictional sliding inside the rock. This idea is schematically illustrated in Figure 9 by the following analogy; the displacements of the points X1 and X2 are respectively analogous to changes of P_c (or P_p), and to the resulting variations of permeability (for example, X1 could represent a distant point, the displacement of which would be caused by the remotely applied P_c or P_p; X2 could represent a point at the surface of a crack). If the initial state is stress free (the spring is not under tension), we need moving X1 twice as much during the second part of the cycle than during the first part in order to initiate sliding. Hence, the second part of the cycle yields less displacement of X2 (analogeously less permeability change) than the first one. Walsh (1965) used similar ideas to explain hysteresis in strain for a cracked isotropic solid subjected to uniaxial compression. Recently, Wissler and Simmons (1985) reported that frictional sliding mechanisms were consistent with the permanent strains they observed on sandstones submitted to pressure cycles. They also studied fused silica glass, a porous material with a homogeneous and isotropic solid matrix. There was almost no hysteresis or permanent strain noticeable. Therefore, it seems likely that the shear stresses developing in the rocks under hydrostatic pressure are caused by the inhomogeneous arrangement of anisotropic grains characteric of geological materials. It should be noted that we do not exclude the possibility of irreversible damage mechanisms such as crushing or cracking, but we believe that their contribution to the permanent permeability changes we observed is only marginal. Such damages were observed

under SEM by Sprunt and Brace (1974) on rocks submitted to pressure cycles (bridge or asperity collapses, flaking and detachment of tiny grains), but they seemed too small to explain the large modifications of permeability observed in our samples. Sprunt and Brace observed that larger damages were produced by thermal cycles at constant pressure, but the corresponding permeability changes were not known.

The path dependency of α can be accounted for in a similar way (Bernabe, 1985). Suppose that we start by shifting P_c by δP, producing a variation of permeability δk_c which is due to both elastic deformations of the cracks and a certain amount of frictional sliding. We then proceed by measuring δk_p corresponding to changing P_p by δP. Like in the previous section, less sliding takes place than what would happen if P_p was changed first, which tend to lower δk_p. Consequently, α is lower in this case than what it would be if the order of application of P_c and P_p was reversed. Our results are in good qualitative agreement with this model. We found α close to 1.0 when P_p was applied before P_c (during unloading with our procedure), and significantly smaller in the other case (during loading with our procedure).

Notice that the spring in Figure 9, which was completely relaxed initially, is under tension after the first cycle is completed. Hence, the initially stress free rock should contain residual shear stresses after completion of a cycle. The recovery experiment mentioned in a previous section (C. Morrow, personal communication), demonstrates clearly the existence of such residual stresses. It also shows that the irreversible damage processes only account for a small portion of the "permanent" changes undergone by the sample. We tried a similar experiment on Pottsville sandstone but failed to observe any

recovery. Perhaps, unlike Westerly granite the sample of Pottsville sandstone experienced heavy irreversible damages concurrently with the sliding mechanisms. Alternatively, the recovery may have been inhibited because we let the sample relax under dry conditions. The weakening effect of water on quartz is well-known (Jaoul et al., 1984). Water also facilitates the slow propagation of cracks (Atkinson, 1984), and lower the frictional strength of rocks (Dieterich and Conrad, 1984). We can reasonably expect that the processes of relaxation of residual stresses may be enhanced by water, and inhibited under dry conditions.

Returning to the analogy of Figure 9, if we apply a second cycle, the permeability loop now closes. Indeed, once the residual stresses are introduced in the rock, the same amount of sliding will occur during both the subsequent loading and unloading stages. That explains why the path dependency of α as well as the permanent permeability change tend to disappear when further cycles are applied. Therefore, after a certain number of cycles, P_p will produce the same permeability variation whether it is applied before or after P_c. In our idealized model, that happens as early as the second cycle, but in the real situation with all the possible interactions between cracks and grains we expect this transition to be more gradual.

In conclusion, our results seem to favor the use of the simple pressure difference, P_c-P_p, for evaluating the effective pressure. Indeed, 1.0 seems to be an universal limit for α in crystalline rocks. However, an important question remains. Are the seasoned samples (submitted to several pressure cycles) representative of the in-situ rocks? As a first condition, the rock masses must have experienced higher pressures in the past than now, at

least once. In connection with this, Wissler and Simmons (1985) found that the state of the samples strongly depended on the maximum pressure reached. A second condition is that there was not enough time between the pressure peak and the present time for allowing the residual stresses to relax. That raises another question. What is the effect of pressure on the relaxation mechanisms? At the present time, we do not have enough data to even give a preliminary answer. All we can say is that relaxation under load seems possible to occur. Brace reduced the hysteresis in strain during an uniaxial stress experiment by simply vibrating the sample still loaded (reported by Walsh, 1965). The vibration was not quantitatively controlled and the effect of the amplitude, frequency, and duration of the vibration are not known. Conceivably, in nature, mechanical vibrations of various sources might play a similar role, and "reset" properties of rocks to a pre-stress value.

In any case, relaxation processes are likely to occur in nature. We saw that large irreversible hysteresis, rapidly vanishing with further cycles, which are characteristic of pre-stress state, are very commonly observed on rock samples in the laboratory. Therefore, we can assume that these samples were naturally in pre-stress state, unless the extraction processes had reset them (laboratory rock samples usually come from quarries or road-cuts at the surface of the Earth, where extraction techniques can be used, that minimize microcracking of the samples, Simmons et al., 1982).

References

Atkinson, B.K., Subcritical crack growth in geological materials, J. Geophys. Res., 89, 4077-4114, 1984.

Bernabe, Y., An effective pressure law for permeability in Chelmsford granite and Barre granite, unpublished manuscript, 1985.

Bernabe, Y., W.F. Brace, and B. Evans, Permeability, porosity, and pore geometry of hot-pressed calcite, Mech. of Materials, 1, 173-183, 1982.

Bernabe, Y., W.F. Brace, and J.B. Walsh, Effective pressure law for permeability for two granites (abstr.), Trans. Am. Geophys. Union, 65, 283, 1984.

Brace, W.F., and R.J. Martin, A test of the law of effective stress for crystalline rocks of low porosity, Int. J. Rock Mech. Min. Sci., 5, 415-426, 1968.

Brace, W.F., and A.S. Orange, Further studies of the effect of pressure on electrical resistivity of rocks, J. Geophys. Res., 73, 5407-5420, 1968.

Coyner, K.B., Effects of stress, pore pressure, and pore fluids on bulk strain, velocity, and permeability on rocks, Ph.D. Thesis, M.I.T., Cambridge, 1984.

Coyner, K.B., W.F. Brace, and J.B. Walsh, New laboratory measurements of permeability and electrical resistivity of crystalline rocks (abstr.), Trans. Am. Geophys. Union, 60, 943, 1979.

Dieterich, J.H., and G. Conrad, Effect of humidity on time- and velocity-dependent friction in rocks, J. Geophys. Res., 89, 4196-4202, 1984.

Gregory, A.R., Fluid saturation effects on dynamic elastic properties of

sedimentary rocks, Geophysics, 41, 895-921, 1976.

Hadley, K., The effect of cyclic stress on dilatancy: another look, J. Geophys. Res., 81, 2471-2474, 1976.

Haimson, B.C., Mechanical behaviour of rock under cyclic loading, in Advances in Rock Mechanics, Proc. 3rd Congr. Int. Soc. Rock Mech., Denver 1974, Washington, D.C., Nat. Acad. Sci., Vol. 2, Part A, 373-378, 1974.

Jaoul, O., J. Tullis, and A. Kronenberg, The effect of varying water contents on the creep behavior of Heavitree quartzite, J. Geophys. Res., 89, 4298-4312, 1984.

Knutson, C.F., and B.F. Bohor, Reservoir rock behavior under moderate confining pressure, Proc. 5th. Symp. on Rock Mech., C. Fairhurst (ed.), Pergamon Press, New York, 627-659, 1963.

Kranz, R.L., A.D. Frankel, T. Engelder, and C.H. Scholz, The permeability of whole and jointed Barre granite, Int. J. Rock Mech. Min. Sci. Geomech. Abstr., 16, 225-234, 1979.

Robin, P-Y.F., Note on effective pressure, J. Geophys. Res., 78(14), 2434-2437, 1973.

Scholz, C.H., and T.A. Koczinski, Dilatancy anisotropy and the response of the rock to large cyclic loads, J. Geophys. Res., 84, 5525-5534, 1979.

Siegfried, R., and G. Simmons, Characterization of oriented cracks with differential strain analysis, J. Geophys. Res., 83, 1269-1278, 1978.

Simmons, G., R. Wilkens, L. Caruso, T. Wissler, and F. Miller, Physical Properties and Microstructures of a set of sandstones, Ann. Rept. to the Schlumberger-Doll Research Center, 1982.

Sprunt, E., and W.F. Brace, Some permanent structural changes in rocks due

to pressure and temperature, in Advances in Rock Mechanics, Proc. 3rd Congr. Int. Soc. Rock Mech., Denver 1974, Washington, D.C., Nat. Acad. Sci., Vol. 2, Part A, 524-529, 1974.

Todd, T., and G. Simmons, Effect of pore pressure on the velocity of compressional waves in low-porosity rocks, J. Geophys. Res., 77(2), 3731-3743, 1972.

Walsh, J.B., The effect of cracks on the uniaxial elastic compression of rocks, J. Geophys. Res., 70, 399-411, 1965.

Walsh, J.B., Effect of pore pressure and confining pressure on fracture permeability, Int. J. Rock Mech. Min. Sci. Geomech. Abstr., 18, 429-435, 1981.

Walsh, J.B., and W.F. Brace, The effect of pressure on porosity and the transport properties of rocks, J. Geophys. Res., 89, 9425-9431, 1984.

Walsh, J.B., and M.A. Grosenbaugh, A new model for analyzing the effect of fractures on compressibility, J. Geophys. Res., 84, 3532-3536, 1979.

Wilhelmi, B., and W.H. Somerton, Simultaneous measurement of pore and elastic properties rocks under triaxial stress conditions, Soc. Pet. Eng. J., 7, 283-294, 1967.

Wissler, T.H., and G. Simmons, The physical properties of a set of sandstones, II: permanent and elastic strains in hydrostatic compression to 200MPa, Int. J. Rock Mech. Min. Sci. Geomech. Abstr., in press, 1985.

Witherspoon, P.A., Y.W. Tsang, J.C.S. Long, and J. Nooriphad, New approaches to problems of fluid flow in fractured rock masses, in Proceedings to the 22nd U.S. Symposium on Rock Mechanics, MIT, Cambridge, pp.1, 1982.

Zoback, M.D., and J.D. Byerlee, The effect of cyclic differential stress on dilatancy in Westerly granite under uniaxial and triaxial conditions, J. Geophys. Res., 80, 1526-1530, 1975.

	cycle #1						cycle #2		
	loading			unloading			loading		
	10MPa	30MPa	10MPa	10MPa	30MPa	10MPa	10MPa	30MPa	10MPa
P_c (MPa)									
40	304.	510.	299.	92.0	252.	116.	92.0	252.	116.
	304.	496.	309.	95.6	242.	115.	95.6	242.	115.
60	149.	202.	148.	49.3	93.4	55.9	60.8	100.	63.7
	156.	213.	157.	48.7	90.8	53.3			
80	83.0	115.	79.4	32.5	47.4	34.2	37.1	54.1	38.9
	88.3	116.	83.2	31.9	47.6	37.5			
100	48.3	62.1	47.7	23.0	31.5	23.5			
	51.6	63.2	48.8	23.4	32.1	24.2			
120	31.7	38.5	31.1	17.3	23.3	17.0			
	33.2	39.3	31.9	18.4	22.8	19.0			
140	23.3	25.0	21.4	15.2	17.4	14.4			
	23.2	26.6	22.7	14.8	18.0	15.5			
160	14.8	17.9	15.8	11.7	14.5	11.8			
	16.0	17.7	15.5	12.4	14.3	11.9			
180	12.0	13.4	11.5	10.4	11.9	10.4			
	13.2	14.2	11.8	10.6	12.2	10.8			
200	9.15	10.8	9.11	9.15	10.8	9.11			
	9.71	10.4	9.68	9.71	10.4	9.68			
n		0.09			0.001				

Table 1: Results of the permeability measurements for Pottsville sandstone ($10^{-21}m^2$ or nd). The exponent n is also given.

	cycle #1			cycle #5		
	10MPa	30MPa	10MPa	10MPa	30MPa	10MPa
P_c (MPa)						
60		112.	72.4	40.4	76.4	45.9
		112.	71.5	40.6	75.1	45.6
80	42.2	56.6	40.5	30.2	43.5	29.4
	41.9	57.0	42.4	31.2	42.8	31.3
100	28.5	35.9	27.4	22.3	29.3	21.7
	28.4	37.4		22.4	30.7	22.2
120	20.8	25.1	20.1	17.0	20.5	16.5
	20.2		20.4	16.8	20.6	16.7
140	15.5	16.9	14.7	13.5	15.2	13.7
	15.1	17.4	14.8	13.5	15.5	13.8
120	17.5	22.0	17.4	15.3	19.4	15.6
	17.7	21.8	17.5	15.5	19.3	15.4
100	22.2	29.0	22.8	20.4	25.9	20.3
	22.6	28.9	23.2	19.9	25.6	20.8
80	29.3	44.8	31.4	26.5	40.3	27.8
	28.7	46.1	31.7	26.6	39.4	27.6
60	43.9	79.2	50.0	39.5	73.8	43.0
	47.6	78.7			72.1	45.5
n loading		0.04			0.2	
n unloading		0.001			0.001	

Table 2: Results of the permeability measurements for Pottsville sandstone after the relaxation time ($10^{-21}m^2$ or nd). The exponent n is also given.

	cycle #1			cycle #2		
	10MPa	30MPa	10MPa	10MPa	30MPa	10MPa
P_c (MPa)						
40	61.9	130.	61.8	41.4	107.	47.2
	62.8	119.	61.5	42.3	105.	47.7
60	37.6	55.0	37.6	30.5	44.5	29.4
	38.5	54.2	39.7	30.8	45.8	30.1
80	27.3	33.2	27.2	20.3	27.8	19.5
	29.2	34.4	26.8	21.8	26.8	21.5
100	20.4	24.5	20.3	15.5	19.7	15.7
	19.9	25.3	19.9	15.0	19.4	15.9
120	15.6	17.9	15.2	13.1	15.1	11.9
	16.4	18.3	15.7	12.4	14.1	12.4
140	13.1	14.3	12.7	9.84	11.1	10.4
	12.8	13.9	13.2	9.92	11.7	10.2
160	10.8	11.4	10.6	8.52	9.27	8.65
	10.3	12.0	10.3	8.92	9.82	8.57
140	11.8	13.3	11.6	9.78	10.8	10.4
	11.8	13.6	11.8	9.66	10.6	9.69
120	13.8	15.1	13.3	11.2	12.9	11.0
	13.8	15.5	14.0	11.2	12.7	11.1
100	15.0	20.0	16.5	13.7	16.0	13.2
	15.7	19.5	16.2	13.4	16.2	13.7
80	19.3	26.7	20.8	16.3	23.0	16.6
	19.6	27.2	20.1	16.2	22.4	16.9
60	26.4	40.6	27.4	22.7	34.5	22.9
	26.3	42.3	27.9	21.5	36.1	23.1
40	41.4	107.	47.2	34.2	91.3	39.2
	42.3	105.	47.7	33.8	87.7	41.2
n loading		0.09			0.009	
n unloading		0.001			0.001	

Table 3: Results of the permeability measurements for Pigeon Cove granite ($10^{-21}m^2$ or nd).

P_c (MPa)	10MPa	30MPa	10MPa
20	7.55		
	7.91		
40	2.18	6.92	1.99
	1.71	7.12	1.95
60	.806	1.59	.747
	.893	1.39	.798
80	.452	.636	.418
	.447	.691	.416
100	.250	.398	.235
	.264	.351	.276
120	.149	.224	.159
	.178	.228	
n		0.002	

Table 4: Results of the permeability measurements for Westerly granite ($10^{-21}m^2$ or nd).

Figure captions

Figure 1: A set of hypothetical curves $k(P_c, P_p)$=constant illustrating the behavior of crystalline rocks as suggested by some experimental data (Todd and Simmons, 1972; Bernabe et al., 1984). α is believed to decrease with increasing P_c and decreasing P_p.

Figure 2: A sketch of the different paths that can be used for measuring δk_c and δk_p.

Figure 3: A sketch of the cycling procedure we used. P_c is changed before P_p during the loading stage, and after during the unloading stage.

Figure 4: A typical set of permeability data. The error bars indicate the expected uncertainty on the relative values of k (in this example, 5%). The best fit curves $k=(a\log P_c+b)^{1/n}$ are also plotted.

Figure 5: The values of α for Pottsville sandstone. The solid symbols correspond to loading and the open ones to unloading. The best fit straight lines are indicated (except for the 2nd cycle; since we have only two data points, the segment drawn just represents the expected trend). The expected error on α is given for low and high P_c. Note that these features will be showed too in the next three Figures.

Figure 6: The values of α for Pottsville sandstone after the relaxation time.

Figure 7: The values of α for Pigeon Cove granite.

Figure 8: The values of α for Westerly granite.

Figure 9: An analogy illustrating the frictional sliding mechanisms responsible for the hysteresis and path dependency effects observed. The exitation is applied by moving the point X1 between A and B. The resulting displacements of the point X2 is explicited in the same diagram as well as the force F_s (F_n is supposed constant). If the spring is relaxed at the beginning of the first cycle, the loop does not close, which is analogous to the permanent changes in permeability observed in our samples. However, the spring is under tension after the first cycle is completed (analogous to the development of residual shear stresses in the rocks), and the loops corresponding to subsequent cycles now close. This is analogous to the decrease in permanent change observed after applying a few pressure cycles to our samples.

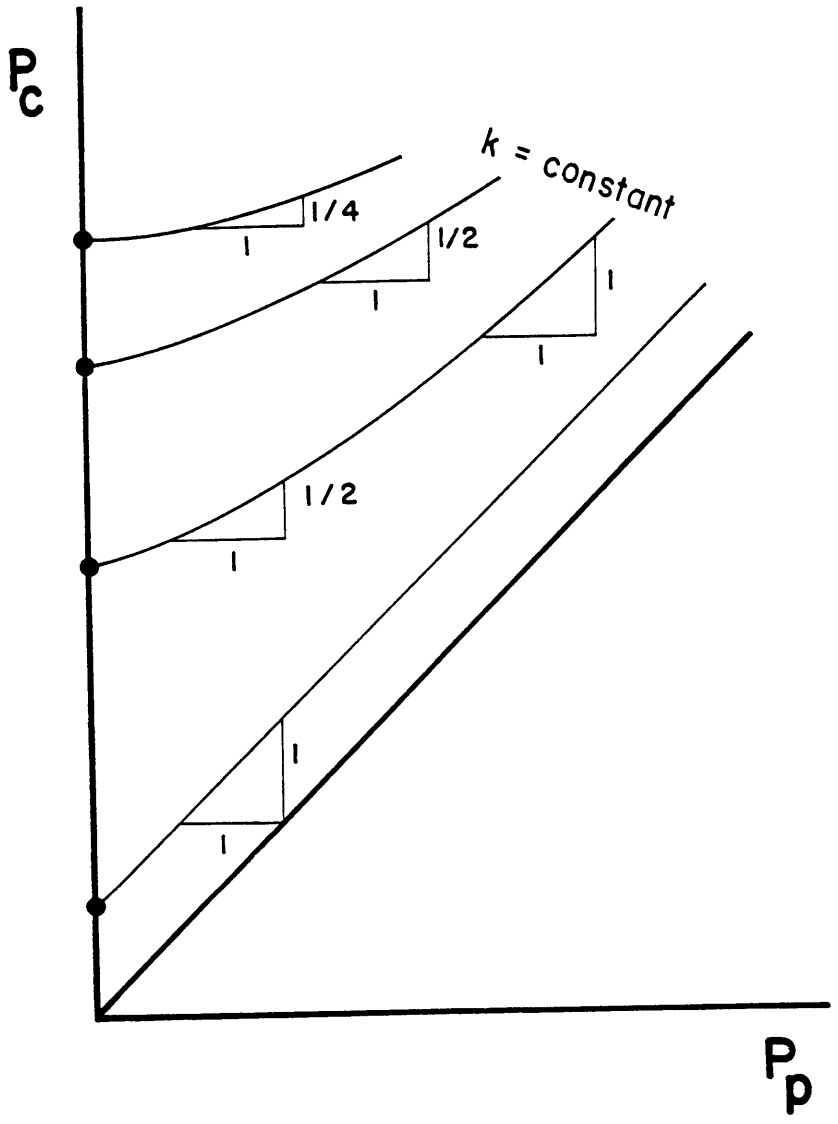

Figure 1:

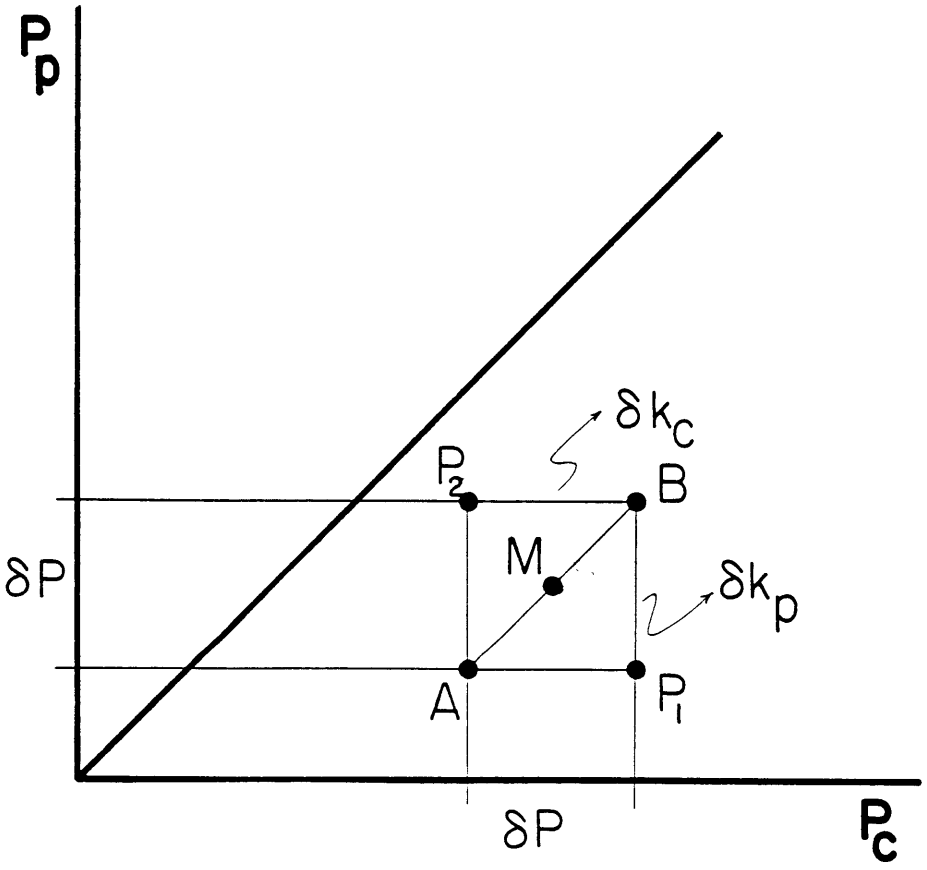

Figure 2:

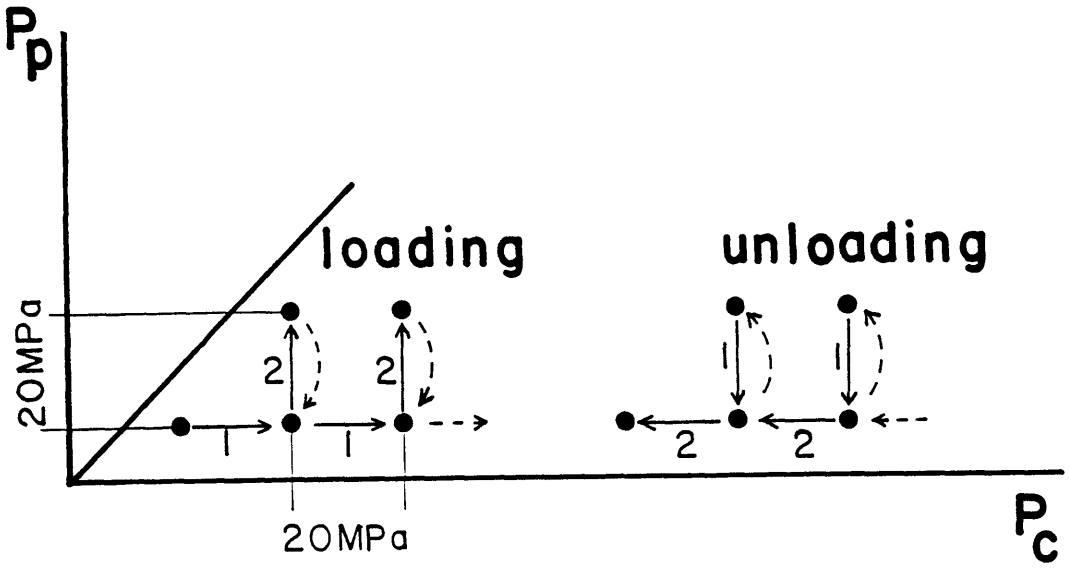

Figure 3:

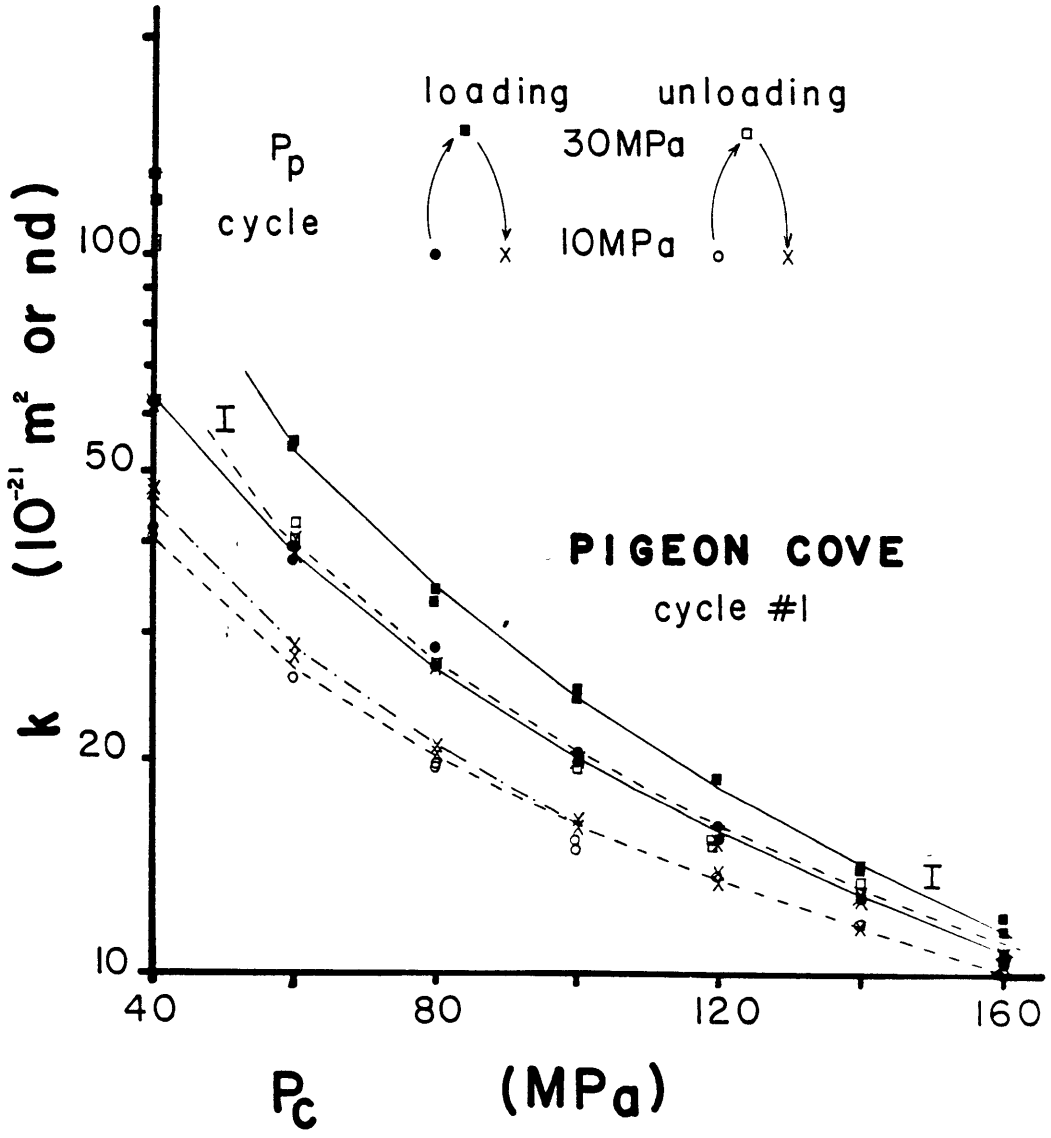
loading
unloading
P_p
cycle
30MPa
10MPa
PIGEON COVE
cycle #1
I
I
k (10^{-21} m^2 or nd)
100
50
20
10
40
80
120
160
P_c (MPa)

Figure 4:

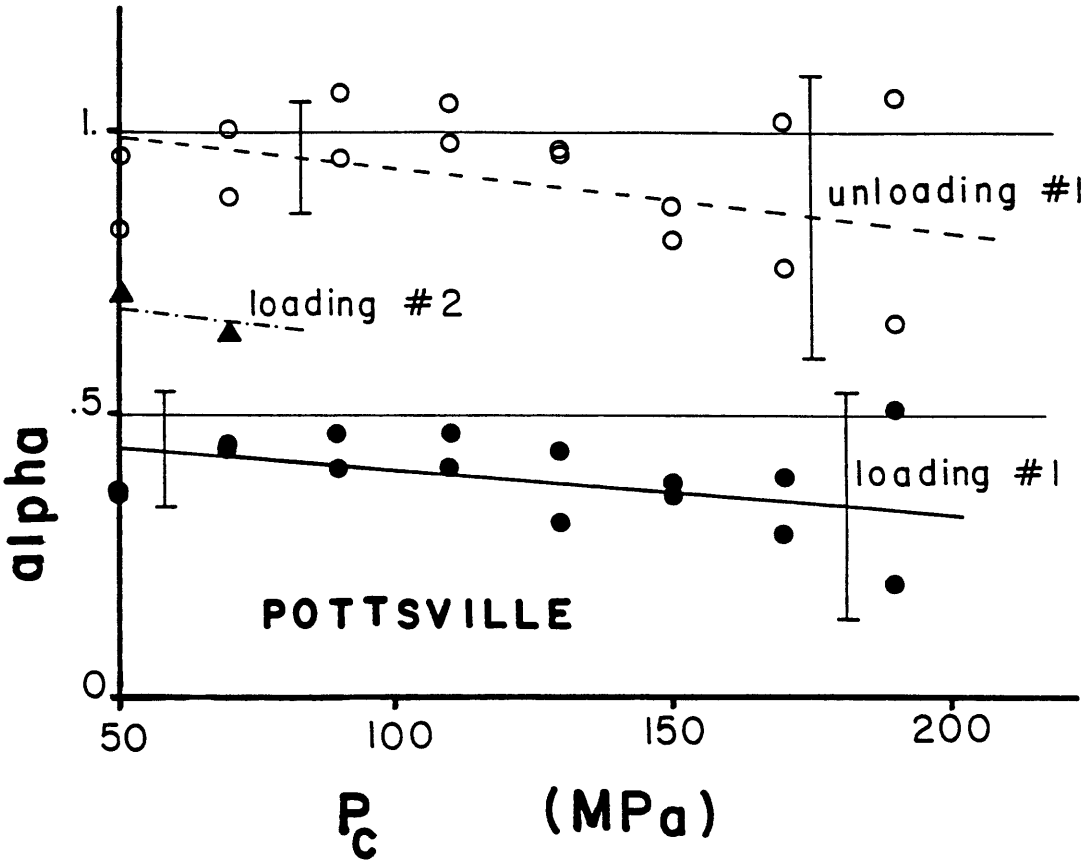
1.
.5
0
alpha
unloading #1
loading #2
loading #1
POTTSVILLE
50
100
150
200
P_c (MPa)

Figure 5:

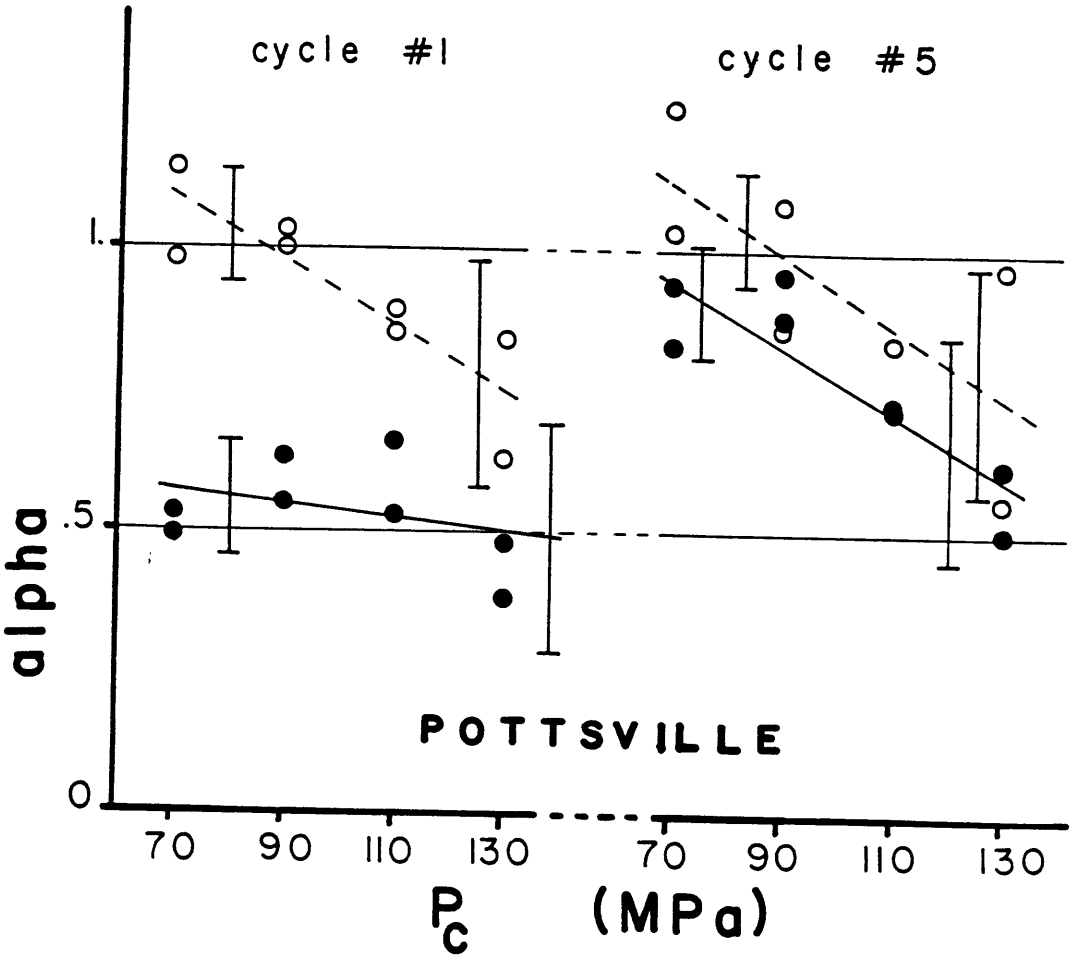
cycle #1
cycle #5
1.
.5
0
alpha
POTTSVILLE
70
90
110
130
70
90
110
130
Pc (MPa)

Figure 6:

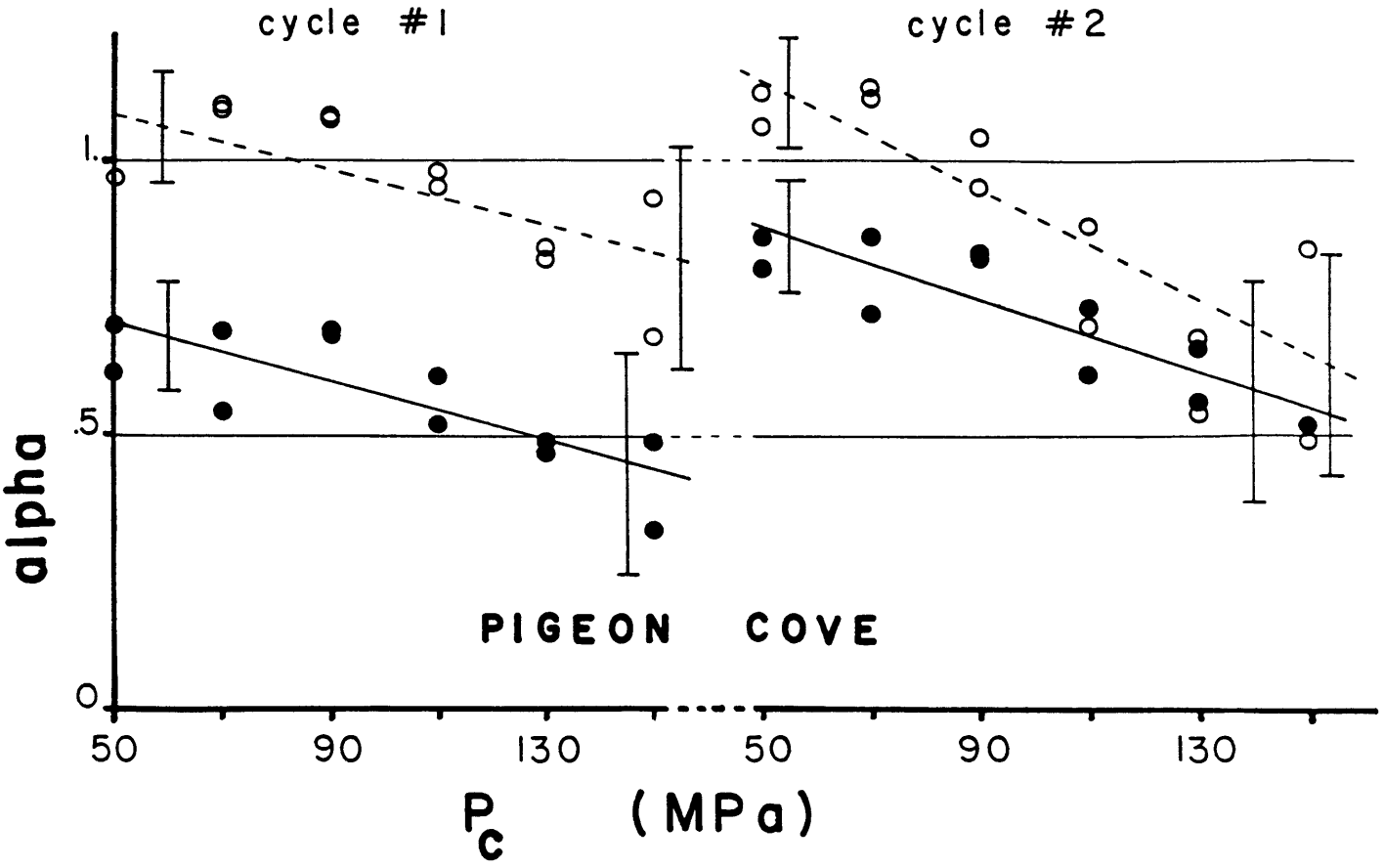

Figure 7:

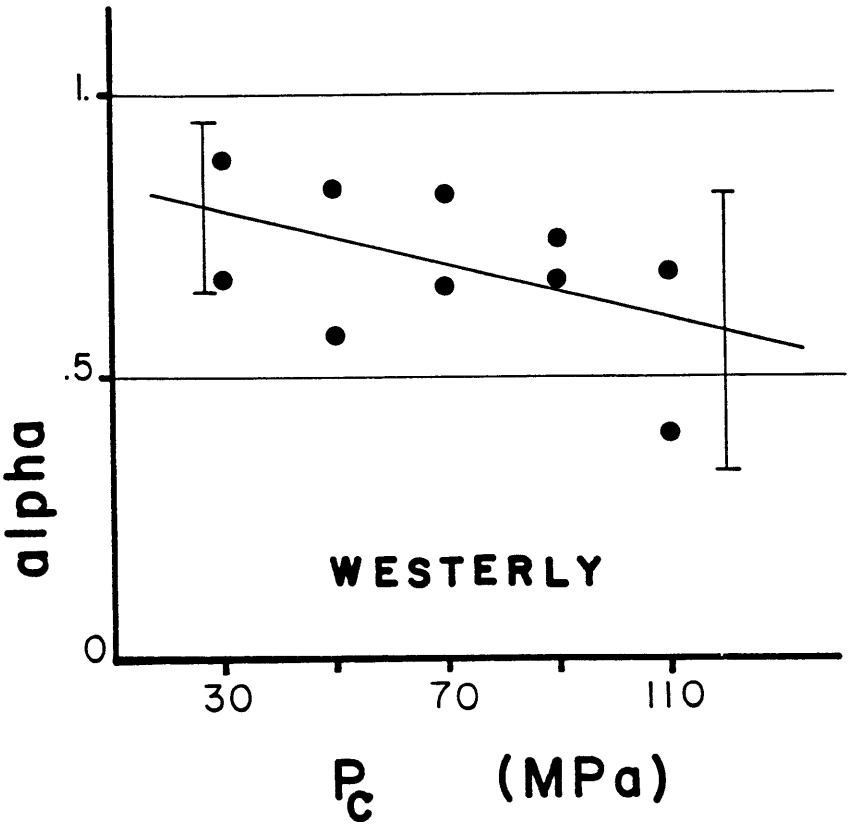

Figure 8:

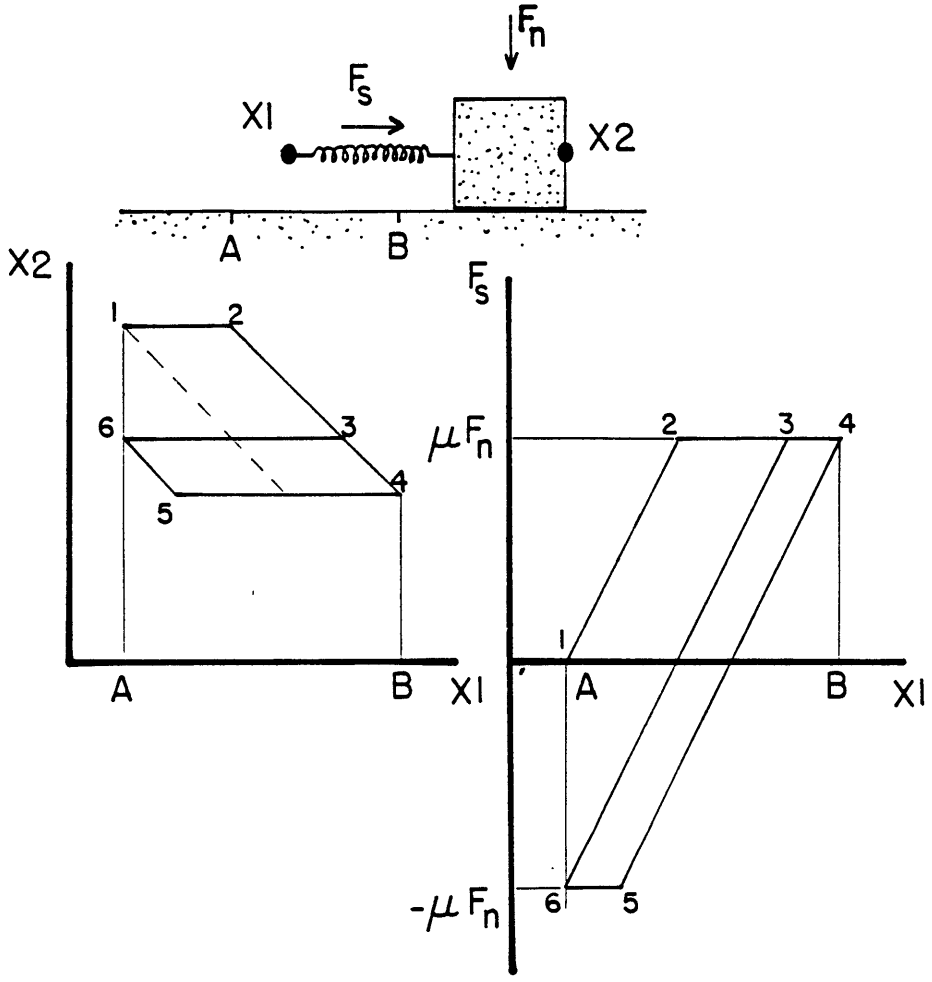

Figure 9:

CHAPTER 4:

PORE VOLUME AND TRANSPORT PROPERTIES CHANGES DURING PRESSURE CYCLING OF SEVERAL CRYSTALLINE ROCKS.

1. Introduction

From loose sand to tight rocks, geological materials present a great variety of pore structures. In the past, numerous models were devised to explain rocks and soils transport properties, but none seems universally applicable (reviews can be found in Bear, 1972, or Dullien, 1979). The so-called "equivalent channel model" (first proposed by Wyllie and Rose, 1950, and recently revised by Paterson, 1983, and, Walsh and Brace, 1984) has yielded satisfactory results for crystalline rocks. This model is extremely simple conceptually. The entire porous network of the rock is just replaced by a single "equivalent" conduit characterized by a number of geometrical parameters like tortuosity, hydraulic radius, or aspect ratio (of course, the porosity of the equivalent channel is supposed to be identical to that of the sample). The replacing operation can always be carried out, but it makes very little physical sense unless the equivalent channel is somehow "representative" of the rock pore structure. The equivalent channel model was used in recent studies (Walsh and Brace, 1984; Katsube and Walsh, 1985) to find values of the hydraulic radius and pore wetted area that were well correlated with those obtained from other independent methods. The reason for this success is probably that the pore phase in crystalline rocks is almost exclusively formed of low aspect ratio cracks (Hadley, 1976; a rather large number of equant pores were observed in plagioclase grains in crystalline rocks but they appeared to be isolated, therefore having no effect on the transport properties; Montgomery and Brace, 1975). Hence, it is reasonable to think that the equivalent channel corresponds to an average of the cracks in the rock. But, the averaging operation is

unknown and can vary depending on the topology of the crack network. For example, the mean hydraulic radius <m> of a set of parallel cracks is given by

$$\langle m \rangle^2 = \int_0^\infty m^2 \, Q(m) \, dm \qquad (1)$$

whereas it is

$$\langle m \rangle^2 = \left[\int_0^\infty m^{-2} \, Q(m) \, dm \right]^2 / \int_0^\infty m^{-6} \, Q(m) \, dm \qquad (2)$$

for a set of cracks in series (Dullien, 1979), where Q(m) is the hydraulic radius distribution function. The symbol < > will thus be used in this paper to remind that the values found correspond to an averaging operation, which will be kept unspecified because the data on crack size distributions available to us were not sufficient to address this problem in greater details. All we can say is that, for any parameter, the "average" value becomes identical to the value at the peak when the distribution is narrow enough.

Another important point was recently raised by Walsh (1981). At different scales, microcracks, and joints or faults play very similar roles in the behavior of rock under pressure. It is therefore tempting to use the models of the mechanical and transport properties of joints recently devised (Gangi, 1978, Walsh and Grosenbaugh, 1979, Tsang and Witherspoon, 1981, Walsh, 1981, Brown and Scholz, 1985, to cite a few), in which joints are always considered as rough surfaces in contact.

In this paper, we report measurements of the pore volume changes during pressure cycling of several crystalline rocks (namely, Chelmsford granite, Barre granite, Pottsville sandstone, Pigeon Cove granite, and Westerly granite). Then we use these data together with permeability and electrical

resistivity data to characterize the equivalent channel (or equivalent crack) for these rocks. But first, in the next section, we are going to briefly present the version of the equivalent channel model used here, based on Walsh and Brace (1984).

2.The equivalent channel model

We must start with the hypothesis that the paths are identical for both fluid flow and electrical current, which implies that both types of flow "see" the same tortuosity. This assumption seems quite reasonable, especially when the crack size distribution is narrow (complications may arise with broad distributions, because the smaller cracks contribute much less to the fluid flow than to the electrical current). Also, we will only consider the actively conducting pore space. This may introduce some complication when evaluating certain parameters like porosity (for example, the porosity determined from point-counting in micrographs includes isolated and dead-end pores which are not actively conducting, whereas that evaluated from immersion techniques excludes the isolated pores but not the dead-ends; in fact, it can be reasonably assumed in most cases that dead-ends represent a negligible fraction of the pore volume). We can then proceed to replacing the whole conducting pore network by a single equivalent conduit, the permeability of which is given by the following equation

$$k = (\langle m \rangle^2 / \langle b \rangle)\ (\Phi / \langle \tau \rangle^2) \qquad (3)$$

where $\langle b \rangle$ is a shape factor ranging from 2 to 3 when the aspect ratio varies from 1 to 0, Φ is the conducting porosity (ratio of the conducting pore volume

V_c to the sample volume V), and $\langle\tau\rangle$ is the tortuosity (ratio of the equivalent channel length to the sample length). We do not need to use the symbol < > for Φ because the equivalent channel porosity and the actual conducting porosity are identical. Similarly, we can assume that the wetted area of the equivalent channel is simply equal to A_c, the real wetted area of the conducting pore space, which leads to the relation

$$\langle m\rangle = \Phi\ (V/A_c) \tag{4}$$

The resistivity formation factor F is given by the expression

$$F = \langle\tau\rangle^2/\Phi \tag{5}$$

which, with (3), yields the important relation

$$\langle m\rangle = (\langle b\rangle kF)^{1/2} \tag{6}$$

We can assume that the aspect ratio of the equivalent channel is near 0. Therefore, $\langle b\rangle$ will be simply taken equal to 3 in the rest of the paper. From (4) and (6) we can derive the following relation

$$(3kF)^{1/2} = \Phi\ (V/A_c) \tag{7}$$

Walsh and Brace (1984) plotted the square root of 3kF against crack porosity for Westerly granite and Chelmsford granite, and found fairly linear relationships, which implies that the wetted area remained nearly constant in the range of pressure investigated. Consequently, most of the deformation taking place at the surface of the pores was elastic.

This is the point where we need to introduce some elements of elastic joint mechanics. The hydraulic radius is identical to the crack half-aperture, and we can write the following approximated equation

$$d\langle m\rangle = -\ 2h\ dP/P \tag{8}$$

where P is the effective pressure (the definition of "effective pressure" will

be discussed latter), and h is the standard deviation of the asperity heights distribution. It is implicitly assumed here that the distribution of asperity heights can be approximated by an exponential distribution. In this analysis, an asperity is defined as a "local" maximum of the crack walls topography. Also, interactions between asperities are excluded. From (6) and (8), one can deduce that the square root of 3kF should be proportional to the natural logarithm of pressure. Walsh and Brace (1984) verified this point on Westerly granite and Chelmsford granite.

It would be very interesting to have direct relations between k or F and P at our disposal, but the model does not provide enough equations to separate all the variables. Rather, we can use empirical relations inferred from experimental data. Walsh and Brace (1984) found that k was approximately proportional to F elevated to a certain power -r. For the data they used, r ranged from 1.5 to 2.8. Remarkably, these values fall between the bounds predicted by the model ($1<r\leq 3$).

Indeed, when r exists, it is defined by the following expression

$$r = - (dk/k)/(dF/F) \tag{9}$$

Since A_c/V is independent of pressure, by combining the equations (3), (4), and (5) with (9) we can derive the following relation

$$r = \frac{-3d\langle m\rangle/\langle m\rangle + d\langle\tau\rangle^2/\langle\tau\rangle^2}{d\langle m\rangle/\langle m\rangle - d\langle\tau\rangle^2/\langle\tau\rangle^2} \tag{10}$$

which leads to

$$\langle\tau\rangle^2/\langle\tau_o\rangle^2 = (\langle m\rangle/\langle m_o\rangle)^{-(3-r)/(r-1)} \tag{11}$$

where the subscript zero arbitrarily refers to the zero pressure state (therefore, $\langle\tau_o\rangle$ represents the intrinsic tortuosity of the crack network,

which is unlikely to take values much larger than 2 or 3). We know that a decrease in hydraulic radius must correspond to an increase in tortuosity. Hence, the exponent $-(3-r)/(r-1)$ must be negative, and $1 < r \leq 3$. For the interpretation of these bounds we can quote Walsh and Brace (1984). "r is a measure of the sensitivity of the tortuosity to changes in hydraulic radius: as r approaches 3, tortuosity is nearly independent of hydraulic radius, whereas small changes in aperture result in very large changes in tortuosity for samples where r is near unity." These two limiting cases can also be interpreted in terms of rugosity of the crack walls: r=3 corresponds to very smooth cracks (it is easy to see that, in this case, k is proportional to $\langle m \rangle^3$, the cube law habitually used for perfectly flat cracks), while r=1 can be related to very rough ones. Now, we need to know what value r takes for the rocks considered in this study. The values referred to by Walsh and Brace (1984) are relatively close to 2.0 (from 1.5 to 2.4 for Westerly granite, from 1.9 to 2.3 for Chelmsford granite, 2.6 for Pottsville sandstone, and 2.1 for Pigeon Cove granite). Katsube and Walsh (1985) studied samples of various granites and found r's ranging between 1.9 and 2.1. Gee and Brace (1985) measured electrical resistivity on the samples of Chelmsford granite and Barre granite that we previously used for permeability measurements (Bernabe, 1985a). They too observed r ranging from 1.9 to 2.1. Therefore, r=2 appears to be an adequate approximation for the rocks we studied. However, we should point out that a set of measurements of electrical resistivity and crack porosity on several other crystalline rocks (Brace, Orange, and Madden, 1965) seems to contradict this statement. Assuming that F^{-r} is proportional to k, we can deduce from equations (4) and (6) that F^n with $n=(1-r)/2$ should be

proportional to Φ. Therefore, the curves Φ vs F on a log-log plot should be straight lines. Their slope n should range between -1 and 0. But, the Brace et al.'s data (1965) plotted in Figure 1 show a different behavior. The curves Φ vs F are not linear. Their slope vary from -1 to $-\infty$ as Φ decreases (or P increases). The apparent vanishing of Φ at a finite value of the electrical resistivity (when $n=-\infty$) probably just shows that the method of measuring Φ used by Brace et al. tends to underestimate Φ, particularly at high pressure where Φ is very small (the crack porosity is defined as the difference between the curve giving the volumetric strain against pressure and its linear portion extended down to zero pressure; in fact, the "linear" part of the curve has an imperceptible curvature; its slope is then slightly underestimated, which leads to smaller values for Φ). If we neglect the high pressure data, the slope n seems to be closer to -1 than -1/2, corresponding to r=3 rather than 2. This discrepancy argues against the first assumption of the model ($\langle\tau\rangle$ is the same for permeability and electrical resistivity). In that case, the relation $n=(1-r)/2$ does not hold anymore. Presumably, this should happen when the distribution of crack widths is broad.

Assuming that r=2, appropriate combinations of the equations previously established in the model, yield the following expressions

$$d\Phi = - A_\Phi \, dP/P \tag{12}$$

$$dk^{1/4} = - A_k \, dP/P \tag{13}$$

$$dF^{-1/2} = - A_F \, dP/P \tag{14}$$

where A_Φ, A_k, and A_F are defined by

$$A_\Phi = 2h \, (A_c/V) \tag{15}$$

$$A_k = 2h \, (A_c/V)^{1/4} \, (3\langle m_o\rangle\langle\tau_o\rangle^2)^{-1/4} \tag{16}$$

$$A_F = 2h\ (A_c/V)^{1/2}\ (\langle m_o\rangle\langle\tau_o\rangle^2)^{-1/2} \qquad (17)$$

Hence, we can calculate h, A_c/V, and $\langle m_o\rangle\langle\tau_o\rangle^2$.

$$h = (A_k^2\ 3^{1/2})/(2\ A_F) \qquad (18)$$

$$A_c/V = (A_\Phi\ A_F)/(A_k^2\ 3^{1/2}) \qquad (19)$$

$$\langle m_o\rangle\langle\tau_o\rangle^2 = (A_\Phi\ A_k^2\ 3^{1/2})/A_F^3 \qquad (20)$$

We can now return to the definition of the effective pressure P which was needed in equation (8). In general, P is given by the following equation

$$P = P_c - \alpha\ P_p \qquad (21)$$

where P_c is the confining pressure, P_p the pore pressure, and α a constant less or equal to unity. We have detailed information about α in the rocks considered only for permeability (Bernabe, 1985a, b), and using α=1 (the most common form of the effective pressure law) seems the simplest and the most objective approach in our case. Furthermore, we can remark that, by using α=1, we slightly underestimate P, and consequently A_Φ, A_k, and A_F as well. But, these effects tend to cancel each other in the equations (19) and (20), yielding adequate values of A_c/V and $\langle m_o\rangle\langle\tau_o\rangle^2$. But, the values calculated for h are only lower bounds.

To summarize, the pressure dependence of the transport properties of crystalline rocks can apparently be explained by the individual behavior of rough cracks which form the conducting network of the rocks. In this model, pressure does not induce important topological changes in the crack network itself, since the asperities prevent the cracks from completely closing. In particular, the connectivity as well as the intrinsic tortuosity of the crack network are assumed to remain nearly unchanged (a distinction must be made between the intrinsic network tortuosity which is approximately equal to $\langle\tau_o\rangle$

and the mean tortuosity of the cracks themselves, caused by their rugosity). Therefore, according to the model, the variations of tortuosity are exclusively caused by the asperities of the crack walls coming into contact.

As an alternative model, one could imagine a network of flat cracks with a broad distribution of aspect ratios. The cracks would close at different pressures depending on their aspect ratios. The changes induced in the crack network would then explain the behavior of the rocks transport properties. But, this model is not very attractive because such a network with few high aspect ratio cracks randomly distributed would rapidly loose its connectivity, causing a dramatic drop in permeability. This is in contradiction with the common observation that permeability tends to decrease at a rate slower at high P_c than at low P_c.

3.Experimental procedures

We used cylindrical samples 1.90cm in diameter and about 2.5cm in length, saturated with distilled water (more details about the preparation of the samples are given in Bernabe, 1985a, b). All the samples except the Chelmsford granite ones, were submitted to various numbers of cycles of confining pressure (1 for Barre granite, 2 for Pigeon Cove, 2 and 5 for Pottsville sandstone, and 1/2 for Westerly granite), during which both permeability and pore volume changes were measured. The confining pressure P_c was increased and decreased step by step with an increment of δP=20MPa causing porosity variations that were measured as is described in the next section. At each step in P_c, the pore pressure P_p was also cycled using procedures described elsewhere (Bernabe,

1985a, b), and the permeability was measured for each value of P_p. Furthermore, we measured two oriented samples of Chelmsford granite (one perpendicular to rift plane and the other to grain plane), which were previously used for a permeability study (Bernabe, 1985a). We subjected these samples to a single confining pressure cycle with δP=20MPa, while keeping the pore pressure constant at 20MPa. We designed the experiments in a way such that, for each sample, the pore pressure always took the same value during the pore volume change measurements (P_p was equal to 10MPa for Pigeon Cove granite, Pottsville sandstone, and Westerly granite, to 20MPa for Chelmsford granite, and to 30MPa for Barre granite).

3.1.Pore volume change measurements

When the confining pressure is increased by a given amount δP, a certain volume of pore fluid (here, distilled water) is squeezed out of the sample, thus increasing the pressure in the pore fluid circuit. The pore pressure is then restored to its initial value by operating a metering valve. Knowing the cross-section of the metering valve piston and its displacement, we can measure the volume of fluid expelled from the sample during pressurization. Of course, the same technique can be applied when lowering confining pressure as well.

The volume of the pore fluid circuit can be set sufficiently small, so that even tiny variations of fluid volume will produce significant changes in pore pressure. Therefore, the fluid volume changes in the pore fluid circuit can be measured with a fair accuracy (the uncertainty on fluid volume changes is around 5%). However, end-plugs, tubings, connections, jacket, and other such elastic elements are enclosed inside the pressure vessel together with the sample. Being submitted to confining pressure, these elements deform and cause

an unknown fraction of the pore pressure variations observed. Hence, our data need being corrected for this effect to give the true pore volume changes in the rock. In order to evaluate that correction, we measured the fluid volume changes with a solid aluminum sample prepared in the same way than the rock samples. The corresponding fluid volume changes were of the order of 10% of the pore volume changes observed for rocks. These values are probably too small to be accurately determined, which brings additional uncertainty into the values of the pore volume changes (about 15%). Finally, we should keep in mind that this method does not yield the absolute values of porosity as a function of pressure. Therefore, we cannot verify our basic assumption (r=2) by simply plotting our values against k or F in a log-log scale as was previously done for Brace et al.'s data (1965).

3.2.The transport properties data

As will be seen latter, there is a large scatter in the values of A_k and A_F calculated from k and F data found in the literature for the rocks considered here. It is, therefore, critical to use transport properties data collected from the same samples under the same conditions of pressure in order to obtain accurate determinations of A_k and A_F. We saw that, in most cases, permeability was measured jointly with the pore volume changes during the same runs (the only exception is Chelmsford granite for which k was measured in the same samples as Φ, but during different experiments). Gee and Brace (1985) measured electrical resistivity on our samples of Barre granite and Chelmsford granite using the same cycling procedures in the same range of pressure. However, we should remark that each cycle applied changes the state of the rock samples (Bernabe, 1985b; Wissler and Simmons, 1985). Hence, the resistivity

data are not strictly comparable to the other data. Nevertheless, the situation was much better in these cases than for the other rocks, for which we had to use data from totally different sources. For Westerly granite and Pigeon Cove granite, we used data from Coyner et al. (1979). For Pottsville sandstone, resistivity data were collected a long time ago by Brace and Orange (1968), and more recently by Brace and Coyner (1980). For these three rocks, we expect an unusually large uncertainty in h, A_c/V, and $\langle m_o \rangle \langle \tau_o \rangle$.

4.Observations and discussion

4,1.Westerly granite

$\delta\Phi$, the values of pore volume changes normalized to the volume of the sample, are given in Table 1. In this form, our data are not easy to compare to other data. Thus, we transformed the $\delta\Phi$'s into a more appropriate form using the following expression

$$\Phi - \Phi_R = \int_{P_R}^{P} \delta\Phi \qquad (22)$$

where Φ_R is the sample porosity at some arbitrary reference effective pressure P_R (as explained before, Φ_R is an unknown quantity). With this presentation, we can first check the linearity of the relationship between Φ-Φ_R and lnP, and second compare the slopes measured for the different data available. In Figure 2, our values of Φ-Φ_R are plotted against P in a semi-log scale, as well as other values from Brace et al. (1965) and Coyner (1984). In all the cases, Φ-Φ_R is a fairly linear function of lnP. Our data show the steepest slope (A_Φ is $0.52 \pm 0.04\ 10^{-3}$ for our data, $0.37\ 10^{-3}$ for Brace,

Orange, and Madden's, and, 0.34 and 0.28 10^{-3} for Coyner's). As explained earlier, a slight underestimation of the Φ's is expected for Brace et al.'s data. Coyner obtained his data by subtracting the volumetric strain of an unjacketed sample (this type of experiment aims at determining the intrinsic bulk modulus of the solid matrix, since P_p is supposed to be identical to P_c) from the volumetric strain of the same jacketed sample at zero pore pressure. Because of the low permeability of Westerly granite, the pressure of the confining fluid inside the rock is not immediately in equilibrium with the applied confining pressure during the unjacketed experiments. Perhaps, the difference of pressure is temporarily large enough to generate shear stresses and frictional sliding inside the rock. The sliding surfaces would stay locked as the pressure difference vanishes, and a certain amount of pore strain can thus be included within the matrix strain measured during the unjacketed experiment, making the intrinsic bulk modulus apparently lower. Furthermore, Coyner (1984) observed that the intrinsic bulk modulus increased with increasing confining pressure. Indeed, increasing P_c probably inhibits sliding inside the rock. Consequently, we expect less contamination of the matrix strain by pore strain at high confining pressure. Finally, this mechanism must be very sensitive to permeability, and as a matter of fact, the other more permeable granites studied by Coyner (1984) showed a less significant increase in intrinsic bulk modulus with increasing P_c.

In the Figure 3, we plotted $k^{1/4}$ as a function of lnP. The relationship appears fairly linear (A_k=2.4±0.1 $10^{-6}m^{1/2}$). We see that using different effective pressure laws (the usual law $P=P_c-P_p$, and a more realistic one with a variable coefficient α; Bernabe, 1985b) does not produce dramatically

different results. Using the data from Coyner, Brace, and Walsh (1979), Brace, Orange, and Madden (1965), and Brace, Walsh, and Frango (1968), we computed the following values: CBW, sample #1, for loading A_k=5.7 $10^{-6}m^{1/2}$, A_F=5.9 10^{-3}, for unloading A_k=4.0 $10^{-6}m^{1/2}$, A_F=5.0 10^{-3}; sample #2, for loading A_k=7.5 $10^{-6}m^{1/2}$, A_F=6.7 10^{-3}; BWF, A_k=5.0 $10^{-6}m^{1/2}$; BOM, A_F=5.4 10^{-3}. These four pairs of values nearly fall on a straight line which can be used to determine A_F for our sample (Figure 4). We found A_F=4.0±1.3 10^{-3} (extrapolating introduces a great deal of uncertainty, but it is the only way to minimize the effect of the sample disparity). Assuming that A_k and A_F are linearly related in a particular rock, implies that A_c/V and $\langle m_o \rangle \langle \tau_o \rangle^2$ are proportional. The microcracking mechanisms in that rock can operate more or less intensely from place to place, but they apparently produce similar structures. When more cracks or longer cracks are created, their width is proportionally increased.

From the equations (18), (19), and (20) we deduced the following results: h=1.3±0.5 10^{-3}μm, A_c/V=2100±1000 cm^{-1}, and $\langle m_o \rangle \langle \tau_o \rangle^2$=0.08±0.08 μm. The wetted area calculated is much larger than the values given by Walsh and Brace (1984): 310cm^{-1} obtained from plotting the square root of 3kF against Φ, and 46 to 170cm^{-1} from microscope studies by others (references can be found in Walsh and Brace, 1984). This large overestimation is certainly due to the inaccuracy of the value of A_F we used. Accordingly, the hydraulic radius calculated must be seriously underestimated. However, we should point out that the A_c/V's obtained from microscope studies are probably underestimated because the smallest cracks may not be counted. As a matter of fact, because of the lower resolution, the optical microscope studies consistently produced the lowest values of A_c/V. In conclusion, we should emphasize that it is critical

to have the resistivity measurements made on the same sample as the permeability and porosity measurements in order to obtain an accurate characterization of the equivalent crack.

4.2.Barre granite

The $\delta\Phi$'s for Barre granite are given in Table 2 (we used the sample labelled #2 in Bernabe, 1985a). Figure 5 shows the Φ-Φ_R's plotted against lnP during a complete pressure cycle. The relationship between Φ-Φ_R and lnP is fairly linear with A_Φ slightly higher for loading ($0.70\pm0.05\ 10^{-3}$) than for unloading ($0.64\pm0.05\ 10^{-3}$). This trend is consistent with the frictional sliding model proposed by Bernabe (1985a) to explain the hysteresis in permeability and the fact that the coefficient of the effective pressure law α depended on the order in which P_c and P_p were applied to the sample. As will be seen latter, similar trends were observed for the other properties (k and F), and for all the rocks considered in this study. Similar data by Coyner (1984) are also drawn in Figure 5, showing a very good agreement with our results ($A_\Phi=0.69\ 10^{-3}$).

Figure 6 shows examples of permeability and formation factor data (Bernabe, 1985a, Gee and Brace, 1985). The linearity is good. The values calculated for A_k and A_F are the following: sample #1, for loading, $A_k=3.7\pm0.1\ 10^{-6}m^{1/2}$, $A_F=5.5\pm0.2\ 10^{-3}$; for unloading, $A_k=3.2\pm0.1\ 10^{-6}m^{1/2}$, $A_F=4.7\pm0.1\ 10^{-3}$; sample #2, for loading, $A_k=4.1\pm0.1\ 10^{-6}m^{1/2}$, $A_F=5.9\pm0.2\ 10^{-3}$; for unloading, $A_k=3.3\pm0.1\ 10^{-6}m^{1/2}$, $A_F=4.9\pm0.5\ 10^{-3}$ (this last value was determined by extrapolation like for Westerly granite). We computed the following results: for loading $h=2.5\pm0.2\ 10^{-3}\mu m$, $\langle m_o\rangle\langle\tau_o\rangle^2=0.10\pm0.02\ \mu m$,and $A_c/V=1400\pm200\ cm^{-1}$. for unloading $h=1.9\pm0.4\ 10^{-3}\mu m$, $\langle m_o\rangle\langle\tau_o\rangle^2=0.10\pm0.04\ \mu m$,and $A_c/V=1700\pm400\ cm^{-1}$.

We can see that, within the uncertainty limits, these three parameters can be considered constant during the entire cycle.

Finally, having resistivity measurements on our samples, we could test the possible discrepancy between the exponents n and r ($\Phi \propto F^n$; $k \propto F^{-r}$ with r ranging between 1.9 and 2.1). In Figure 7 we plotted F^{-1} and $F_{-1/2}$ against lnP ($\Phi \propto \ln P$). The scales were chosen so that the two curves have comparable slopes. We can see that the linearity is better for $F^{-1/2}$ than for F^{-1}. As an alternative test, we tried to find a reasonable value of Φ_R which would produce Φ inversely proportional to F. In Figure 8, the Φ's corresponding to Φ_R=0.2, 0.3, and 0.4% are plotted against F in a log-log scale. Apparently, we did not obtain a good straight line with a slope of -1. On the other hand, the curve corresponding to 0.3% is fairly linear with a slope of -1/2. Therefore, our data seem to support values of n and r consistent with the equivalent channel model.

4.3.Pigeon Cove granite

The $\delta\Phi$'s for Pigeon Cove granite during two successive cycles are given in Table 3, and the corresponding Φ-Φ_R's are plotted in Figure 9. Like for Westerly granite and Barre granite, the linearity is excellent. We found the following results: first cycle, for loading A_Φ=1.1±0.1 10^{-3}, for unloading A_Φ=0.71±0.06 10^{-3}; second cycle, for loading, A_Φ=0.91±0.07 10^{-3}, for unloading A_Φ=0.67±0.05 10^{-3}. For both cycles we can observe the same feature than for Barre granite (A_Φ larger for loading than for unloading). This effect is slightly less pronounced during the second cycle.

Figure 10 presents examples of the permeability data (Bernabe, 1985b). As usual the linearity is quite good. The following values were calculated: first

cycle, for loading A_k=3.3±0.1 $10^{-6}m^{1/2}$, for unloading A_k=2.9±0.1 $10^{-6}m^{1/2}$; second cycle, for loading, A_k=3.1±0.1 $10^{-6}m^{1/2}$, for unloading A_k=2.8±0.1 $10^{-6}m^{1/2}$. We also obtained values of A_k and A_F from data by Coyner et al. (1979): for loading A_k=8.6 $10^{-6}m^{1/2}$, A_F=6.7 10^{-3}, and for unloading A_k=5.4 $10^{-6}m^{1/2}$, A_F=4.6 10^{-3}. Using the same procedure than for Westerly granite we evaluated A_F for our sample (for loading 3.2±0.6 10^{-3}, and for unloading 2.9±0.6 10^{-3}). From these values we derived the following results: h=2.6±0.7 10^{-3}μm, A_c/V=1600±500 cm^{-1}, and $\langle m_o \rangle \langle \tau_o \rangle^2$=0.47±0.34 μm (these values were averaged over the loading and unloading stages of the two cycles; the detailed values are reported in Table 7). Again, within the uncertainty limits, these parameters remained unchanged during the two cycles ($\langle m_o \rangle \langle \tau_o \rangle^2$ seemed to decrease slightly, but this trend cannot be considered significant).

4.4.Chelmsford granite

The $\delta\Phi$'s for the two samples of Chelmsford granite are given in Table 4, and the corresponding Φ-Φ_R's are plotted in Figure 11. The linearity is very good. We found the following results: R-sample (perpendicular to rift plane), for loading A_Φ=1.2±0.1 10^{-3}; G-sample (perpendicular to grain plane), for unloading A_Φ=1.2±0.1 10^{-3}, for unloading A_Φ=1.0±0.1 10^{-3}, which confirm the observations already made for the other rocks (A_Φ larger for loading than for unloading). Furthermore, we should note that there is no dependence on the direction in which the samples were cored. This is expected since all the cracks contribute to the fluid and electric flows independently of their relative orientations. Had a significant directional effect been observed, that would have meant that the samples were not submitted to a perfectly hydrostatic pressure due to defaults in the experimental setting (for example,

end-effects or misalignment). Measurements by Coyner (1984) are also plotted in Figure 11, showing a good agreement with our results (A_Φ=0.97 10^{-3}).

Figure 12 shows examples of the permeability data (Bernabe, 1985a), and the formation factor data (Gee and Brace, 1985). Again, the linearity is quite good. We computed the following values: R-sample, for loading A_k=8.0±0.2 $10^{-6}m^{1/2}$, A_F=7.6±0.2 10^{-3}, for unloading A_F=6.8±0.2 10^{-3}; G-sample, for loading A_k=7.0±0.2 $10^{-6}m^{1/2}$, A_F=7.5±0.2 10^{-3}, for unloading A_F=6.6±0.2 10^{-3}; H-sample (perpendicular to hardway plane), for loading A_k=7.3±0.2 $10^{-6}m^{1/2}$, A_F=8.2±0.2 10^{-3}, for unloading A_F=7.3±0.2 10^{-3}. For comparison, we report values calculated from data by Coyner et al. (1979): R-sample, for loading A_k=18.7 $10^{-6}m^{1/2}$, A_F=13.6 10^{-3}, for unloading A_k=11.4 $10^{-6}m^{1/2}$, A_F=7.3 10^{-3}; G-sample, for loading A_k=9.6 $10^{-6}m^{1/2}$, A_F=7.9 10^{-3}, for unloading A_k=6.3 $10^{-6}m^{1/2}$, A_F=6.0 10^{-3}; H-sample, for loading A_k=10.2 $10^{-6}m^{1/2}$, A_F=9.8 10^{-3}, for unloading A_k=7.3 $10^{-6}m^{1/2}$, A_F=7.1 10^{-3}. From the loading values we calculated the following results (lacking A_k for the unloading stage made the calculations impossible in this case): h=6.1±0.5 10^{-3}μm, A_c/V=1000±200 cm^{-1}, and $\langle m_o \rangle \langle \tau_o \rangle^2$=0.25±0.07 μm. These values were averaged for the different orientations (the detailed values can be found in Table 7). As already mentioned, no dependence on the orientation was observed. We found A_c/V's relatively close to 640cm^{-1}, the value reported by Walsh and Brace (1984).

With the electrical resistivity measured in the same samples than permeability and pore volume change, we could test the exponents n and r as was done for Barre granite. Again, the results seemed to support the use of the equivalent channel model.

4.5.Pottsville sandstone

The $\delta\Phi$'s for Pottsville sandstone are given in the Tables 5 and 6 (two sets of measurements were performed on the same sample; in the mean time, the sample was kept at atmospheric pressure under dry conditions; Bernabe, 1985b). Figure 13 shows the corresponding Φ-Φ_R's. As usual, the linearity is fairly good. The following values were calculated: first set, cycle #1, for loading A_Φ=3.2±0.2 10^{-3}, for unloading A_Φ=1.6±0.1 10^{-3}; cycle #2, for loading A_Φ=1.9±0.1 10^{-3}; second set, cycle #1, for loading A_Φ=2.2±0.2 10^{-3}, for unloading A_Φ=1.6±0.1 10^{-3}; cycle #5, for loading A_Φ=1.8±0.1 10^{-3}, for unloading A_Φ=1.6±0.1 10^{-3}. Again, we found A_Φ larger for loading than for unloading. Furthermore, this effect rapidly decreased with the number of cycles. After five cycles, an equilibrium state was reached where A_Φ was nearly unchanged by loading or unloading. Similar vanishing of irreversible hysteresis and stress history dependency with the number of cycles was previously observed on the same rocks (Bernabe, 1985b). These observations can be easily explained with the frictional sliding model mentioned in previous paragraphs (see also Bernabe, 1985a, b). A_Φ was also calculated for Coyner's data (1984). We found 1.6 10^{-3}, very near the equilibrium value reached after several cycles. This is in excellent agreement with our results, since Coyner submitted his samples to several seasoning cycles before running the experiments.

Figure 14 shows examples of the permeability data (Bernabe, 1985b). Again, we observed a good linearity, and we calculated the following values of A_k ($10^{-6}\mu m$): first set, cycle#1, for loading 6.6±0.2, for unloading 4.3±0.1; cycle #2, for loading 4.2±0.1; second set, cycle #1, for loading 5.0±0.1, for unloading 3.9±0.1; cycle #5, for loading 4.0±0.1, for unloading 3.9±0.1. We also obtained the following results from data by Brace and Coyner (1980), and

Brace and Orange (1968): BC, for loading A_k=5.5 $10^{-6}m^{1/2}$, A_F=10.8 10^{-3}, for unloading A_k=4.6 $10^{-6}m^{1/2}$, A_F=9.2 10^{-3}; BO, A_F=10.2 10^{-3}. Once again, we used the extrapolation technique already mentioned to evaluate A_F for our sample for loading and unloading. Then, we computed the corresponding values of the three parameters h, A_c/V, and $\langle m_o \rangle \langle \tau_o \rangle^2$, and average them. We found respectively 2.0±0.4 $10^{-3}\mu m$, 4900±1100cm^{-1}, and 0.10±0.06μm (the detailed values can be found in Table 7). Within the precision limits of this study, these parameters did not seem clearly affected by loading, unloading, and further cycling.

5.Conclusion

The general observation that $\Phi-\Phi_R$, $k^{1/4}$, and $F^{-1/2}$ were all well represented by linear functions of lnP provides sufficient justification for using the equivalent channel model. This model allows the determination of three geometrical parameters h, A_c/V, and $\langle m_o \rangle \langle \tau_o \rangle^2$ characterizing the equivalent channel. The precision in these parameters critically depends on the homogeneity of the data (simultaneously measuring all the needed quantities on the same sample is the ideal case).

Within the uncertainty limits, our results seemed to produce a fairly consistent image for the five rocks studied. A_c/V did not show any obvious correlation with porosity or permeability (for example, Chelmsford granite is more porous and more permeable than Barre granite, but presents a smaller A_c/V). h ranged from 1.5 to 6.0 $10^{-3}\mu m$ clearly increasing with increasing permeability. A similar trend was observed with $\langle m_o \rangle \langle \tau_o \rangle^2$ which roughly varied

from 0.10 to 0.35μm (but the trend was less pronounced than for h, perhaps because $\langle m_o \rangle$ and $\langle \tau_o \rangle$ cannot be separated). This suggest that permeability is predominantly controlled by the hydraulic radius (intuitively one expects h to increase with increasing m).

Within the uncertainty limits, we did not observe significant changes in these parameters with loading, unloading or the number of cycles. However, this conclusion is not definitive because of the large uncertainties in the results for Westerly granite, Pigeon Cove granite and Pottsville sandstone, and the lack of permeability data for the unloading cycles on Chelmsford granite. In fact, the results for Pigeon Cove granite suggest a slight decrease in hydraulic radius with the number of cycles. However, since the equivalent channel model seems to work satisfactorily in crystalline rocks, such trends should be observable, provided that electrical resistivity is measured in the same samples as permeability and pore volume changes.

Finally, a strong hysteresis was observed in the pore volume change data. But, this effect rapidly diminished with the number of cycles. These observations are consistent with frictional sliding models proposed in previous works (Bernabe, 1985a, b; Wissler and Simmons, 1985).

References

Bear, J., Dynamics of Fluids in Porous Media, American Elsevier Publ., New York, pp.764, 1972.

Bernabe, Y., An effective pressure law for permeability in Chelmsford granite and Barre granite, unpublished manuscript, 1985.

Bernabe, Y., The effective pressure law for permeability during pore pressure and confining pressure cycling of several crystalline rocks, unpublished manuscript, 1985.

Brace, W.F., and K.B. Coyner, unpublished data, 1980.

Brace, W.F., and A.S. Orange, Further studies of the effect of pressure on electrical resistivity of rocks, J. Geophys. Res., 73, 5407-5420, 1968.

Brace, W.F., A.S. Orange, and T.R. Madden, The effect of pressure on the electrical resistivity of water-saturated crystalline rocks, J. Geophys. Res., 70, 5669-5678, 1965.

Brace, W.F., J.B. Walsh, and W.T. Frango, Permeability of granite under high pressure, J. Geophys. Res., 73, 2225-2236, 1968.

Brown, S.R., and C.H. Scholz, Closure of random elastic surfaces in contact, J. Geophys. Res., 90, 5531-5545, 1985.

Coyner, K.B., Effects of stress, pore pressure, and pore fluids on bulk strain, velocity, and permeability on rocks, Ph.D. Thesis, M.I.T., Cambridge, 1984.

Coyner, K.B., W.F. Brace, and J.B. Walsh, New laboratory measurements of permeability and electrical resistivity of crystalline rocks (abstr.), Trans. Am. Geophys. Union, 60, 943, 1979.

Dullien, F.A.L., Porous Media: Fluid Transport and Pore Structure, Academic Press, New York, pp.396, 1979.

Gangi, A.F., Variation of whole and fractured porous rock permeability with confining pressure, Int. J. Rock Mech. Min. Sci. Geomech. Abstr., 15, 249-257, 1978.

Gee, L.S., and W.F. Brace, The dependence of electrical resistivity in granites on effective pressure (abstr.), Trans. Am. Geophys. Union, 66, 366, 1985.

Hadley, K., Comparison of calculated and observed crack densities and seismic velocities in Westerly granite, J. Geophys. Res., 81(20), 3484-3494, 1976.

Katsube, T.J., and J.B. Walsh, Effective aperture for fluid flow in crystalline rocks, unpublished manuscript, 1985.

Montgomery, C.W., and W.F. Brace, Micropores in plagioclase, Contrib. Mineral. Petrol., 52, 17-28, 1975.

Paterson, M.S., The equivalent channel model for permeability and resistivity in fluid-saturated rock - a re-appraisal, Mech. Mat., 2, 345-352, 1983.

Tsang, Y.W., and P.A. Witherspoon, Hydromechanical behavior of a deformable rock fracture subject to normal stress, J. Geophys. Res., 86, 9287-9298, 1981.

Walsh, J.B., Effect of pore pressure and confining pressure on fracture permeability, Int. J. Rock Mech. Min. Sci. Geomech. Abstr., 18, 429-435, 1981.

Walsh, J.B., and W.F. Brace, The effect of pressure on porosity and the

transport properties of rocks, J. Geophys. Res., 89, 9425-9431, 1984.

Walsh, J.B., and M.A. Grosenbaugh, A new model for analyzing the effect of fractures on compressibility, J. Geophys. Res., 84, 3532-3536, 1979.

Wissler, T.H., and G. Simmons, The physical properties of a set of sandstones, II: permanent and elastic strains in hydrostatic compression to 200MPa, Int. J. Rock Mech. Min. Sci. Geomech. Abstr., in press, 1985.

Wyllie, M.R.J., and W.D. Rose, Some theoretical considerations related to the quantitative evaluation of the physical characteristics of reservoir rock from electrical log data, Trans. Am. Inst. Mech. Eng., 189, 105-118, 1950.

	Loading
P_c (MPa)	
20	
	-0.52
40	
	-0.28
60	
	-0.19
80	
	-0.14
100	
	-0.12
120	

Table 1: The fluid volume changes $\delta\Phi$ during confining pressure cycling of a sample of Westerly granite (P_p=10MPa). The results showed here are normalized to the sample volume ($7.2cm^3$), and must be multiplied by 10^{-3}.

P_c (MPa)	Loading	Unloading
40		
	-0.78	+0.73
60		
	-0.35	+0.35
80		
	-0.22	+0.19
100		
	-0.19	+0.16
120		
	-0.15	+0.12
140		
	-0.11	+0.10
160		

Table 2: The $\delta\Phi$'s during confining pressure cycling of a sample of Barre granite (labelled #2 in Bernabe, 1985a; P_p=30MPa). These values must be multiplied by 10^{-3}.

P_c (MPa)	cycle #1		cycle #2	
	Loading	Unloading	Loading	Unloading
40	-0.48	+0.36	-0.38	+0.32
60	-0.36	+0.24	-0.30	+0.22
80	-0.28	+0.17	-0.24	+0.17
100	-0.24	+0.14	-0.19	+0.14
120	-0.19	+0.13	-0.18	+0.13
140	-0.19	+0.10	-0.19	+0.10
160				

Table 3: The $\delta\Phi$'s for Pigeon Cove granite during two confining pressure cycles (P_p=10MPa). These results must be multiplied by 10^{-3}.

P_c (MPa)	G-sample		R-sample
	Loading	Unloading	Loading
40	-0.72	+0.73	-0.70
60	-0.46	+0.40	-0.51
80	-0.35	+0.29	-0.37
100	-0.30	+0.23	-0.27
120	-0.24	+0.18	-0.24
140	-0.21	+0.15	-0.20
160	-0.17	+0.14	-0.18
180			

Table 4: The $\delta\Phi$'s during confining pressure cycling of two oriented samples of Chelmsford granite (P_p=20MPa). These results must be multiplied by 10^{-3}.

	cycle #1		cycle #2
P_c (MPa)	Loading	Unloading	Loading
40	-2.36	+0.73	-0.94
60	-0.83	+0.52	-0.68
80	-0.73	+0.39	
100	-0.58	+0.33	
120	-0.50	+0.29	
140	-0.44	+0.27	
160	-0.36	+0.24	
180	-0.31	+0.21	
200			

Table 5: The $\delta\Phi$'s for a sample of Pottsville sandstone during two confining pressure cycles (P_p=10MPa). These results must be multiplied by 10^{-3}.

P_c (MPa)	cycle #1		cycle #5	
	Loading	Unloading	Loading	Unloading
60	-0.91			
80	-0.79	+0.48	-0.57	+0.50
100	-0.58	+0.38	-0.44	+0.39
120	-0.49	+0.34	-0.40	+0.34
140	-0.44	+0.28	-0.35	+0.29
160				

Table 6: The $\delta\Phi$'s for Pottsville sandstone during five confining pressure cycles (P_p=10MPa). The measurements were made during the first and the fifth cycles only. These results must be multiplied by 10^{-3}.

			h ($10^{-3}\mu m$)	A_c/V (cm^{-1})	$\langle m_o \rangle \langle \tau_o \rangle^2$ (μm)
Westerly (10nd)		L	1.3±0.5	2100±1000	0.08±0.08
Barre (100nd)		L	2.5±0.2	1400±200	0.10±0.02
		U	1.9±0.3	1700±400	0.10±0.04
Pigeon Cove (150nd)	#1	L	2.9±0.7	1900±600	0.63±0.46
		U	2.5±0.6	1400±500	0.42±0.31
	#2	L	2.6±0.7	1700±600	0.46±0.33
		U	2.3±0.6	1400±500	0.37±0.27
Pottsville (500nd)					
1st. set	#1	L	3.0±0.7	5400±1600	0.12±0.08
		U	1.8±0.2	4400±800	0.07±0.04
	#2	L	1.8±0.3	5200±1200	0.10±0.06
2nd. set	#1	L	2.7±0.5	4000±900	0.19±0.09
		U	1.7±0.3	4700±1100	0.09±0.06
	#5	L	1.8±0.3	5100±1200	0.11±0.07
		U	1.7±0.3	4700±1100	0.09±0.06
Chelmsford (1000nd)	R	L	7.3±0.6	800±150	0.30±0.06
	G	L	5.7±0.5	1100±200	0.24±0.05
	H	L	5.6±0.5	1100±300	0.20±0.06

Table 7: The values of h, A_c/V, and $\langle m_o \rangle \langle \tau_o \rangle^2$ calculated for all our samples in all the cycling conditions (the letters L and U respectively refer to loading and unloading, the number of the cycle is given for Pigeon Cove granite and Pottsville sandstone, and also the orientation of the samples for Chelmsford granite). The order of magnitude of permeability is indicated for each rock.

Figure captions

Figure 1: Electrical resistivity ρ plotted versus crack porosity Φ_c on a log-log scale for Casco granite (C), Stone Mountain granite (SM), Rutland quartzite (R), Westerly granite (W), and Cape Cod granodiorite (CC) after Brace, Orange, and Madden (1965). The scales are not specified because we had to translate the data for some of the rocks in order to have the complete set fitting into a single diagram (this operation does not change the slope of the curves).

Figure 2: Φ-Φ_R versus lnP for Westerly granite (solid circles). The other symbols represent similar data from Coyner (1984), and Brace, Orange, and Madden (1965). The reference point is indicated by a larger solid circle labelled P_R. Error bars were drawn to show the precision in the determination of the slope A_Φ.

Figure 3: $k^{1/4}$ versus lnP for Westerly granite (Bernabe, 1985b). The solid symbols correspond to the ordinary effective pressure law ($P=P_c-P_p$), and the open ones to a more realistic law derived from Bernabe (1985b). We can see that the slope A_k does not vary much when the effective pressure law is changed.

Figure 4: A_F versus A_k for several samples of Westerly granite (the circles and the square correspond to CBW, and the triangle to BOM-BWF). The point interpolated for our sample is also given as well as the expected error bar.

Figure 5: Φ-Φ_R versus lnP for Barre granite. The solid symbols correspond to loading, and the open ones to unloading. Similar data from

Coyner (1984) are also plotted for comparison. The error bars indicated for the unloading cycle were calculated without including the errors previously made during the loading cycle (we are only interested in evaluating the uncertainty on the slope A_Φ).

Figure 6: Examples of $k^{1/4}$ (solid symbols) and $F^{-1/2}$ (open symbols) versus lnP for Barre granite (the data were collected on the same sample; for permeability, Bernabe, 1985a; for resistivity, Gee and Brace, 1985).

Figure 7: The average values of F^{-1} (circles) and $F^{-1/2}$ (triangles) plotted against lnP for Barre granite (Gee and Brace, 1985). The linearity is better for $F^{-1/2}$ than for F^{-1}.

Figure 8: The conducting porosity Φ for several reasonable values of Φ_R (0.2, 0.3, and 0.4%) plotted against F in a log-log scale for Barre granite. Two segments with slope of -1 and -1/2 are also indicated for comparison with the different curves.

Figure 9: Φ-Φ_R versus lnP for Pigeon Cove granite (the circles correspond to the first cycle, and the triangles to the second).

Figure 10: An example of $k^{1/4}$ versus lnP for Pigeon Cove granite (cycle #1, for loading; Bernabe, 1985b).

Figure 11: Φ-Φ_R versus lnP for Chelmsford granite (the circles correspond to the G-sample, and the triangles to the R-sample). Similar data from Coyner (1984) are also plotted for comparison.

Figure 12: Examples of $k^{1/4}$ (solid symbols; data for G-sample from Bernabe, 1985a) and $F^{-1/2}$ (open symbols; data for R-sample from Gee and Brace, 1985) versus lnP.

Figure 13: Φ-Φ_R versus lnP for Pottsville sandstone (the circles

correspond to the first set of measurements, and the triangles and squares to the second set). Similar data from Coyner (1984) are also plotted for comparison. Remark that the reference point had to be changed twice during these experiments.

Figure 14: Examples of $k^{1/4}$ versus lnP for Pottsville sandstone (the circles correspond to the first set, cycle #1, for loading, and the squares to the second set, cycle #1, for loading).

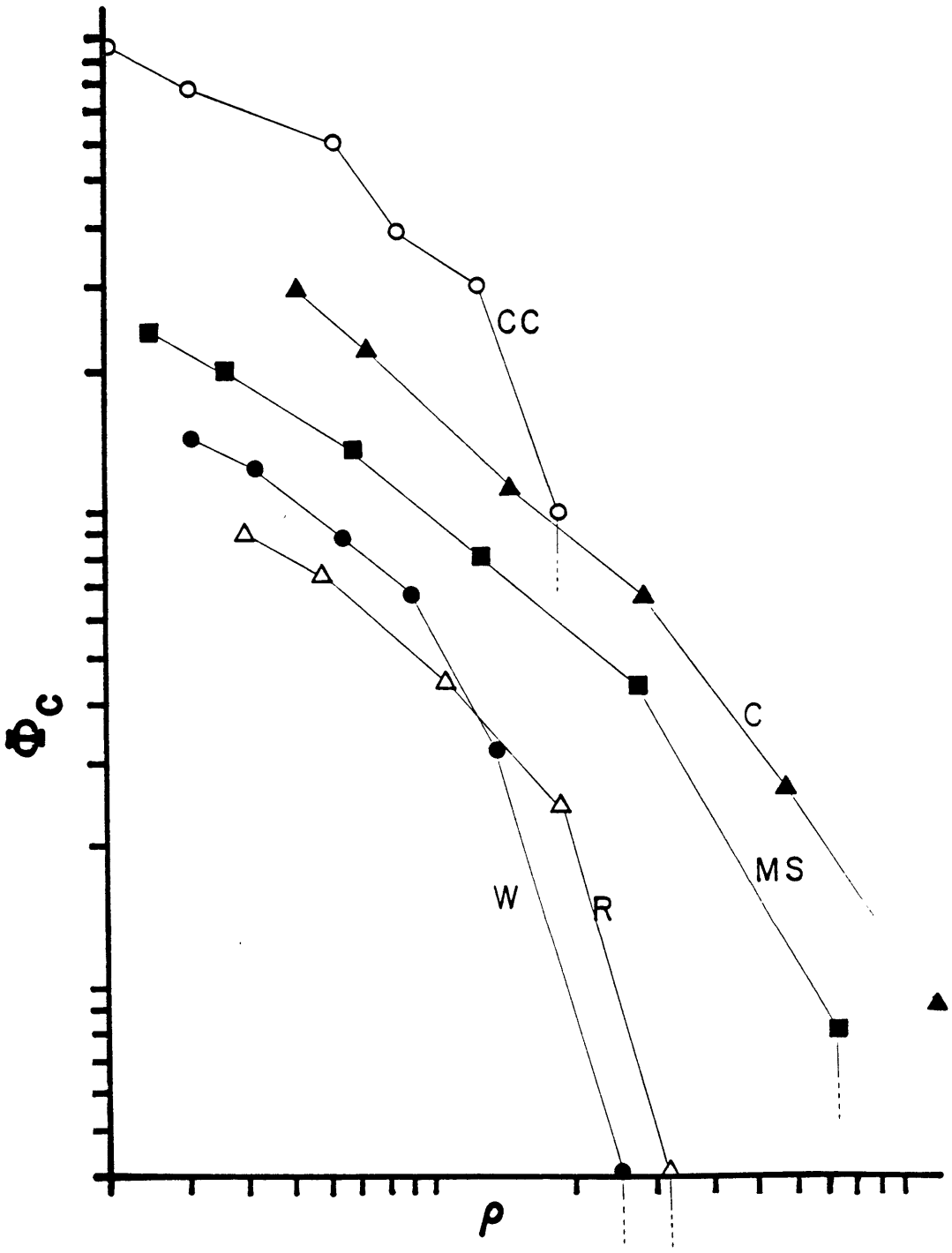

Figure 1:

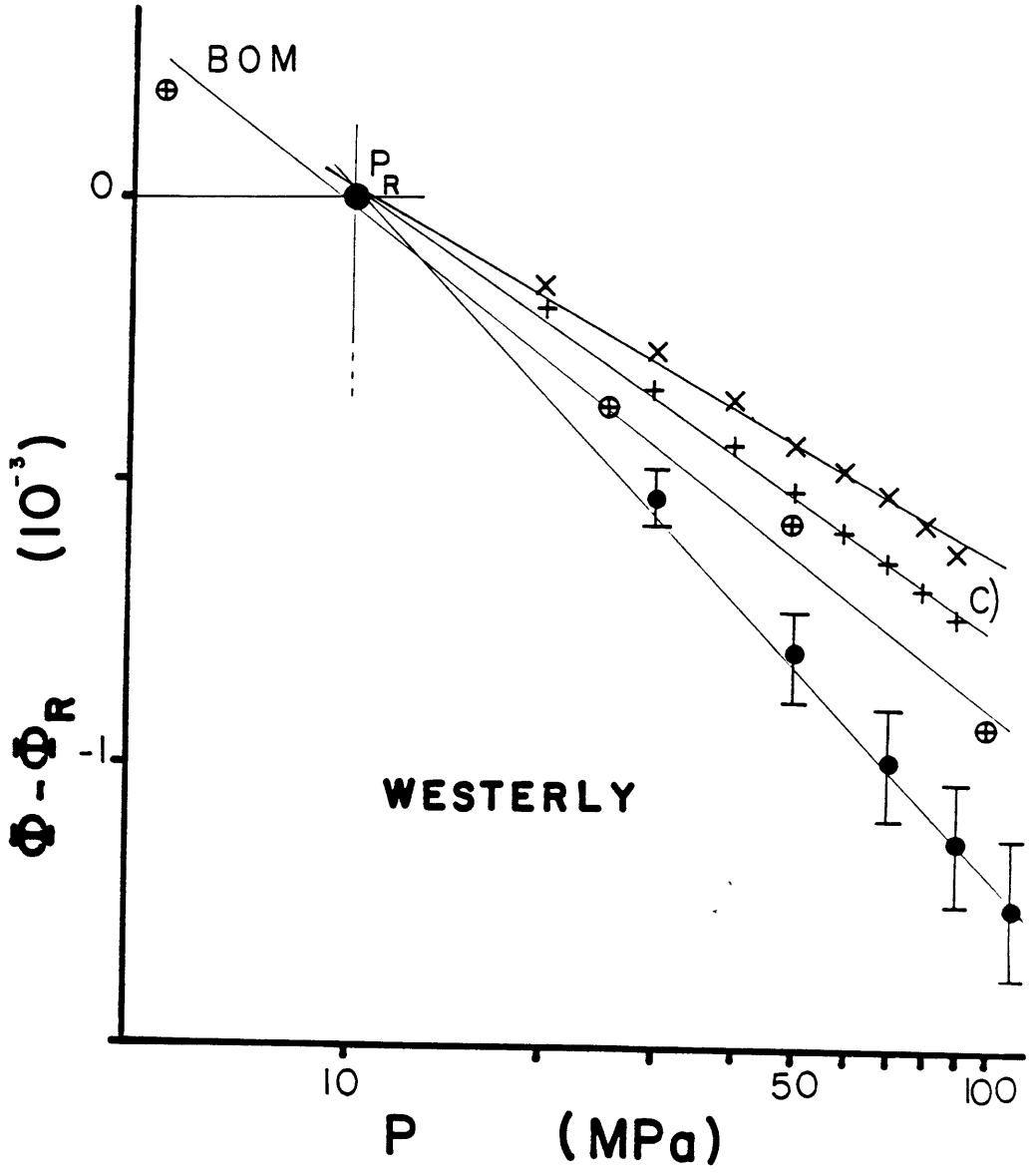

Figure 2:

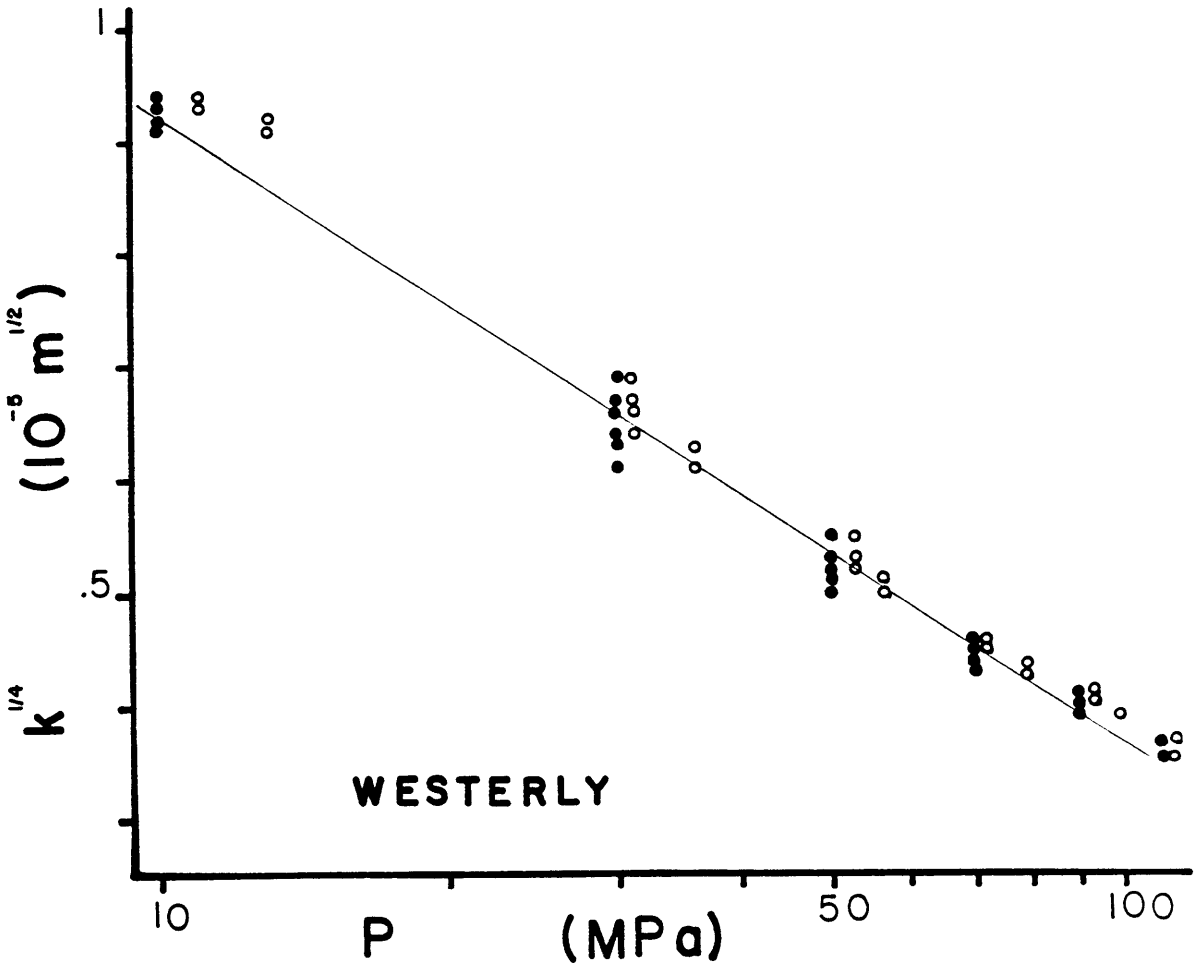

Figure 3:

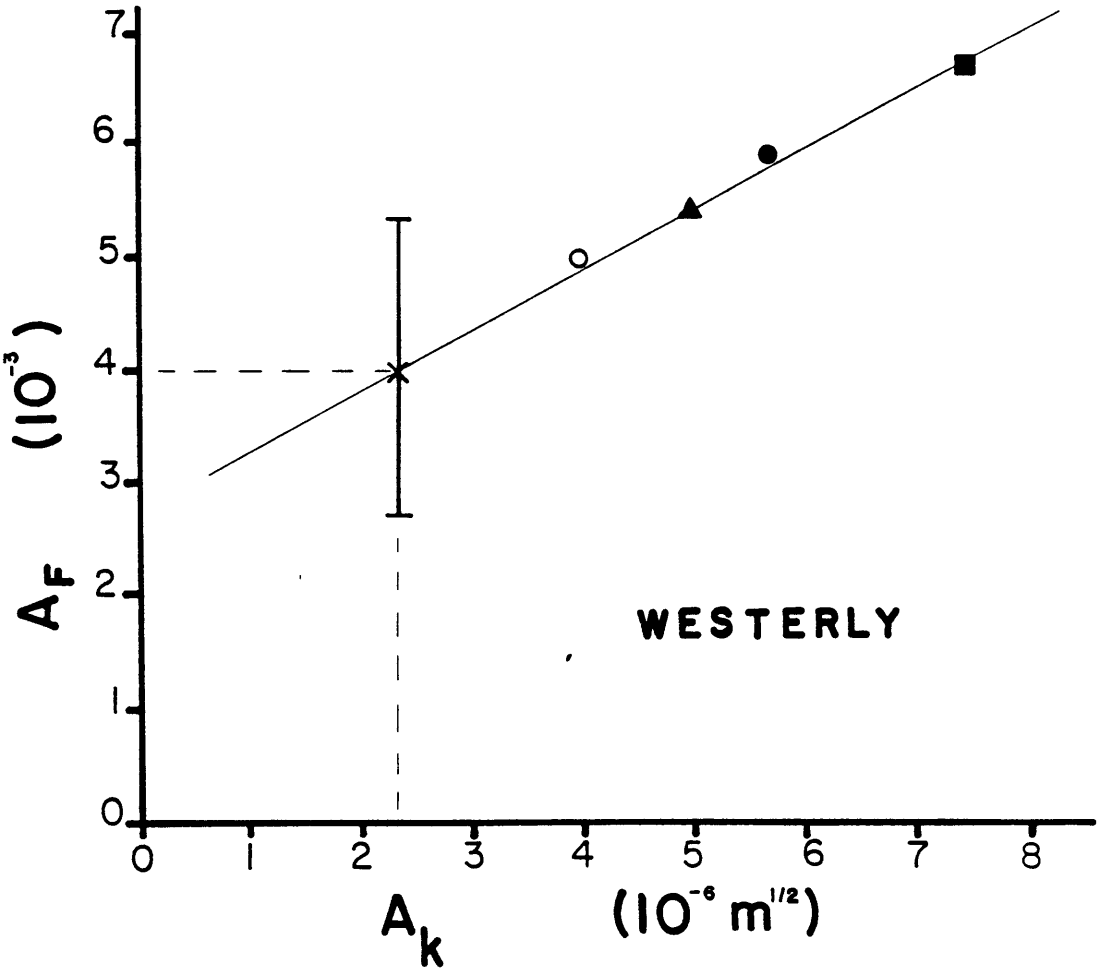

Figure 4:

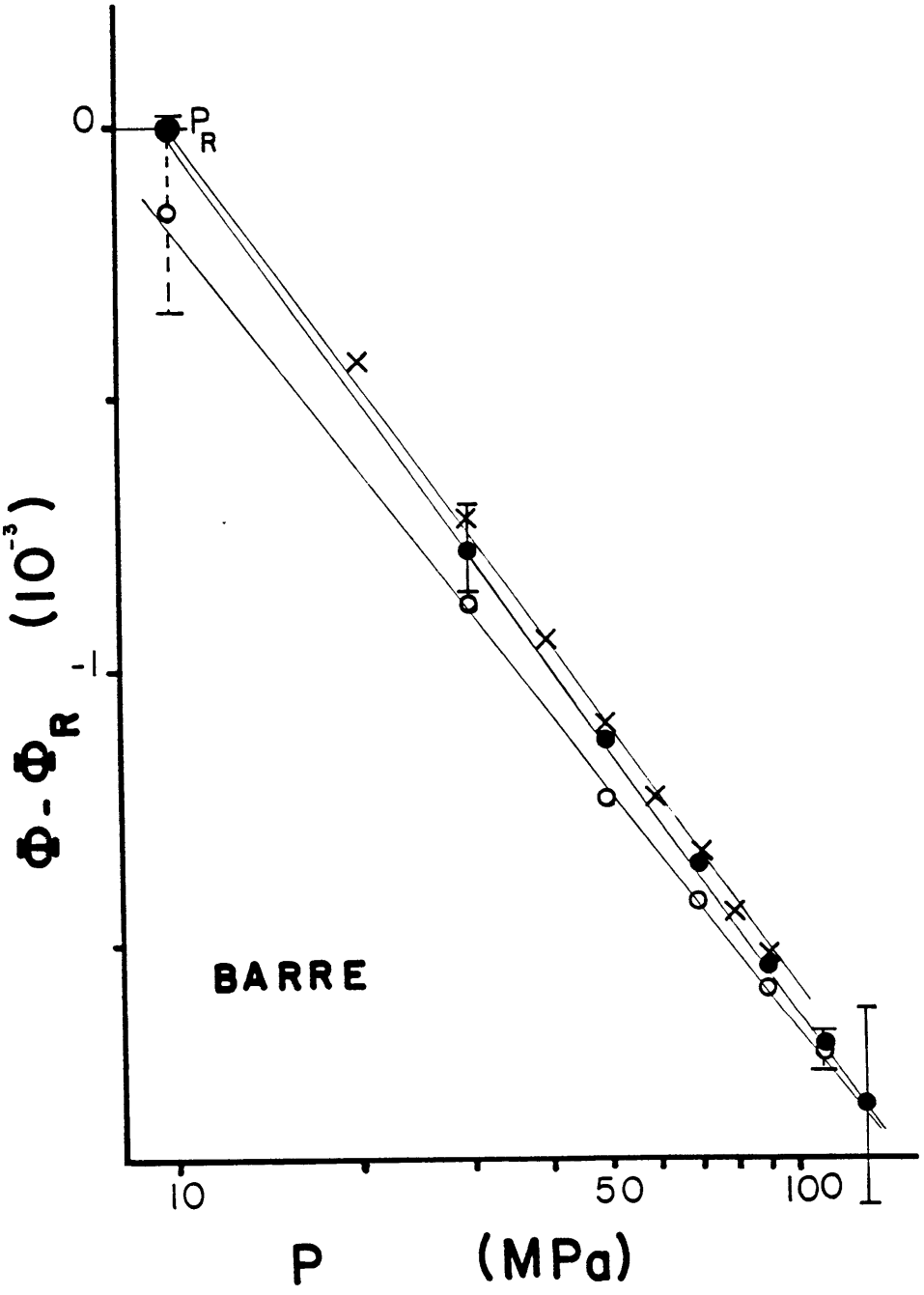

Figure 5:

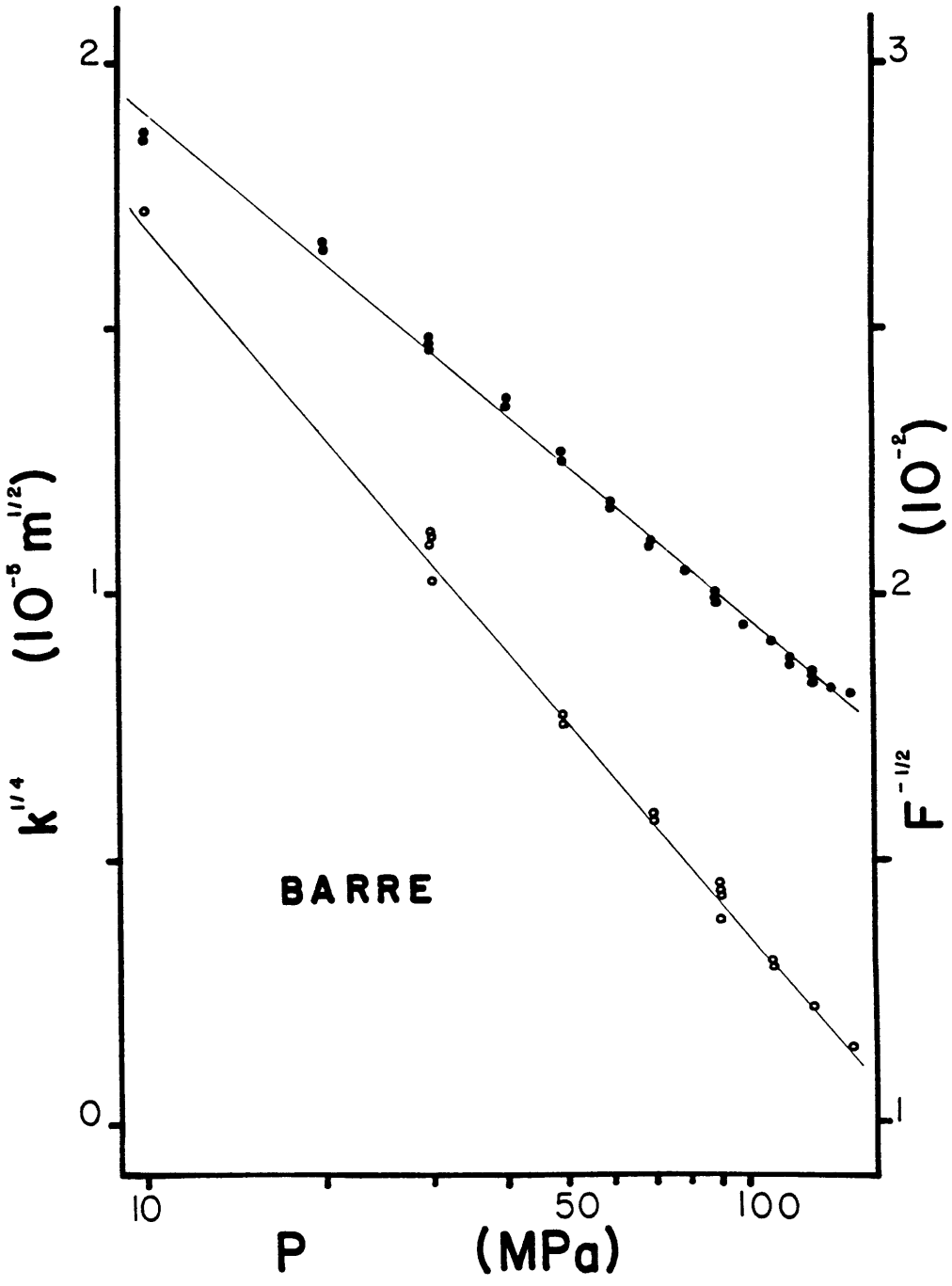

Figure 6:

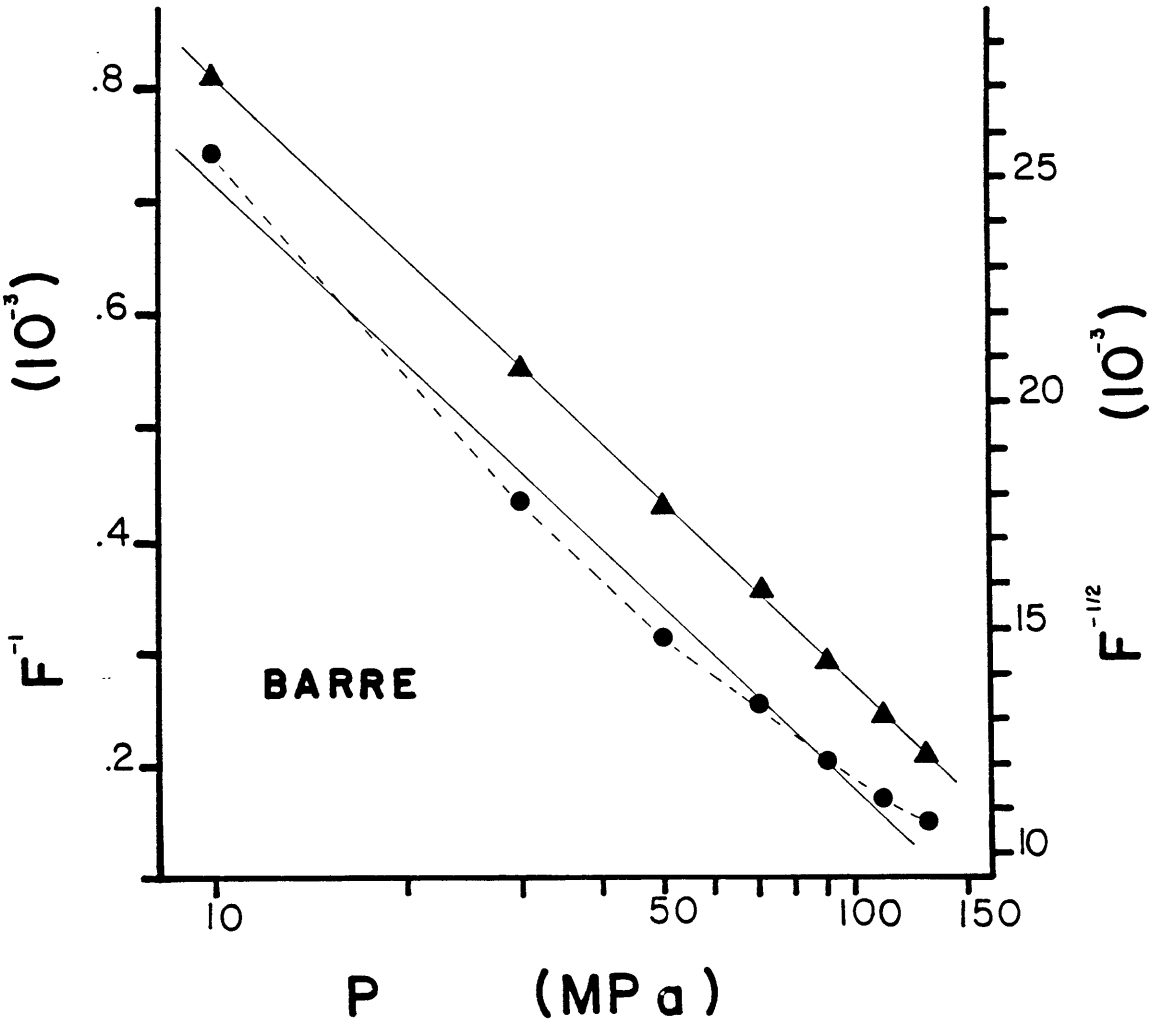

Figure 7:

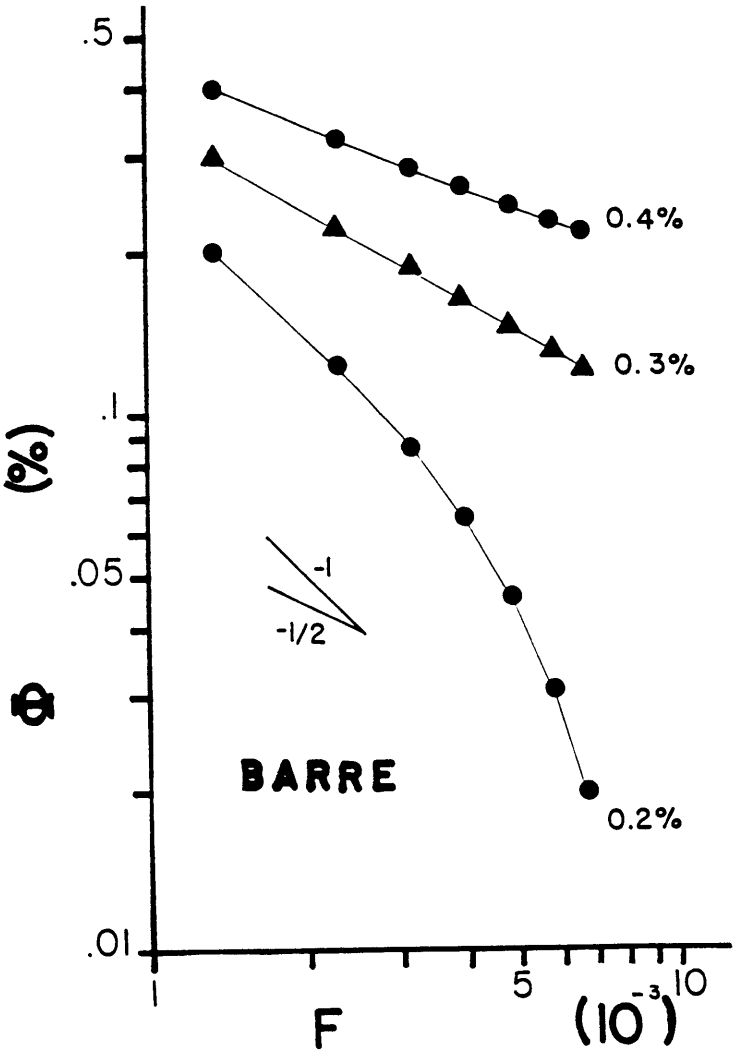

Figure 8:

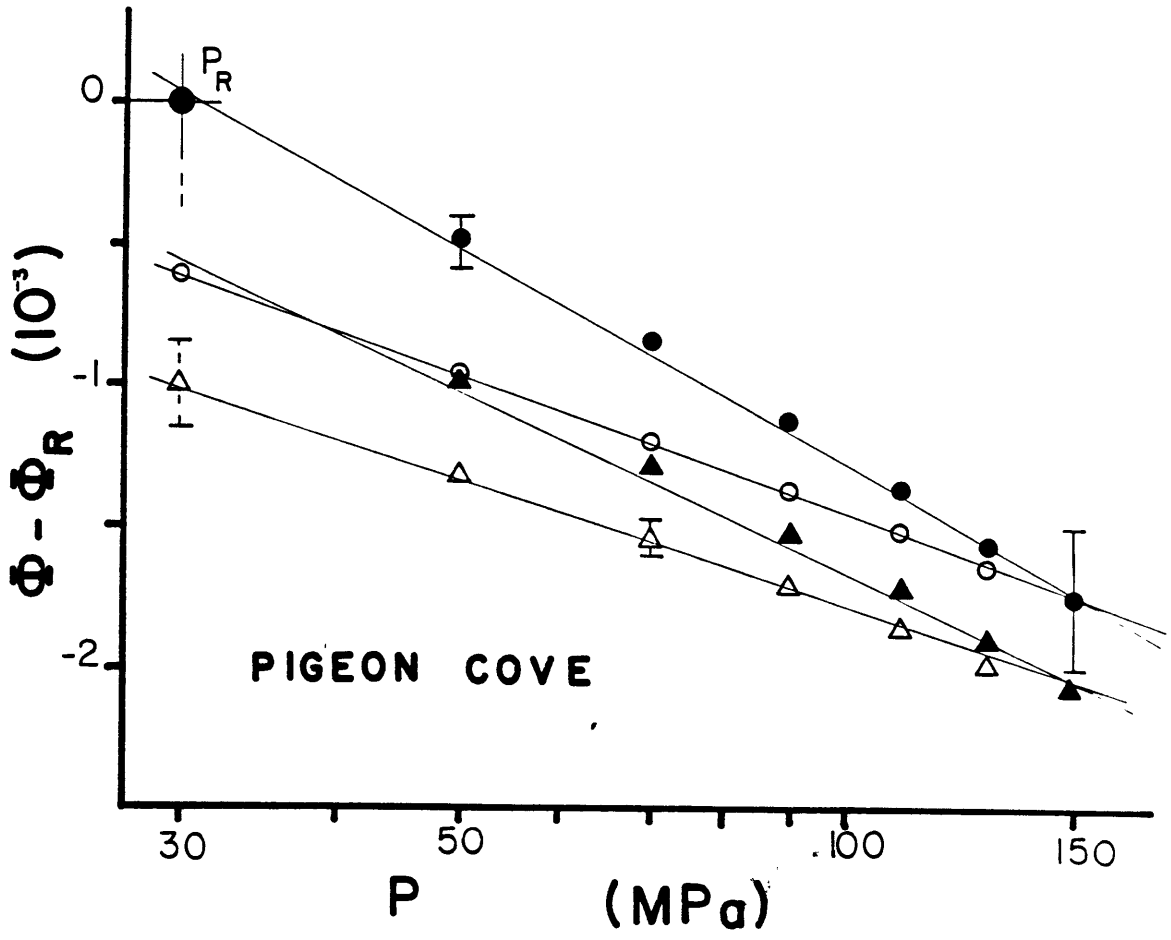

Figure 9:

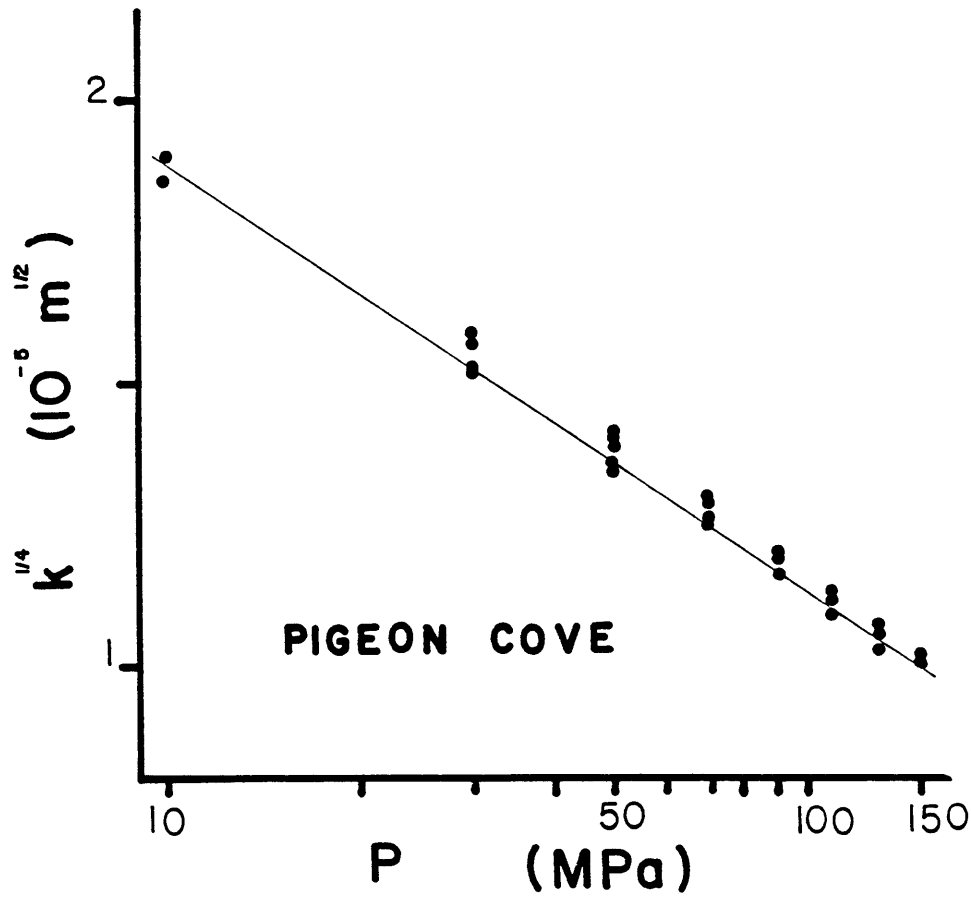

Figure 10:

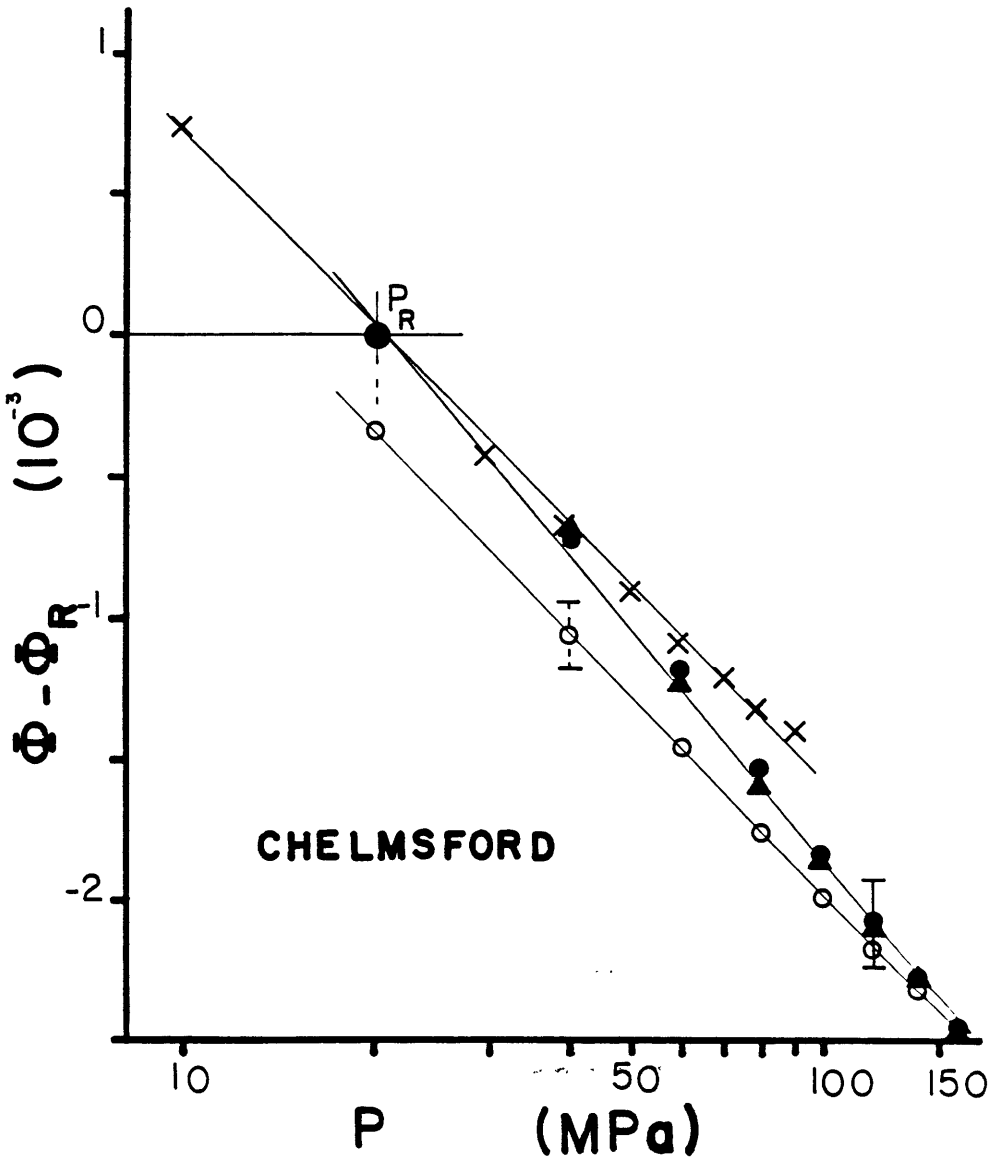

Figure 11:

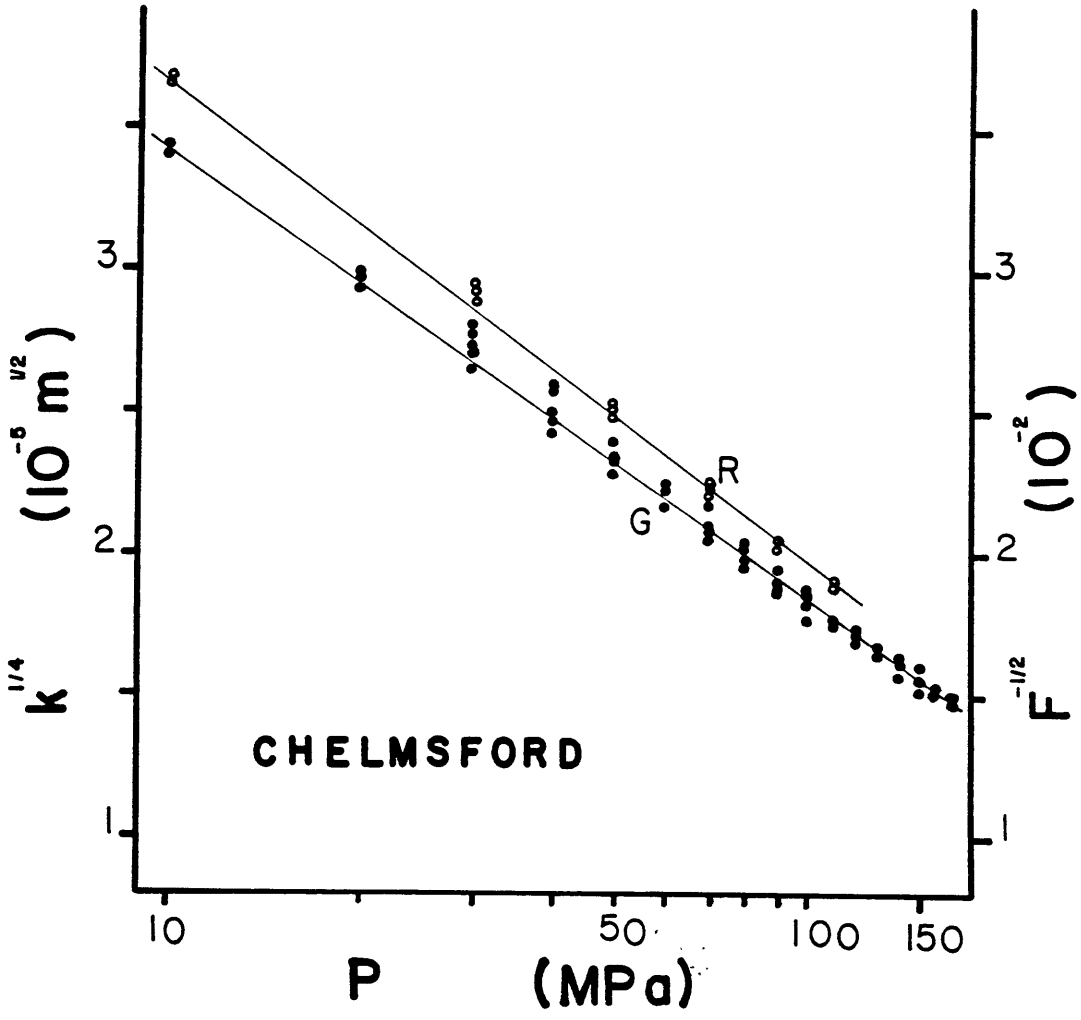

Figure 12:

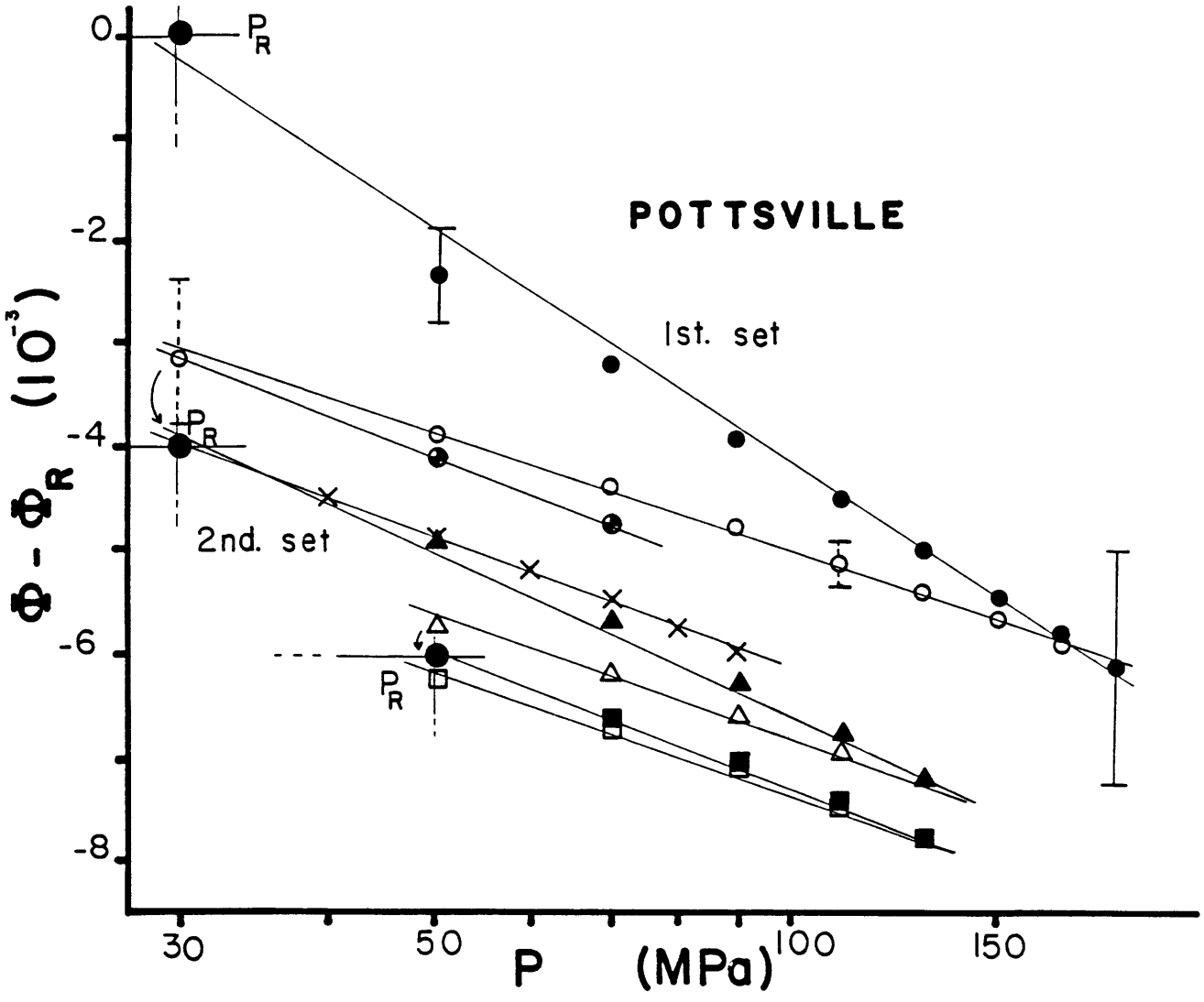
POTTSVILLE
1st. set
2nd. set
P_R
P_R
P_R
0
-2
-4
-6
-8
$\Phi - \Phi_R$ (10^{-3})
30
50
100
150
P (MPa)

Figure 13:

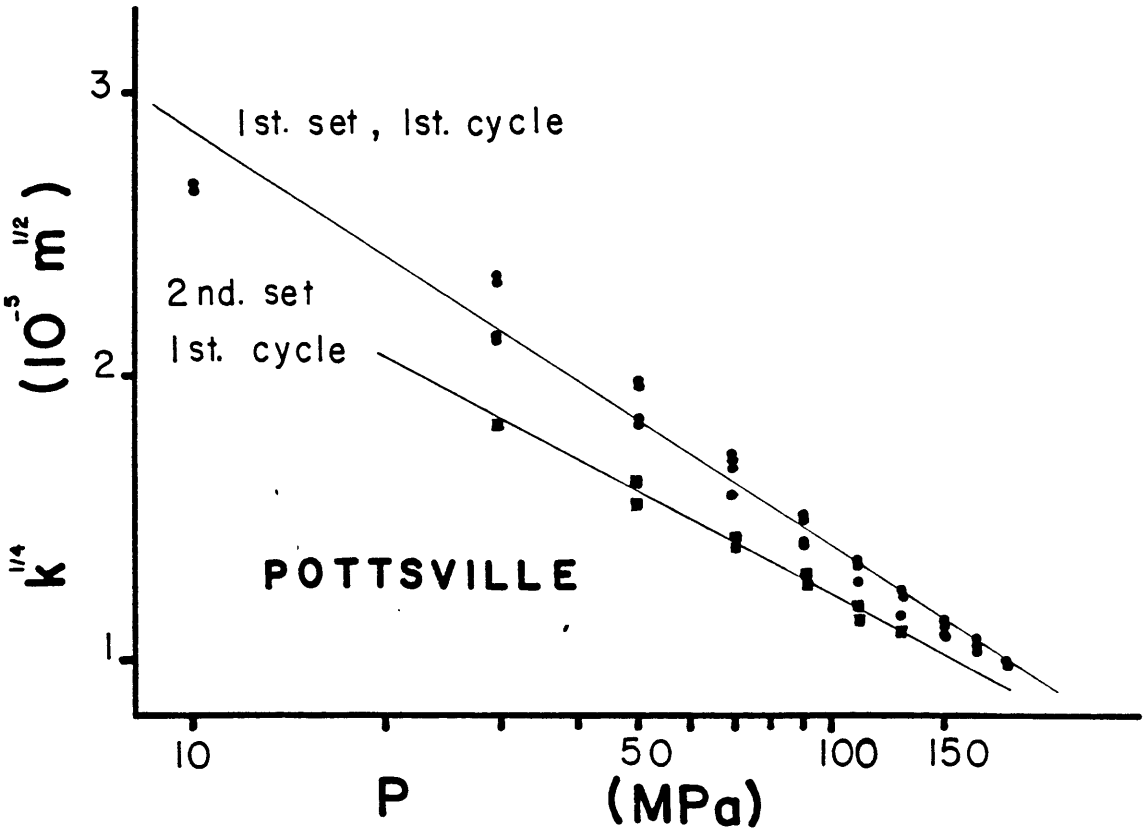
3
2
1
1st. set , 1st. cycle
2nd. set
1st. cycle
POTTSVILLE
$K^{1/4}$ $(10^{-5}\ m^{1/2})$
10
50
100
150
P (MPa)

Figure 14:

CHAPTER 5:

A WIDE RANGE PERMEAMETER FOR USE IN ROCK PHYSICS: TECHNICAL NOTE.

INTRODUCTION

The permeability of geological materials ranges over more than 10 orders of magnitude, from as high as $10^{-11}m^2$ (or 10.darcys) in sand to as low as $10^{-23}m^2$ (or 0.01nd) in shales [1]. Moreover, within a single class of rocks the permeability can vary dramatically. Sandstones range from 10^{-12} to $10^{-16}m^2$, limestones and dolomites from 10^{-14} to $10^{-21}m^2$, and granites from 10^{-17} to $10^{-21}m^2$. Also, a single rock may show a strong dependence of permeability on confining pressure and pore pressure. To study such dependence, an apparatus was designed which was capable of measuring about 8 orders of magnitude in permeability under high confining pressure. A first version of this permeameter was built in 1981 and used for synthetic rocks (hot-pressed quartz and calcite) prepared in the laboratory to different porosities; permeability ranged from 10^{-15} to $10^{-20}m^2$. To extend this work to even less permeable samples, a second, more elaborate version capable of permeabilities as low as $10^{-22}m^2$ under pressures up to 200MPa was built. The upper limit is around $10^{-14}m^2$. This new system also enabled the pore volume changes to be measured.

THE DESIGN PRINCIPLE

The main idea was to extend the range of the apparatus by making it usable under both the steady-state flow method and the transient flow method [2]. Trimmer et al. [3] built a similar system for permeabilities ranging from 10^{-11} to $10^{-21}m^2$. They even attempted to extend the capability of their apparatus to $10^{-24}m^2$ by using only a portion of the decay curve (see paragraph on transient

flow method), but this technique is likely to increase the uncertainty drastically. Our system is schematically represented in Figure 1. It was designed to allow switching from one operating mode to the other as necessary, without changing the conditions of pressure (therefore avoiding unnecessary pressure cycles). Figures 2 and 3 show photographs of the newest version of the permeameter.

Steady-state flow method

A constant pore pressure gradient is applied across the sample and the volume of fluid flowing through it per unit time is measured. the permeability k is given by Darcy's law

$$(V_f/A\delta t) = k\ (\delta P_p/\mu L) \qquad (1)$$

where V_f is the volume of fluid measured, δt the time interval, A the cross-sectional area of the sample, L the sample length, δP_p the pore pressure difference across the sample, and μ the fluid viscosity. Since very small volumes of fluid are not easily measured, this method is better suited for high permeabilities. The system is set on steady-state mode by closing the valves 1,4, and 7 (see Figure 1). A small "leak" is then created on the downstream side of the sample by slightly opening the metering valve (see Appendix). The leakage flow is adjusted in order to keep δP_p constant at a value small enough to ensure that the flow is laminar (0.1 to 0.5MPa). δP_p is recorded using a differential pressure transducer (see Appendix), which was calibrated by comparison with a Heise bourdon tube gage (at 45°C, 1mV=0.538±0.002MPa). A bladder-type accumulator (see Appendix) maintains the pressure nearly constant on the upstream side of the sample despite large variations of volume of fluid. The upstream pressure is measured by an absolute

pressure transducer (see Appendix; at 45°C, 1mV=1.16±0.01MPa). The accumulator has a fixed operating pressure of 15MPa. As a consequence, the pore pressure cannot be varied when using the steady-state flow method. The flow is determined by simply measuring the volume of fluid coming out of the system during a given length of time.

The accuracy of the measurements essentially depends on how constant δP_p can be kept (A, L, μ, V_f, and δt are all measured with a precision of a few tenth of percent). Since they are made with different elements (tubing, valves, O-rings, and so on), the upstream and downstream reservoirs react differently to temperature changes. Therefore, ambient temperature fluctuations can induce perturbations of δP_p. In the first version of this apparatus, despite an imperfect temperature control, the uncertainty was estimated around 10% [2]. As will be showed latter, the temperature control of the new system was vastly improved. But, the new apparatus has not been tested yet in steady-state flow mode, and it is difficult to guess how much was gained in measurement quality.

Transient flow method

When the sample permeability is too low for the steady-state flow method, the transient flow method (also called pulse decay method) must be used [4]. We start with the pressure in equilibrium in the whole system. Then, the pressure is suddenly changed on one side of the sample. As a convention, this side will be called the upstream side, without considering in which direction the fluid actually flows (that depends on the sign of the pressure pulse generated). We can remark that, with this convention, upstream and downstream are exchanged when switching from steady-state flow method to transient flow method. The pressure is then let free to return to equilibrium. Under certain conditions,

the pressure decay is approximately exponential and the decay time inversely proportional to the permeability as showed by the following equations [4]

$$\delta P_p(t) \propto \exp(-\alpha t) \tag{2}$$

and

$$\alpha = \{Ak(C_u+C_d)\}/\{\mu L C_u C_d\} \tag{3}$$

where t is the time, C_u and C_d are the compressive storages of the upstream and downstream reservoirs, defined as the ratios of the change of fluid volume by the corresponding pore pressure variation ($C=\partial V/\partial P$). They are physical constants of the apparatus, and, hence, must be experimentally determined. Following Lin's suggestion [5], the system was designed so that reservoirs with different compressive storage could be used to better suit the rock properties. The system is set on transient flow mode by closing the valves 1, 2, 7, and either 4 or 6 depending on which one of the two possible upstream reservoirs needs to be used (in the first case C_u=1.22±0.06 $10^{-9}m^3$/MPa, and C_d=49.2±0.3 $10^{-9}m^3$/MPa; in the second case C_u=8.93±0.08 $10^{-9}m^3$/MPa, and C_d=41.5±0.5 $10^{-9}m^3$/MPa). Notice that the accumulator can be included in the downstream reservoir when the pore pressure is 15MPa. In this case, C_d can be considered infinitely large. In their excellent analysis of the transient flow method Hsieh et al. [6] and Neuzil et al. [7] show that the validity of the exponential approximation depends on the comparison of C_u and C_d with the sample compressive storage C_s. They considered the parameters $\beta=C_s/C_u$ and $\gamma=C_d/C_u$. The Figure A-2 in [7] shows that, when γ is larger than 1.0 (always true in this apparatus), the condition of validity is $\beta<0.2$ (the error is of the order of 2% for $\beta=0.2$). An upper limit of C_s can be evaluated by simply remembering that the effect of pore pressure on pore volume is at the

most equal to that of confining pressure. And, the variations of pore volume when shifting the confining pressure were routinely measured for all the rocks considered [8]. C_s was then found ranging between 0.2 and 0.04 $10^{-9}m^3/MPa$ except for Pottsville sandstone at low confining pressure (0.8 $10^{-9}m^3/MPa$). Therefore, the condition of validity was satisfied for all the rocks studied. Of course, for other rocks it may be necessary to use the general solutions of [6], rather than the exponential approximation.

Here also, unstable ambient temperature is the main source of noise in the data. Figures 4 and 5 show examples of decay curves at high and low permeabilities and the effect of temperature fluctuations. The good linearity of these curves in a semi-log plot provides another justification for using the exponential approximation. In the average, the uncertainty in α was estimated around 5%. But, the uncertainty increases with decreasing permeabilities, since the thermal fluctuations tend to increase with increasing intervals of time. In any case, it is important to record the longest possible portion of the decay curve (at least until δP_p decayed to one quarter of its initial value). Otherwise, it might not be possible to appreciate the effect of temperature fluctuations.

All the possible configurations of upstream and downstream reservoirs were tested on Pottsville sandstone under constant conditions of pressure. There was very little discrepancy observed on the k's measured (<10%). Let's also recall that the first apparatus was tested under both steady-state flow method and transient flow method on samples of hot-pressed quartz, the permeability of which precisely ranged in the overlapping region where both methods are applicable, showing a good agreement of the two methods (about 10% [2]).

THE TEMPERATURE CONTROL SYSTEM

As shown schematically in Figure 1, the system is almost completely enclosed inside an isothermal air-flow oven (see Appendix) represented in Figure 6. The controlling system in the oven is compensated for room temperature fluctuations. During the experiments, the oven temperature was set at 45°C and constantly recorded using a chromel-constantan thermocouple and an electronic ice point reference (see Appendix). The Figures 4 and 5 give typical examples of the oven temperature variations with time. The oven temperature was usually very stable for small intervals of time (1 hour). When the temperature was accidentally unstable, the measurements were systematically done again. The fluctuations were as high as 0.2°C for longer length of time (1 day). These temperature variations arose because the temperature of the outside air providing the cooling, was not constant, and these changes in cooling were only imperfectly compensated by the heating system.

In order to evaluate the effect of a known temperature change on the decay curves, I performed the following experiment: during a measurement the door of the oven was opened for one minute producing a temperature drop of about 1.0°C. Figure 7 shows how the pressure decay was affected by this temperature perturbation. Before the temperature pulse was generated, the curve was fairly linear. Afterwards, the decay curve remained perturbed for about 20 minutes, and then, became linear again. The two linear segments are fairly parallel but a significant offset can be observed. A similar behavior was sometimes observed for certain measurements at very low permeabilities (Figure 8). In these cases, α was measured using the segments where the temperature was relatively stable.

TESTING THE PERMEAMETER FIDELITY

The measurements were usually repeated twice with pressure pulses of opposite signs. Let's call δk_o the difference between the two measurements normalized to their mean value ($\delta k_o = 2|k^+ - k^-|/[k^+ + k^-]$). The values of δk_o for all the measurements are given in Figure 9 in the form of a histogram. 75% of the measurements yielded δk_o's lower than 0.05, while it was only less than 0.08 in 90% of the cases. Thereafter, these two values will be noted $\delta k_o(75)$ and $\delta k_o(90)$. Similar histograms corresponding to different ranges of permeability are plotted in Figure 10. For permeabilities higher than $10^{-20} m^2$, $\delta k_o(75)$ and $\delta k_o(90)$ are equal to 0.05 and 0.07 respectively, whereas they take higher values (0.07 and 0.13) for lower permeabilities. This indicates that the uncertainty on the relative values of k increases with decreasing k. The histograms for each rock are given in Figure 11. There is a significant improvement for Pottsville sandstone and Pigeon Cove granite in comparison with Chelmsford granite and Barre granite which were studied first (Chelmsford and Barre: $\delta k_o(75)=0.06$, $\delta k_o(90)=0.09$; Pottsville and Pigeon Cove: $\delta k_o(75)=0.04$, $\delta k_o(90)=0.06$). These rocks cover comparable ranges of permeability, and the behavior of the temperature control system has never noticeably changed. Therefore, this amelioration reflects an improvement of the operator's patience, waiting longer intervals of time to ensure that the system was at equilibrium before starting a measurement (about 5 times the decay time after a change in pore pressure or confining pressure, and of the order of the decay time between the repeated measurements). The results for Westerly granite are not as accurate as for the other rocks ($\delta k_o(75) \approx 0.10$, $\delta k_o(90) \approx 0.17$), which is due to

its very low permeability. Among other things, it was not always possible to wait the required intervals of time (2 weeks for a 3 days decay time).

PORE VOLUME CHANGE MEASUREMENTS

During pressurization a certain volume of pore fluid is squeezed out of the sample. As a consequence, the fluid pressure increases in the system. But it can be restored to its initial value with the help of the metering valve or the volumometer (1 turn of the metering valve produces a variation of volume of $1.095 \pm 0.002 cm^3$, and 1 turn of the volumometer changes the reservoirs volume by $0.3572 \pm 0.0007 cm^3$). The system is set in volume measurement mode by closing the valves 2, 3, and 4 (or 6), and opening the valve 1 (Figure 1). The pressure change is measured with both the absolute pressure transducer and the differential pressure transducer (one side of it is isolated from the sample, and therefore, provides a constant pressure reference). Valve 1 is used to allow a fast communication between the two sides of the sample. Without it, the measurements would be very long and difficult for samples with a low permeability. As a matter of fact, the fluid pressure would change differently on both sides of the sample, and it would be necessary to wait until equilibrium is established. For the same reason, restoring the initial pressure with the metering valve would be almost unmanageable.

A small portion of the volume changes measured is caused by the elastic deformation of the tubings, end-plugs, and other elements inserted inside the pressure vessel. In order to evaluate the necessary correction, fluid volume changes were measured on a solid aluminum sample prepared in the same way than

the rock samples. The values obtained are presented in Table 1. They are very small, on the order of a few percent of the values obtained for the rock samples themselves. However, the uncertainty in these values is probably quite large, due to small but unavoidable differences in sample preparation and assembly.

SAMPLE PREPARATION AND ASSEMBLY

Rock cores were ground to a cylindrical shape, 1.90cm in diameter and about 2.5cm in length (the sample assembly with the spiral tubing described in [2] can accommodate little variations in sample length). Special care was taken to produce parallel faces precisely perpendicular to the cylinder axis. The samples were then carefully cleaned of cutting-oil and dried.

The Tygon and P.V.C. jackets previously used by Bernabe et al. [2] appeared to be permeated by kerosene at 45°C. In order to perform experiments of duration longer than a few days, it was necessary to devise a new jacketing procedure, schematically represented in Figure 12. The main jacket consisted of a thick layer of a urethane rubber compound called Flexane (see Appendix). Flexane proved consistently resistant to kerosene for intervals of time as long as 3 months. But, using this rubber induced a cascade of small difficulties. A very thin copper foil (.002") had to be used to prevent the curing compound from filling the interfaces between the end-plugs and the sample. However, considerable leakage could occur along the rock-copper interface. To avoid this, a thin layer of soft silicon rubber was placed between the sample and the copper foil. To prevent penetration of the soft

silicon rubber into cracks in the samples, the sides of the samples were coated with a very thin layer of epoxy. This rather complicated jacketing procedure was successfully tested by exposing an impermeable aluminum sample to a differential pressure of several MPa's for more than a week without observing a drop in δP_p.

Finally, the assembled sample need to be saturated with distilled water before being set inside the pressure vessel. The saturation is better achieved under vacuum. Otherwise, air bubbles would remain inside the pore network spoiling the permeability measurements.

Appendix

Differential Pressure Transducer

model HHD

B.L.H.

Absolute Pressure Transducer

model DHF

B.L.H.

Bladder-type Accumulator

model 30A-1WS

Greer Olaer Products

Isothermal Oven

horizontal air-flow

mechanical convection

model POM-333B-1

Blue-M Electric

Metering Valve

model 60-13HF4-V

H.I.P.

Volumometer

pressure generator

model 37-5.75-60

H.I.P.

Thermocouple

model CO3-E

Omega Engineering

Electronic Ice-point Reference

model CJ-E (calibrated at 45°C)

Omega Engineering

Flexane

80-Putty

Devcon

References

[1] Brace, W.F., Permeability of crystalline and argillaceous rocks, Int. J. Rock Mech. Min. Sci. Geomech. Abstr., 17, 241-251, 1980.

[2] Bernabe, Y., W.F. Brace, and B. Evans, Permeability, porosity, and pore geometry of hot-pressed calcite, Mech. of Materials, 1, 173-183, 1982.

[3] Trimmer, D., B. Bonner, H.C. Heard, and A. Duba, Effect of pressure and stress on water transport in intact and fractured gabbro and granite, J. Geophys. Res., 85, 7059-7071, 1980.

[4] Brace, W.F., J.B. Walsh, and W.T. Frango, Permeability of granite under high pressure, J. Geophys. Res., 73, 2225-2236, 1968.

[5] Lin, W., Parametric analyses of the transient method of measuring permeability, J. Geophys. Res., 87, 1055-1060, 1982.

[6] Hsieh, P.A., J.V. Tracy, C.E. Neuzil, J.D. Bredehoeft, and S.E. Silliman, A transient laboratory method for determining the hydraulic properties of "tight" rocks - Theory, Int. J. Rock Mech. Min. Sci. Geomech. Abstr., 18, 245-252, 1981.

[7] Neuzil, C.E., C. Cooley, S.E. Silliman, J.D. Bredehoeft, and P.A. Hsieh, A transient laboratory method for determining the hydraulic properties of "tight" rocks - application, Int. J. Rock Mech. Min. Sci. Geomech. Abstr., 18, 253-258, 1981.

[8] Bernabe, Y., Pore volume and transport properties changes during confining pressure cycling of several crystalline rocks, unpublished manuscript, 1985.

P_c (MPa)	Loading	Unloading
40	0.030	0.024
60	0.022	0.018
80	0.018	0.011
100	0.015	0.009
120	0.014	0.008
140	0.011	0.008
160	0.010	0.007
180	0.010	0.007
200		

Table 1: The fluid volume changes during confining pressure cycling of a solid aluminum sample. The results showed here are normalized to the sample volume ($7.2cm^3$), and must be multiplied by 10^{-3}.

Figure captions

Figure 1: A sketch of the apparatus. The various elements are indicated by the following abbreviations: MV - metering valve; PV - pressure vessel; S - sample; IOC - isothermal oven chamber; RD - rupture disk; APT - absolute pressure transducer; DPT - differential pressure transducer; A - accumulator; V - volumometer; R - $40cm^3$ reservoir; HG - Heise gage; P - pump; 1 to 8 - valves. The solid lines represent the tubings of the upstream reservoir (transient flow method), and the dotted lines those of the downstream reservoir. The reservoir drawn with dashed lines can be added to either the upstream or the downstream reservoirs in order to increase their compressive storage.

Figure 2: A photograph of the isothermal oven, the pore pressure and confining pressure generating systems, the recording devices, and the sample assembly.

Figure 3: A photograph of the isothermal oven chamber containing the pressure vessel and other elements of the apparatus (see Figure 1).

Figure 4: An example of pressure decay curve corresponding to high permeabilities and the concomitant temperature fluctuations (Pottsville sandstone: $k=112.\ 10^{-21}\ m^2$).

Figure 5: An example of pressure decay curve corresponding to low permeabilities and the concomitant temperature fluctuations (Westerly granite: $k=.806\ 10^{-21}\ m^2$).

Figure 6: A sketch of the isothermal oven. IOC - isothermal oven chamber; I - insulation; EV - exhaust vent; LAF - laminar air flow; CA - cool air; F - fan; HE - heating elements; TS - temperature sensor; CS - control system.

Figure 7: The effect of a provoked temperature perturbation on the pressure decay curve.

Figure 8: The effect of temperature fluctuations during a measurement at very low permeability (Westerly granite: $k=.452\ 10^{-21}\ m^2$).

Figure 9: δk_o for all the measurements made with the second version of the permeameter. The solid arrow indicate $\delta k_o(75)$, and the dashed arrow corresponds to $\delta k_o(90)$ (they will also be plotted in the next two Figures).

Figure 10: a) δk_o for permeabilities less than $10\ 10^{-21}\ m^2$. The portion corresponding to $k<5\ 10^{-21}\ m^2$ is indicated in black.

b) δk_o for permeabilities higher than $10\ 10^{-21}\ m^2$. The portion corresponding to $k>100\ 10^{-21}\ m^2$ is indicated in black.

Figure 11: δk_o for the different rocks. The histograms are normalized to facilitate their comparison.

Figure 12: The jacketing procedure. EP - end-plug; OR - O-ring; SCR - spacing copper ring; F - Flexane; S - sample; CF - copper foil; SR - silicon rubber; EC - epoxy coating.

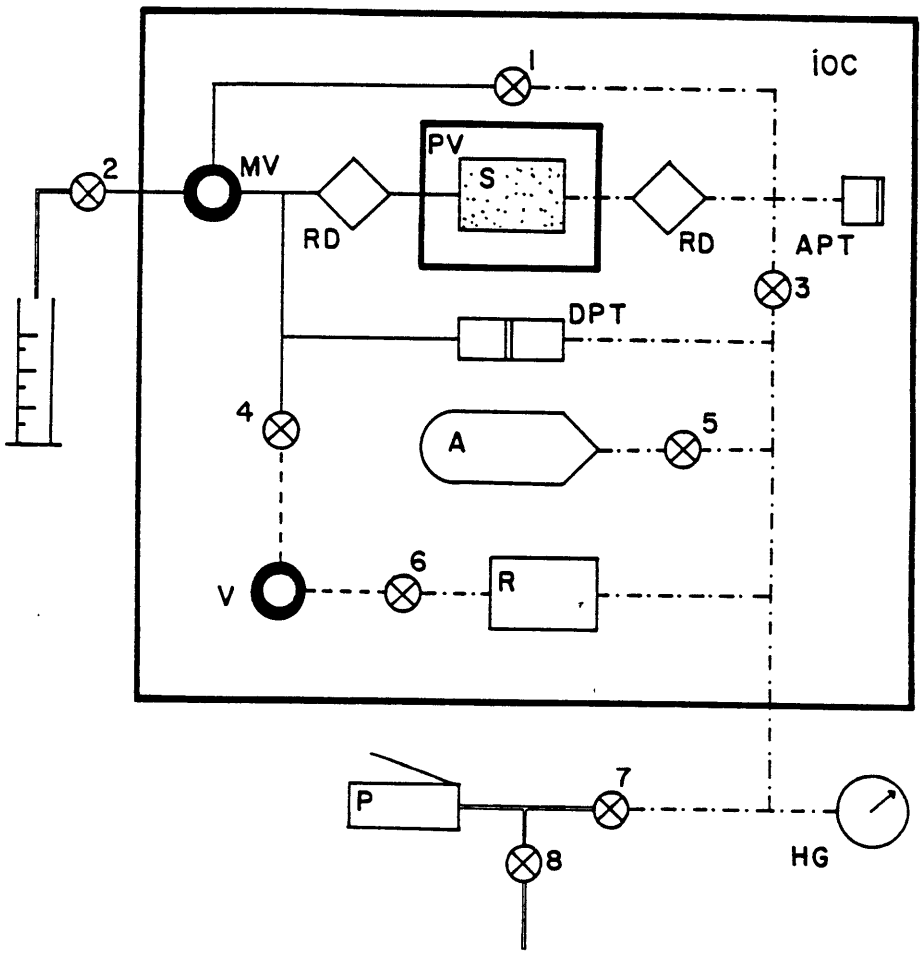

Figure 1:

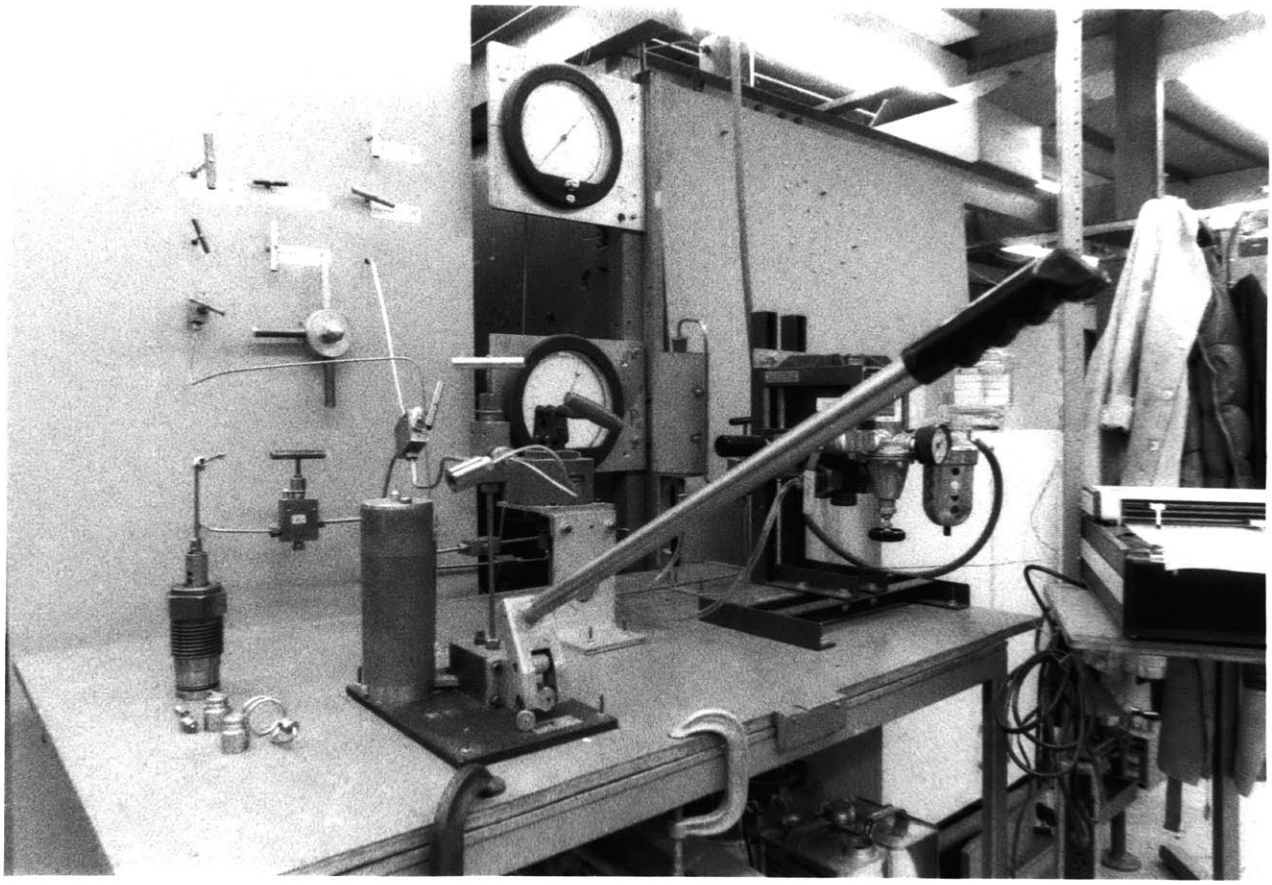

Figure 2:

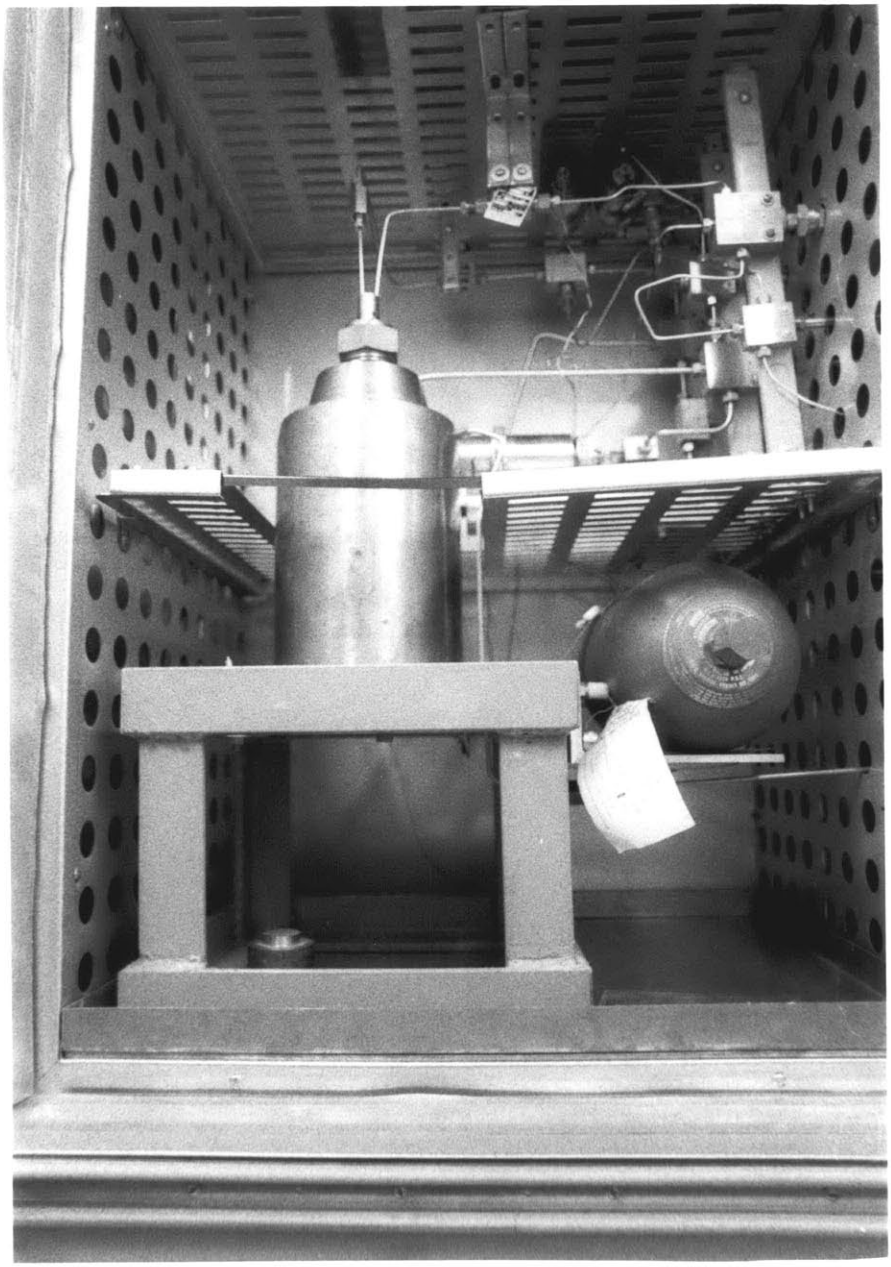

Figure 3:

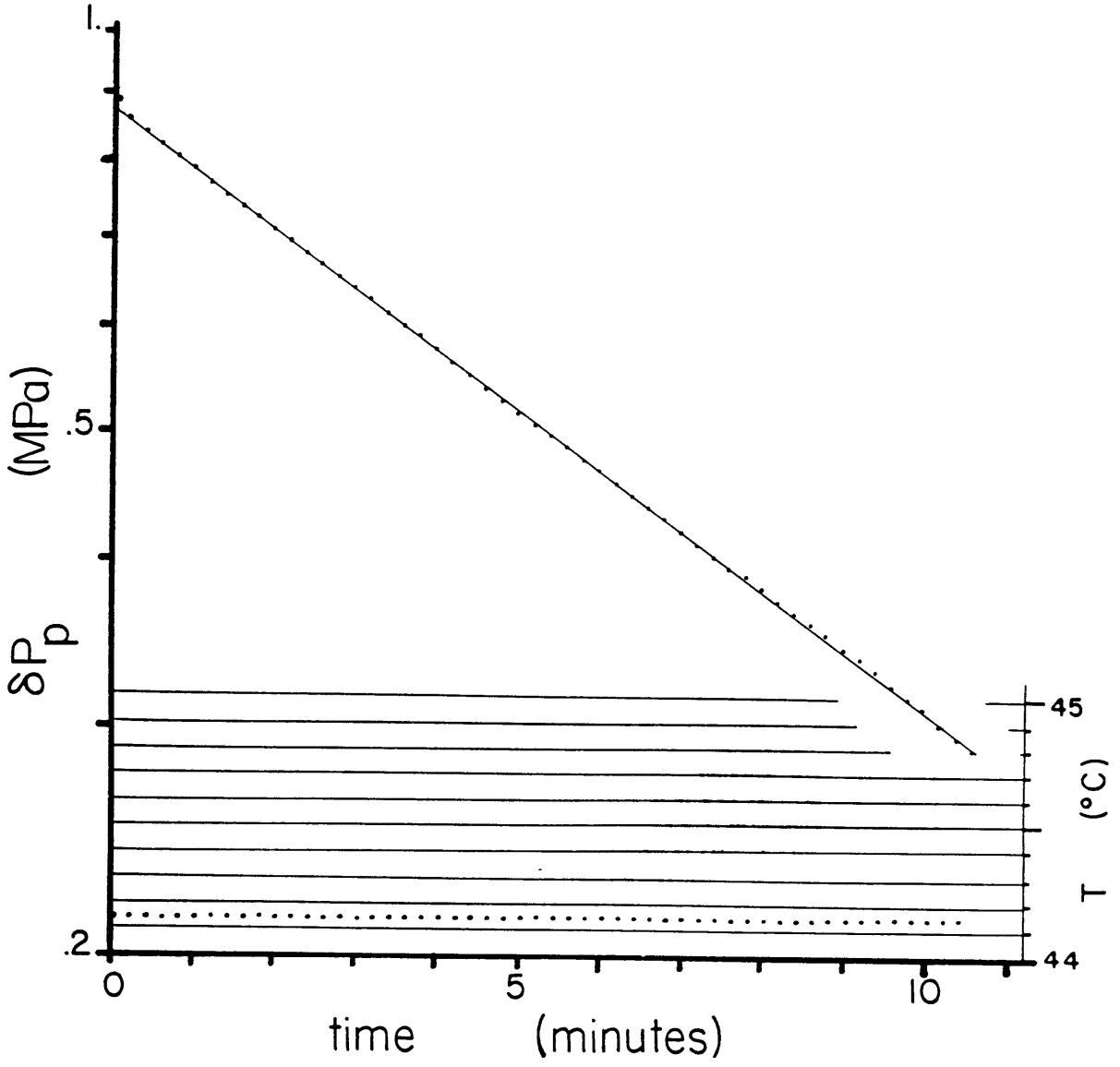

Figure 4:

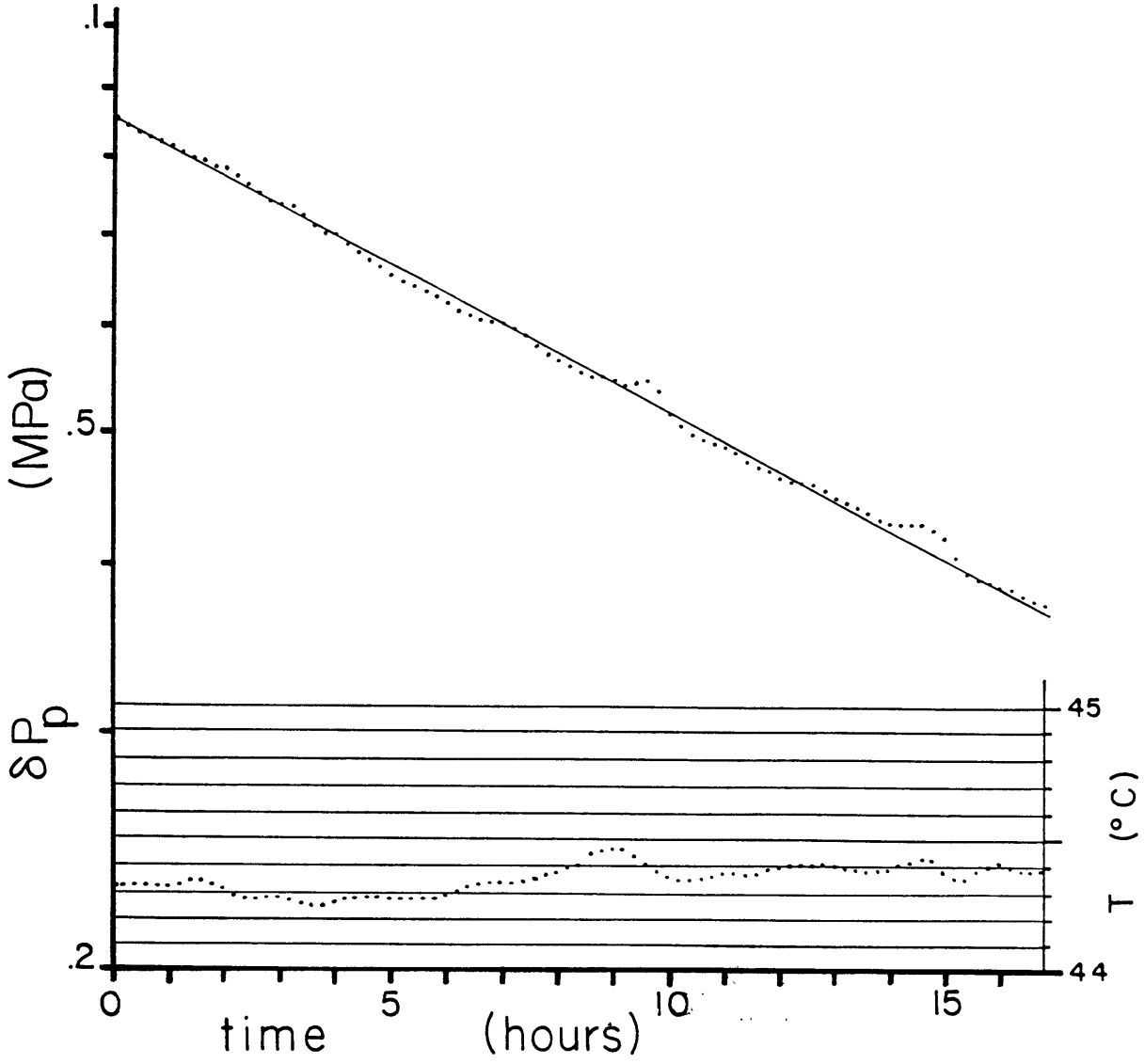

Figure 5:

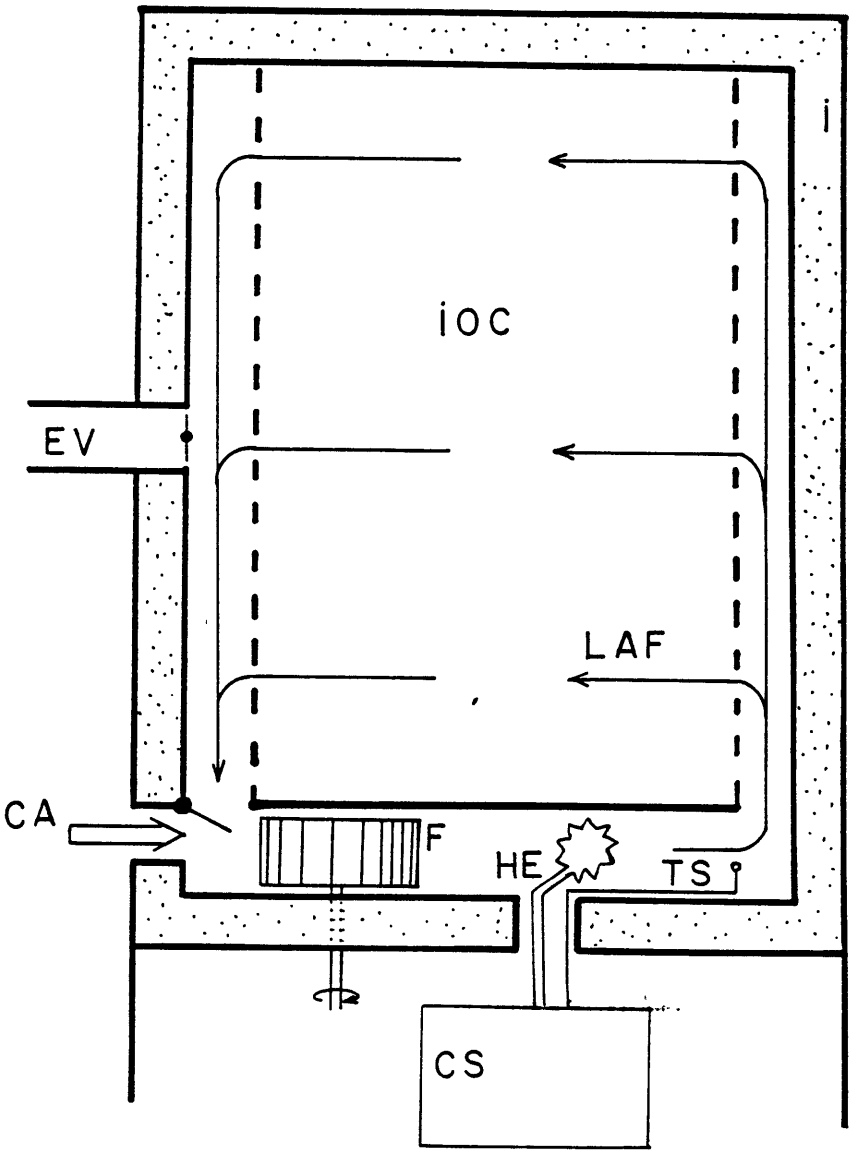

Figure 6:

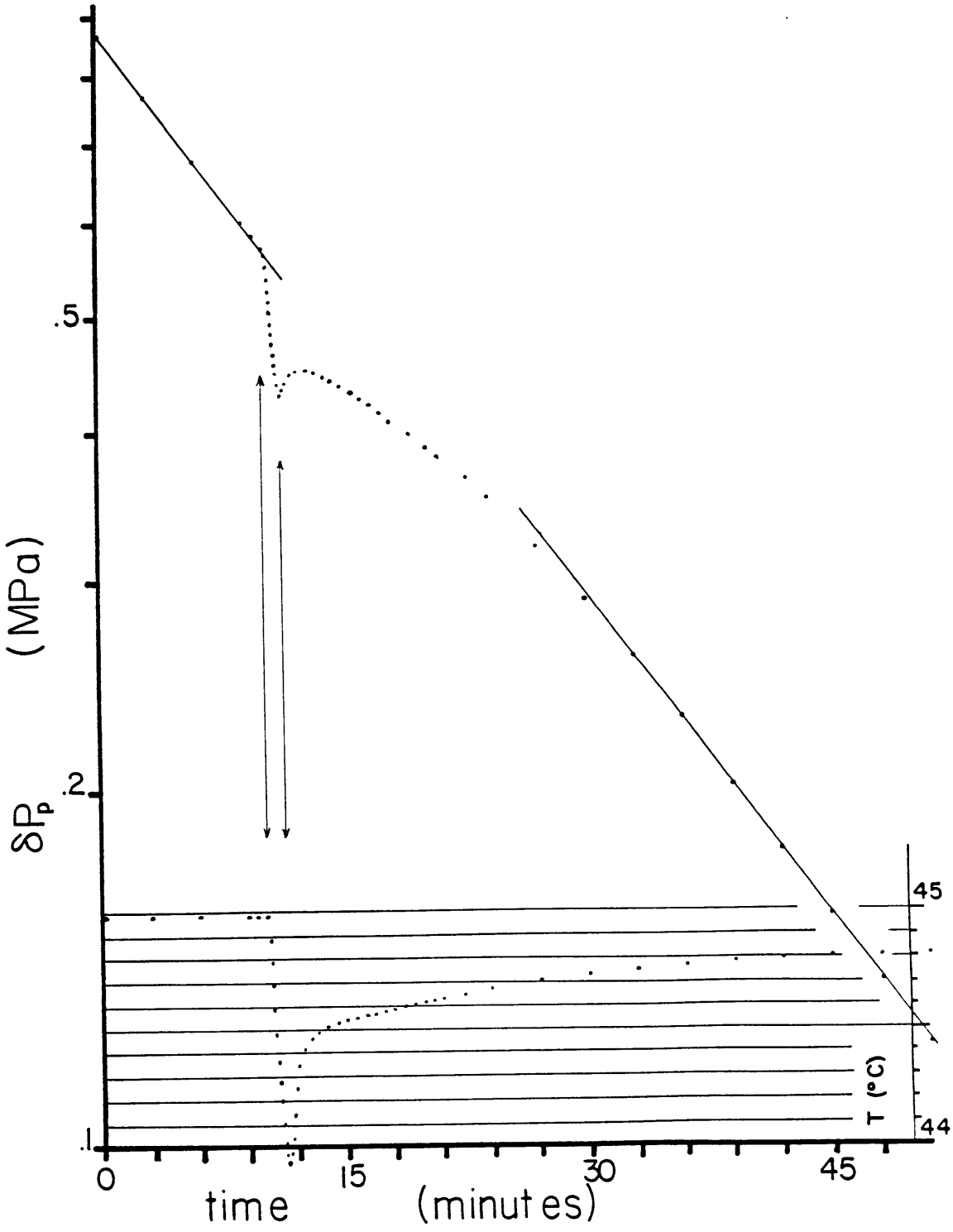

Figure 7:

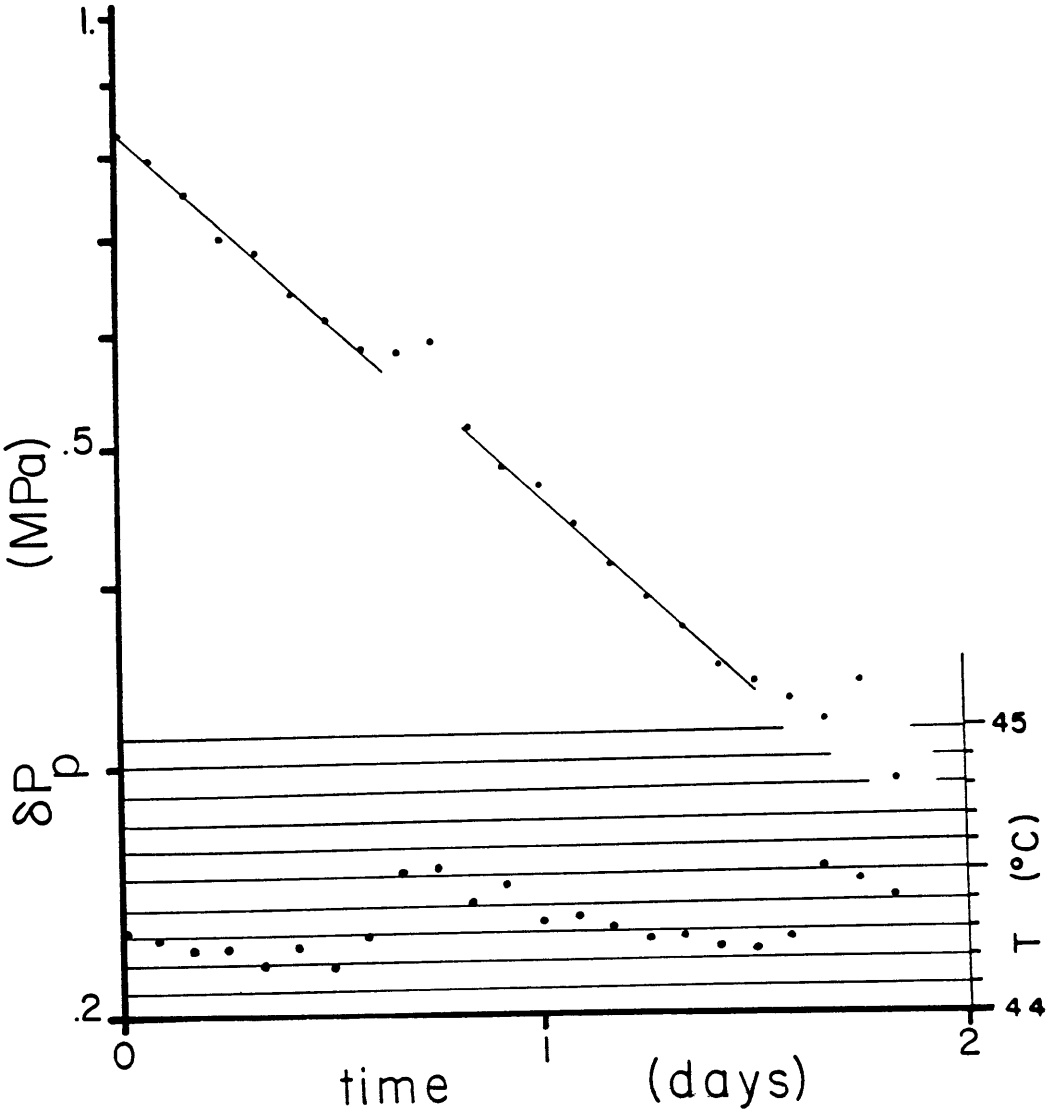

Figure 8:

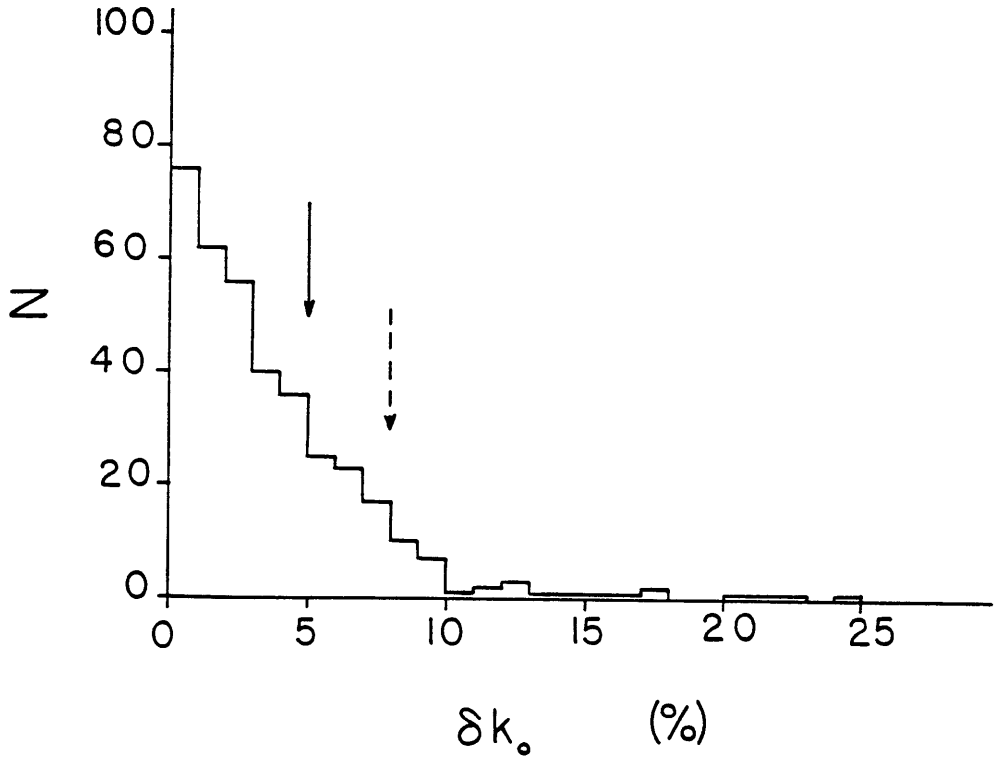

Figure 9:

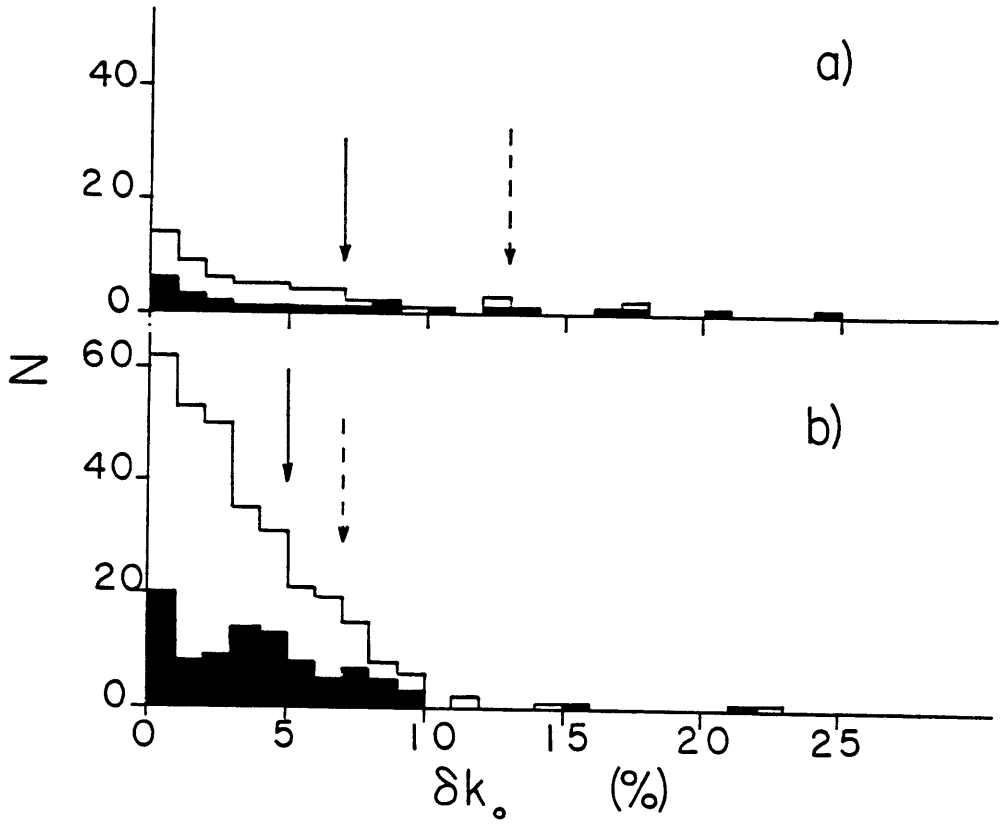

Figure 10:

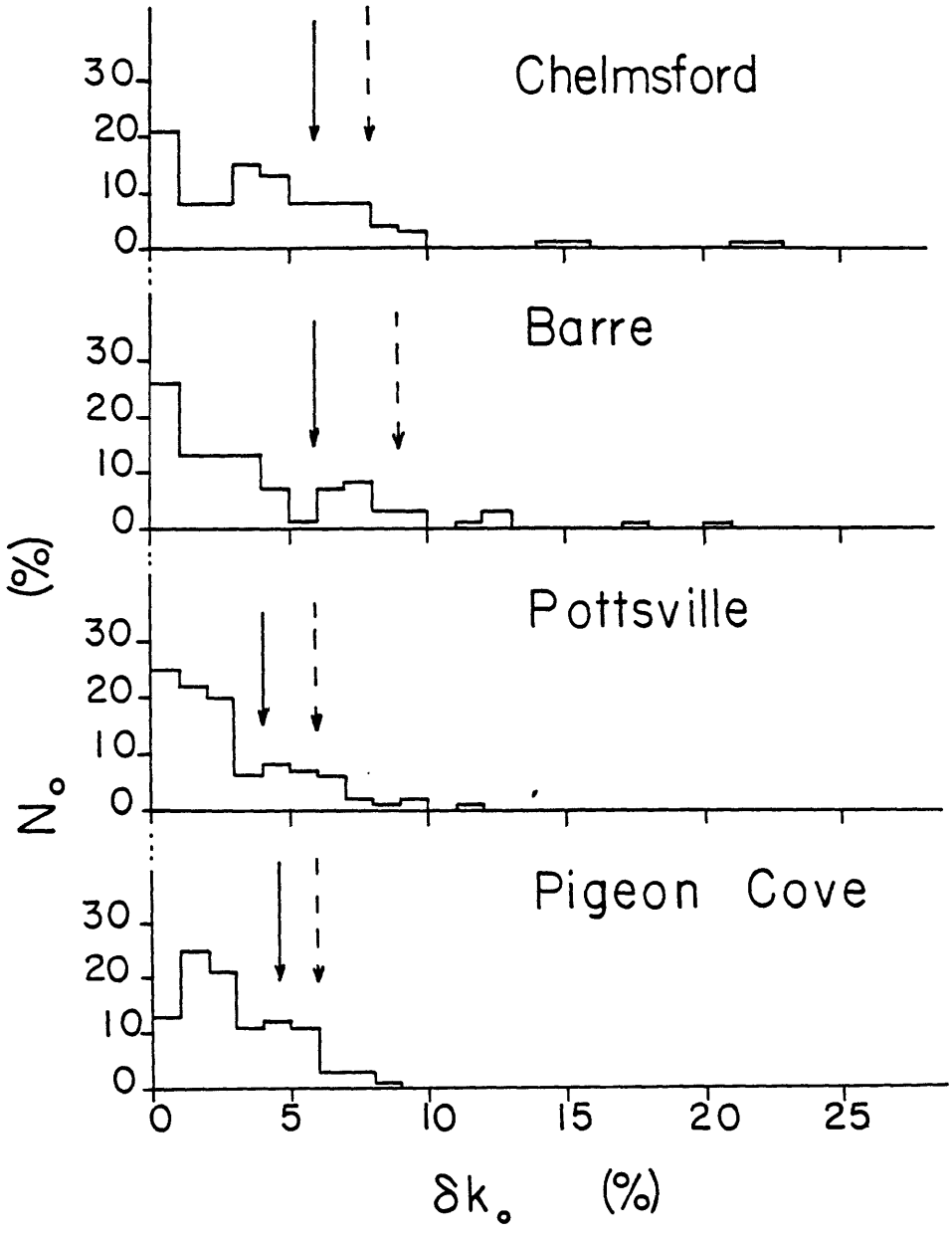
Chelmsford
Barre
Pottsville
Pigeon Cove
30
20
10
0
(%)
N°
0
5
10
15
20
25
δk° (%)

Figure 11:

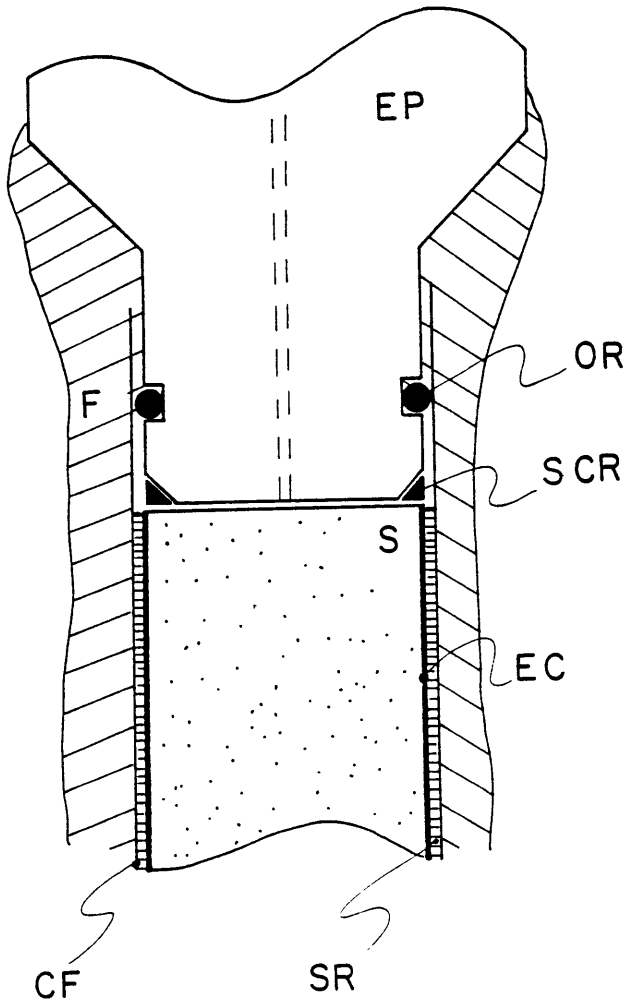

Figure 12:

Thesis examination committee

William F. Brace (advisor)

Theodore R. Madden (chairman)

Ronald F. Scott (Cal. Tech.)

Joseph B. Walsh (MIT)